الجمهورية الجزائرية الديمقراطية الشعبية

République Algérienne Démocratique et Populaire

Ministère de L'Enseignement Supérieur et de la Recherche Scientifique

Université Ferhat ABBAS Sétif 1

UNIVERSITÉ FERHAT ABBAS - SETIF1

FACULTÉ DE TECHNOLOGIE

THÈSE

Présentée au Département de Génie des Procédés

Pour l'obtention du diplôme de

DOCTORAT

Domaine : Sciences et Technologie

Filière: Génie des procédés

Option: Génie des procédés pharmaceutiques

Par

MOKHNACHE Kamel

THÈME

Synthesis, Characterization, Toxicological and Antioxidant Activities of New Hydrazone derived from Isoniazid.

Soutenue le 29/04/2019 devant le Jury:

Mohamed T. Benaniba	**Professeur**	**Univ. Ferhat Abbas Sétif 1**	**Président**
Noureddine Charef	**Professeur**	**Univ. Ferhat Abbas Sétif 1**	**Directeur**
Mohammad S. Mubarak	**Professeur**	**Univ. de Jordanie Amman**	**Co-directeur**
Lekhmici Arrar	**Professeur**	**Univ. Ferhat Abbas Sétif 1**	**Examinateur**
Meriem M. ElKolli	**Professeur**	**Univ. Ferhat Abbas Sétif 1**	**Examinateur**
Noureddine Gherraf	**Professeur**	**Univ. Oum el Bouaghi**	**Examinateur**

الجمهورية الجزائرية الديمقراطية الشعبية

DEMOCRATIC AND POPULAR REPUBLIC OF ALGERIA

MINISTRY OF HIGHER EDUCATION AND SCIENTIFIC RESEARCH

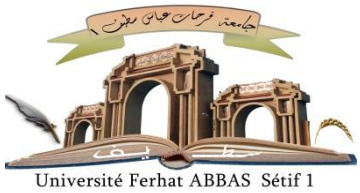

UNIVERSITY FERHAT ABBAS SETIF1

FACULTY OF TECHNOLOGY

THESIS

Presented at the Department of Process Engineering

SUBMITTED FOR THE DEGREE OF:

DOCTORAT

Sciences and Technology

Field: Process Engineering **Special filed: Pharmaceutical process engineering**

By

MOKHNACHE Kamel

TOPIC

Synthesis, Characterization, Toxicological and Antioxidant Activities of New Hydrazone derived from Isoniazid

Presented publically in: 29/04/2019

Jury:

Mohamed T. Benaniba	**Professor**	**Univ. Ferhat Abbas Sétif 1**	**President**
Noureddine Charef	**Professor**	**Univ. Ferhat Abbas Sétif 1**	**Supervisor**
Mohammad S. Mubarak	**Professor**	**The Univ. of Jordan, Amman**	**Co- Supervisor**
Lekhmici Arrar	**Professor**	**Univ. Ferhat Abbas Sétif 1**	**Examinor**
Meriem M. ElKolli	**Professor**	**Univ. Ferhat Abbas Sétif 1**	**Examinor**
Noureddine Gherraf	**Professor**	**Univ. Oum el Bouaghi**	**Examinor**

Acknowledgements

First of all, I am grateful to *Al-mighty ALLAH* who gave me strength and perseverance, whatever I am today is just thanks to Him (*ALLAH subhana-Wa-Taala*).

I would like to express my appreciation and grateful thanks to my supervisor **Pr. Noureddine Charef** for his advice, guidance, encouragements and support throughout my doctoral work.
I would deeply like to thank my co-supervisor, **Pr. Mohammad S. Mubarak** for his enriching advices, keen interest, guidance and support throughout my doctoral work.

I would also like to show my gratitude for my committee; thank you to **Pr. Mohamed T. Benaniba**, **Pr. Lekhmici Arrar**, **Pr. Meriem M. ElKolli** and **Pr. Noureddine Gherraf**.
I want to offer my special thanks to **Pr. Abderrahmane Baghiani** for his valuable advices, continuous support, assistance, and to all other technical supports. I am also thankful to **Pr. Seddik Khennouf**, for help and provision of research facilities in their laboratories.

My sincere gratitude to **Dr. Soraya Ouhida**, Doctor of pathologic anatomy in laboratory of Hospitalo-Public Establishment (HPE) of Sétif, for providing all the facilities to realise histological slides and interpreting them.

Many thanks send to all my colleagues in laboratory of applied biochemistry, who provided the most amicable and lively working environment.

Dedication

To my parents

To my sisters and brothers

To all my family

And to all my

Friends and colleagues

List of abbreviations

ALP: Alkaline phosphatase

ALT: Alanine transaminase

AST: Aspartate transaminase

ATP: Adenosine Triphosphate

CAT: Catalase

CYP2E1: Cytochrome P4502E1

DFT: Density functional theory

DILI: Drug induced liver injury

DMSO: Dimethylsulfoxide

DPRA: Direct peptide reactivity assay

Eco: Econazol

Gent: Gentamicine

GSH: Glutathione

HBA: Hydrogen-bond acceptor

HBD: Hydrogen-bond donors

h-CLAT: Human cell line activation test

HRMS: High Resolution Mass Spectrometry

Hyd1: (N'-[(*E*)-(4-chloro-3-nitrophenyl)methylidene] pyridine-4-carbohydrazide

Hyd2: N'-[(3*Z*)-6-bromo-2-oxo-2,3-dihydro-1*H*-indol-3-ylidene] pyridine-4-carbohydrazide

IND: Indomethacine

INH: Isoniazid

LLNA: Murine local lymph node assay

MAH: Monoacetylhydrazine

MPT: Mitochondrial Permeability Transition

NA: Nicotinamide

NAT2: N-acetyltransferase 2

NMR: Nuclear Magnetic Resonance

PDB: Protein Data Bank

ROS: Reactive Oxygen Species

S_NAr: Aromatic nucleophil substitution

TBABF4: Tetrabutylammoniumtetrafluoroborate

List of Figures

Figure 1. The synthesis methodologies for hydrazone linkages **3**

Figure 2. Standard Mechanism of hydrazones formation **4**

Figure 3. Semi-synthesis of hydrazones **6**

Figure 4. Active centers of hydrazones **6**

Figure 5. Reactions of hydrazones with different type of reagents **7**

Figure 6. Heterocyclic compounds formed from hydrazide-hydrazones **8**

Figure 7. Structure of Nifuroxazide **8**

Figure 8. Structures of thiazolylidene-isonicotino hydrazide derivatives **9**

Figure 9. Structure of anticancer ; monohydroxylated, dihydroxylated and methoxylated hydrazones **10**

Figure 10. Structure of leishmanicidal hydrazones (HPAmIH and HPCIH) **10**

Figure 11. Structure of antibacterial hydrazones (**3**, **4**, and **5**) **11**

Figure 12. Structure of antifungal hydrazones (**A**, **B**, and **C**) **11**

Figure 13. The liver **12**

Figure 14. Mechanisms of DILI **15**

Figure 15. Factors affecting drug-induced hepatotoxicity **16**

Figure 16. Structure of the anti-tubercular drug (isoniazid) **16**

Figure 17. Mechanism of action of **INH** on susceptible bacilli **17**

Figure18. Isoniazid induced oxidative stress in hepatocyte cell. **18**

Figure 19. Isoniazid metabolic pathways **19**

Figure 20. Direct oxidation of **INH** and covalent binding with macromolecules **20**

Figure 21. Biotransformation and bioactivation of **INH** **20**

Figure 22. **INH**-induced oxidative stress and apoptosis in hepatocyte **21**

Figure 23. Pathway for preparation of **Hyd1** **25**

Figure 24. Pathway for preparation of **Hyd2** **25**

Figure 25. Optimized molecular structures of **INH, Hyd1** and **Hyd2**. **32**

Figure 26. Frontier molecular orbitals of **INH, Hyd1** and **Hyd2**; ΔE_{gap} in gas phase. **33**

Figure 27. Ionization centers of **INH, Hyd1** and **Hyd2** **35**

Figure 28. pH-dependent distribution of species derived from **Hyd1**. **35**

Figure 29. pH-dependent distribution of species derived from **Hyd1**. **36**

Figure 30. H-bond donor/acceptor centers of **INH, Hyd1** and **Hyd2** **36**

Figure 31. Partial atomic charges of **INH, Hyd1** and **Hyd2** **38**

Figure 32. Steric hindrance of **INH, Hyd1** and **Hyd2** **39**

Figure 33. logP values distribution of **INH, Hyd1** and **Hyd2** **40**

Figure 34. pH-dependent distribution coefficient; logD of **INH, Hyd1** and **Hyd2** **42**

Figure 35. Proposed mechanism of **Hyd1** biotransformations to their reactive metabolite, nitrenium ion intermediate. **48**

Figure 36. Effect of **Hyd1** on: **a**).Human skin sensitization, **b**). Murine local lymph node assay (LLNA), **c**). Direct peptide reactivity assay (DPRA), **d**). Human cell line activation test (h-CLAT), and **e**). KeratinoSens™. **51**

Figure 37. Effect of **Hyd2** on: **a**).Human skin sensitization, **b**). Murine local lymph node assay (LLNA), **c**). Direct peptide reactivity assay (DPRA), **d**). Human cell line activation test (h-CLAT), and **e**). KeratinoSens™. **51**

Figure 38. Effect of **INH** on: **a**)**.** Human skin sensitization, b). Murine local lymph node assay (LLNA), c). Direct peptide reactivity assay (DPRA), d). Human cell line activation test (h-CLAT), and e). KeratinoSens™. **52**

Figure 39. Effect of **AA** on : a**).** Human skin sensitization, b). Murine local lymph node assay (LLNA), c). Direct peptide reactivity assay (DPRA), d). Human cell line activation test (h-CLAT), and e). KeratinoSens™. **53**

Figure 40. Anti-tubercular activity prediction of **Hyd1** and **Hyd2** **54**

Figure 41. Visualization of binding of : a) **Hyd2**, b) **Hyd1**, c) **INH**, to enoyl ACP reductase (InhA) enzyme (PDB code: 4DRE), Visualization is performed using UCSF Chimera. **56**

Figure 42. Biodegradation products of **Hyd1** **57**

Figure 43. Proposed mechanism of the formation of **Hyd1** **59**

Figure 44. Proposed mechanism of the of formation **Hyd2** **60**

Figure 45. FT-IR spectrum of **Hyd1** **62**

Figure 46. FT-IR spectrum of **Hyd2** **62**

Figure 47. Electronic spectrum of **Hyd1** and **Hyd2** **63**

Figure 48. ^{1}H-NMR spectrum of **Hyd1** **64**

Figure 49. ^{1}H-NMR spectrum of **Hyd1** (7.6-8.9 ppm) **64**

Figure 50. ^{13}C-NMR spectrum of **Hyd1** **65**

Figure 51. ^{13}C-NMR spectrum of **Hyd1** (120-165 ppm) **66**

Figure 52. ^{13}C-NMR; DEPT 135 spectrum of **Hyd1** **66**

Figure 53.^{1}H-NMR spectrum of **Hyd2** **67**

Figure 54. ^{13}C-NMR spectrum of **Hyd2** (114 to 165 ppm) **67**

Figure 55. ^{13}C-NMR spectrum of **Hyd2** (114 to 165 ppm) **68**

Figure 56. High resolution mass spectrum (HMRS) of **Hyd1** **69**

Figure 57. High resolution mass spectrum (HMRS) of **Hyd2** **69**

Figure 58. Development of mice body weight **71**

Figure 59. Histopathological analysis of mousse females' liver and kidney treated with **Hyd1** and **Hyd2** in acute toxicity (x10 and x 40). **72**

Figure 60. Cyclic voltammograms showing superoxide anion scavenging effect of **Hyd1** **74**

Figure 61. Cyclic voltammograms showing superoxide anion scavenging effect of **Hyd2** **74**

Figure 62. Superoxide anion scavenging effect of **Hyd1, Hyd2, IND,** and **AA** **75**

Figure 63. IC_{50} values of **Hyd1, Hyd2, IND** and **AA** **75**

Figure 64. Hydrogen peroxide scavenging effect of **Hyd1, Hyd2, IND,** and **AA** **76**

Figure 65. IC_{50} values of **Hyd2, IND,** and **AA** **76**

Figure 66. Structures of **Hyd2** and **IND** **77**

Figure 67. Body weight estimation during 7 days **79**

Figure 68. Histopathological analysis of mousse females' liver and kidney treated with **Hyd2** in hepatotoxicity assay (x10 and x 40). **81**

Figure 69. Biodegradation of **Hyd1, INH,** and **NA** by *Aspargillus niger* **82**

Figure 70. Diameter of *Aspargillus niger* growth after 7 days in mineral media containing: **a**) **NA**, **b**) **Hyd1** and **c**) **INH.** **82**

List of Tables

Table 1. Origin, chemical structures and names of natural hydrazones **5**

Table 2. Types of DILI **13**

Table 3. Online software programs for toxicity and bioactivity prediction **23**

Table 4. Comparison of HOMO, LUMO, and related molecular properties of **INH, Hyd1** and **Hyd2** in DMSO and in gas state **34**

Table 5. Topological polar surface area and absorption parentage of **INH, Hyd1** and **Hyd2** **42**

Table 6. Toxic substructure prediction of **INH, Hyd1,** and **Hyd2** **44**

Table 7. Acute rat toxicity prediction of **INH, Hyd1,** and **Hyd2** **45**

Table 8. Carcinogenicity prediction of **INH, Hyd1,** and **Hyd2** **46**

Table 9. Hepatotoxicity prediction of **INH, Hyd1,** and **Hyd2** **46**

Table 10. Mutagenicity prediction of **INH, Hyd1,** and **Hyd2** **47**

Table 11. Immunotoicity prediction of **INH, Hyd1,** and **Hyd2** **49**

Table 12. Cytotoxicity prediction of **INH, Hyd1,** and **Hyd2** **49**

Table 13. P values and predicted sensitization effect of **INH, Hyd1, Hyd2,** and **AA.** **50**

Table 14. Skin sensitization predictions of **Hyd1, Hyd2, INH,** and **AA.** **50**

Table 15. Clustering results obtained from the docking of **INH, Hyd1,** and **Hyd2** into InhA **55**

Table 16. Yields, physical appearance, uncorrected melting points, and Rf values **Hyd1** and **Hyd2** **61**

Table 17. Characteristic IR bands of **Hyd1,** and **Hyd2** **61**

Table 18. Elemental analysis of the **Hyd1,** and **Hyd2** **63**

Table 19. ^{13}C-NMR of **Hyd1** **65**

Table 20. ^{13}C-NMR of **Hyd2** **68**

Table 21. Effect of the **INH, Hyd1, Hyd2,** gentamicine, and econazol on bacteria and fungi strains **70**

Table 22. Biochemical parameters of control and mice treated with **Hyd1** and **Hyd2** **71**

Table 23. Effect of **Hyd2** on oxidative stress parameters **78**

Table 24. Organs weight estimation **79**

Table 25. Biochemical parameters **80**

Contents

Acknowledgment……. I

Dedication……..... II

List of abbreviations …… III

List of figures …… IV

List of tables ……..... VII

Contents……. VIII

Introduction ……..... 1

Chapter I

Overview of synthesis, reactivity and biological activity of hydrazones

I. Hydrazones …… 3

I.1. Definition……... 3

I.2. Synthetic pathways……. 3

I.3. Mechanism of formation……..... 3

I.4. Biosynthetic hydrazones…… 4

I.5. Semi-synthetic hydrazones…… 5

I.6. Reactivity of hydrazones…….. 6

I.7. Heterocyclization of hydrazide-hydrazones…… 7

I.8. Biological activity of hydrazones……. 8

I.8.1. Anti-mycobacterial activity…… 9

I.8.2. Anticancer activity……..……. 9

I.8.3. Leishmanicidal activity…….. 10

I.8.4. Antibacterial activity……..... 10

I.8.5. Antifungal activity…….. 11

Chapter II

Overview of Isoniazid and its hepatotoxicity

II. **Hepatotoxicity**……..... 12

II.1. Liver…… 12

II.2. Drug induced liver injury (DILI)…… 12

II.2.1. Types of DILI……..... 13

II.2.2. Mechanism of DILI…… 13
II.2.2.1. First step… …… 13
II.2.2.2. Second step ……..... 14
II.2.2.3. Third step ……..... 14
II.2.3. Factors affecting DILI…….. 15
II.2. Isoniazid induced oxidative stress and hepatotoxicity…… 16
II.2.1. Isoniazid proprieties……. 16
II.2.2. Isoniazid-induced oxidative stress…… 17
II.2.3. Isoniazid induced hepatotoxicity……..... 18
II.2.3.1. Isoniazid -metabolism…… 18
II.2.3.2. Mechanisms of **INH**-hepatotoxicity……..... 19

Chapter III:

Material and methods

III.1. **Computational methods**……..... 22
III.1.1. DFT study…… 22
III.1.2. Physicochemical proprieties calculation……. 22
III.1.3. Toxicity and bioactivity predictions…… 22
III.1.4. Biodegradability prediction……. 23
III. 2. **Experimental methods**…….. 23
III 2.1. Reagents…….. 23
III 2.2. Equipments…….. 23
III 2.2.1. Thin layer chromatography……... 23
III.2.2.2. Nuclear Magnetic Resonance (NMR)…….. 23
III.2.2.3. High Resolution Mass Spectra (HRMS)…… …….. 24
III.2.2.4. Melting point (Mp°)…… 24
III.2.2.5. Elemental analysis……..... 24
III.2.2.6. Fourier transform infrared (FT-IR) spectrum……. 24
III.2.2.7. Electronic absorption spectrum……..... 24
III.2.3. Animals…… 24
III.2.4. Microbial stains and culture medium…….. 24
III.2.5. Synthesis…… 25
III.2.5.1. Synthesis of **Hyd1**…… 25
III.2.5.2. Synthesis of **Hyd2**……. 25
III.2.6. Toxicological studies……..... 26
III.2.6.1. *In vitro* evaluation using bacteria……. 26
III.2.6.2. *In vitro* evaluation using fungus……..... 26
III.2.6.3. *In vivo* acute toxicity evaluation…….. 26

III.2.6.3.1. Observations…… 27
III.2.6.3.2. Animal weight……..... 27
III.2.6.3.3. Biochemical analysis…….. 27
III.2.6.3.4. Histopathological analyses……. 27
III.2.7. *In vitro* antioxidant activity evaluations…….. 27
III.2.7.1. Superoxide anion scavenging activity…… 27
III.2.7.1.1. Chemical assay…….. 27
III.2.7.1.2. Electrochemical assay……..... 28
III.2.7.2. Hydrogen peroxide scavenging activity……..... 28
III.2.8. *In vivo* antioxidant activity evaluation…… 28
III 2.8.1. Preparation of tissue homogenates……..... 29
III.2.8.2. Determination of CAT activity……. 29
III.2.8.3. Estimation of GSH…… 29
III.2.8.4. Estimation of MDA……... 29
III.2.9. Hepatoprotective activity evaluation……..... 30
III.2.9.1. Body weight estimation……. 30
III.2.9.2. Organs weight estimation…….. 30
III.2.9.3. Biochemical analysis……. 30
III.2.9.4. Histopathological analyses……..... 30
III.2.10. *In vitro* biodegradability evaluations……. 30
III.3. Statistical analysis…… 31

Chapter IV:

Results and discussion

IV. 1. **Computational chemistry** …… 32
IV.1.1. DFT study……. 32
IV.1.1.1. Structures optimization……. 32
IV.1.1.2. HOMO and LUMO analysis……. 32
IV.1.2. Physicochemical proprieties calculation…… 34
IV.1.2.1. Protonation/deprotonation forms …… 34
IV.1.2.2. H-bond donor/acceptor centers and number of rotatable bonds…… 36
IV.1.2.3. Partial atomic charges…….. 37
IV.1.2.4. Steric hindrance…… 38
IV.1.2.6. Lipophilicity descriptors…….. 39

IV.1.2.7. Topological polar surface area and absorption percentage…… 42
IV.1.3. *In Silico* Toxicological studies……. 43
IV.1.3.1. Toxic substructure prediction……..... 43
IV.1.3.2. Acute rat toxicity prediction……. 44
IV.1.3.3. Carcinogenicity prediction……..... 45
IV.1.3.4. Hepatotoxicity prediction……. 46
IV.1.3.5. Mutagenicity prediction……..... 46
IV.1.3.6. Immunotoxicity prediction……..... 48
IV.1.3.7. Cytotoxicity prediction……. 49
IV.1.3.8. Skin sensitization prediction…… 49
IV.1.4. *In silico* anti-tubercular activity evaluation…….. 53
IV.1.4.1. Molecular docking…… 54
IV.1.5. *In silico* biodegradability prediction……..... 56
IV.2. Chemistry and biological studies…… 58
IV.2.1. Chemistry……. 58
IV.2.1.1. Mechanisms of formation……. 58
IV.2.1.2. Identification and characterizations ……..…… 60
IV.2.1.2.1. Melting point determination……. 60
IV.2.1.2.2. Thin layer chromatography (TLC)……..... 60
IV.2.1.2.3. Infrared spectrum…… 61
IV.2.1.2.4. Electronic spectrum…… 62
IV.2.1.2.5. Elemental analysis……..... 63
IV.2.1.2.6. NMR spectrum……..... 63
a. NMR spectrum of **Hyd1**…… 63
b. NMR spectrum of **Hyd2**…… 66
IV.2.1.2.7. Mass spectrometry……..... 68
IV.2.2. Biological studies…….. 69
IV.2.2.1. *In vitro* toxicological evaluation……... 69
IV.2.2.2. *In vivo* acute toxicity evaluation……..... 70
IV.2.2.2.1. Behavioral observations and mortality patterns…… 70
IV.2.2.2.2. Body weight estimation……. 70
IV.2.2.2.3. Biochemical parameters…… 71
IV.2.2.2.4. Histopathological analysis……. 72
IV.2.2.3. *In vitro* antioxidant activity evaluation…… 73
IV.2.2.3.1. Superoxide Anion Radical Scavenging effect……..... 73
IV.2.2.3.2. Hydrogen peroxide scavenging effect……..... 76
IV.2.2.4. *In vivo* antioxidant activity evaluation……. 77
IV.2.2.5. Hepatoprotective effect…… 78

IV.2.2.5.1. Body and organs weight estimation…….. 79
IV.2.2.5.2. Biochemical parameters…… 79
IV.2.2.5.3. Histopathological analysis……. 80
IV.2.2.6. *In vitro* biodegradability evaluation……. 81
Conclusion……. 83
References ……... 85

Introduction

Introduction

Hydrazones can find applications in several fields including, among others, organic synthesis, polymer chemistry, biomaterials, hydrogels, dynamic combinatorial chemistry, and chemical biology [1]. Similarly, hydrazone-hydrazide is a particular class of compounds which play an important role in biological activities. This class of compounds exhibit excellent antibacterial, antifungal, antimicrobial, and anticonvulsant activity [2]. In this context, hydrazone-hydrazoides derived from isonicotinyl hydrazide (isoniazid **INH**) and different aldehydes or ketones showed activity against *M. tuberculosis*, and some of these compounds were more potent and less toxic than isoniazid [3]. On the basis of the preceding discussion, and in light of the bioactivity profile of hydrazine-hydrazides, this thesis deals with the synthesis and characterization of a new isonicotinylhydrazide analogs; N'-[(*E*)-(4-chloro-3-nitrophenyl)methylidene] pyridine-4-carbohydrazide (**Hyd1**) and N'-[(3*Z*)-6-bromo-2-oxo-2,3-dihydro-1*H*-indol-3-ylidene] pyridine-4-carbohydrazide (**Hyd2**) *via* condensation of isonicotinylhydrazide (**INH**) and 4-chloro-3-nitrobenzaldehyde or 6-Bromoindoline-2,3-dione, respectively. The structure of this work (four chapters) has been divided into two different parts: a theoretical background section represented by chapters I and II, and studies, applications, and results as in chapters III and IV.

Chapter I is an Overview of synthesis, reactivity and biological activity of hydrazones, whereas Chapter II is an Overview of isoniazid and its hepatotoxicity, including the adverse effect of drug towards liver, drug induced liver injury (DILI) and information about the principle adverse effects of isoniazid, oxidative stress and hepatotoxicity with different proposed mechanisms and hypotheses. Chapter III, on the other hand, deals with material and methods including computational chemistry of the investigated compounds **INH**, **Hyd1** and **Hyd2**, along with the programs used for molecular structure calculations and the online software programs for toxicological, bioactivity, and biodegradability predictions (density functional theory (DFT), the package Marvin, e-MolTOX, ProToxII, Predskin and UMBBD software). Chapter III also contains various instruments and protocols for the synthesis and characterization of hydrazones, *in vitro* and in *vivo* toxicological evaluations towards microorganisms and animals, biological studies, *in vitro* antioxidant activity using superoxide anion and hydrogen peroxide assays, and in *vivo* against oxidative stress in mice induced by **INH**, the hepatoprotective effect against the hepatotoxicity of **INH**, and ecological studies by *in vitro* biodegradability evaluation.

Chapter IV is devoted to results and discussion. In this chapter, we will present the discussion of results obtained from computational experimental sections. In first part, we present computational chemistry results (*in silico*); chemical reactivity prediction from DFT study, physicochemical proprieties calculations, toxicological, biological and biodegradation

predictions. In the second part, we present results of experimental section; various characterizations (NMR, mass spectrometry, elemental analysis and IR). Additionally, results of *in vitro* and *in vivo* from the toxicity study, the antioxidant, the hepatoprotective effect, and the biodegradability evaluation to confirm results of the computational part.

Chapter I: Overview of synthesis, reactivity, and biological activity of hydrazones

I. Hydrazones

I.1. Definition

Hydrazones are a special class of organic compounds in the Schiff base family [4]. They have a general formula of (R_1R_2-C=N-NH) [5]. Duo to the ease of preparation, increased hydrolytic stability and tendency toward crystallinity, hydrazones have been under study for a long time in organic chemistry [6].

I.2. Synthetic pathways

Hydrazones can be prepared by three synthetic pathways: (**a**) condensation between hydrazines and ketones or aldehydes, (**b**) Japp–Klingemann reaction; coupling between aryl diazonium salts and beta-keto esters or acids, and (**c**) coupling reaction between aryl halides and non-substituted hydrazones. These methods lead to the formation of hydrazones with crystalline forms, which facilitate their purification (**Figure1**) [7].

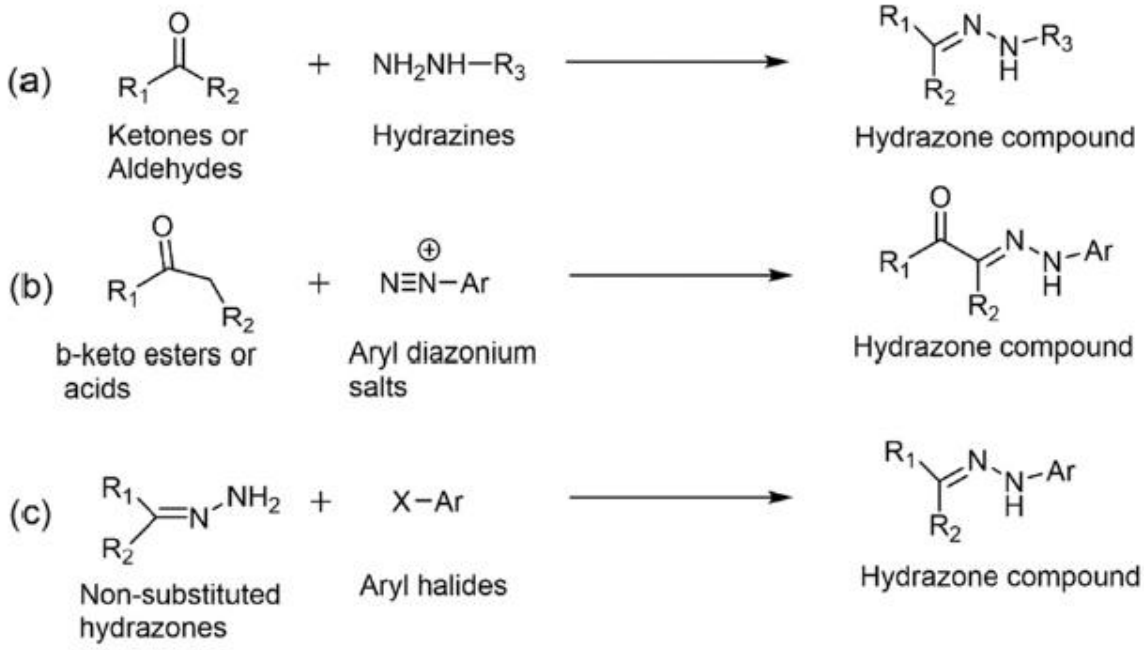

Figure 1. The synthesis methodologies for hydrazone linkages (a) condensation between hydrazine and ketone/aldehyde (b) the Japp-Klingemann reaction and (c) substitution of aryl halide with non-substituted hydrazones [7].

I.3. Mechanism of formation

Hydrazones are formed from the condensation of hydrazine (**A**) and a carbonyl compound (aldehyde or ketone) (**B**) with water being the sole byproduct. The reaction starts by a proton-catalyzed attack of the nucleophile on the carbonyl carbon atom of electrophile. Upon proton transfer, tetrahedral intermediate (**C**) was formed. This intermediate can undergo dehydration

via protonation of the hydroxyl function and subsequent elimination of water. The resulting protonated intermediate is represented by two resonance forms (**D**/**E**). The final deprotonation yields hydrazone [1] (**Figure 2**).

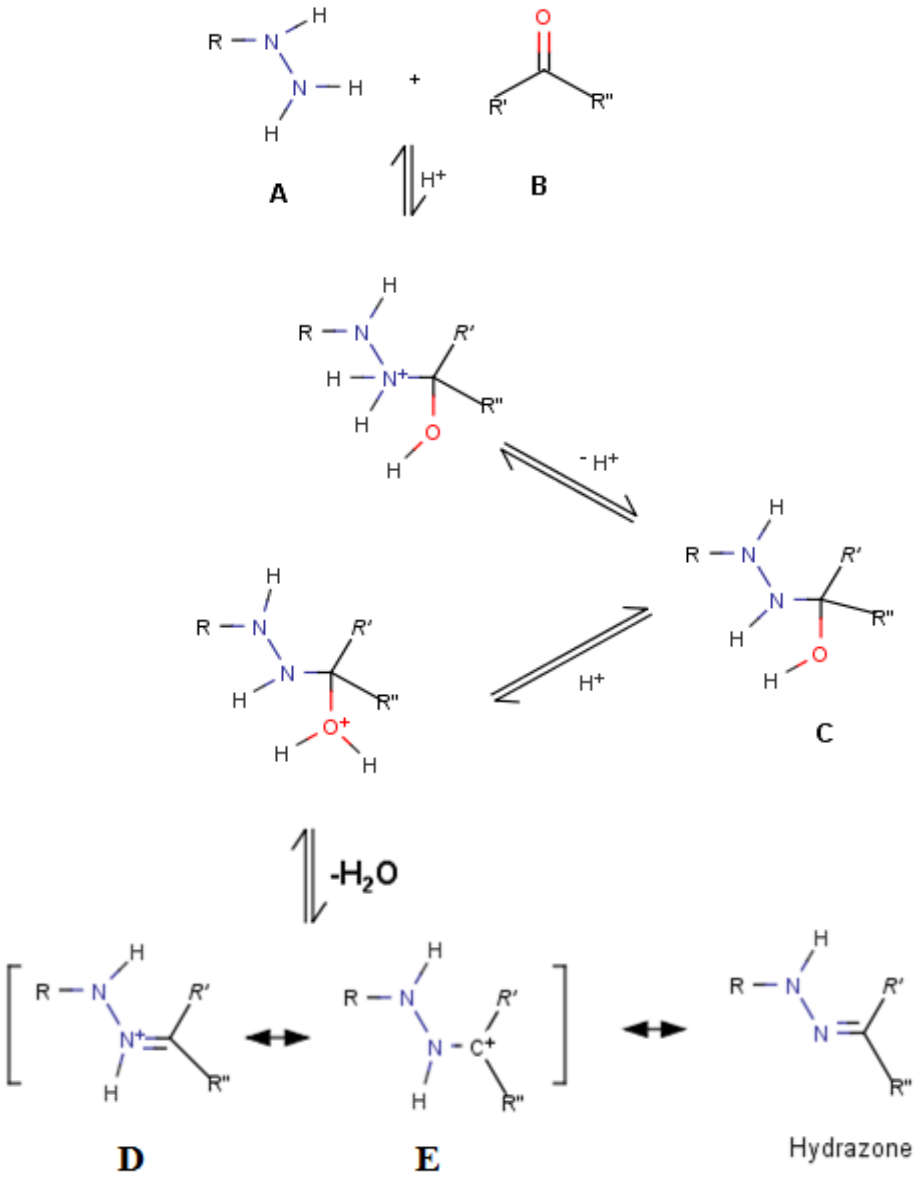

Figure 2. Standard Mechanism of hydrazones formation [1]

I.4. Biosynthetic hydrazones

Hydrazones are widely present in nature [8], which could be biosynthesized by bacteria, fungi, plants, and marine organisms, and can be isolated by different ways such as solvent extraction and fermentation. **Table1** summarizes various natural hydrazones and their sources.

Table 1. Origin, chemical structures, and names of natural hydrazones

Origin	Chemical structure	Name/ Date of isolation
Bacteria [9] *Streptomyces sp*. IFM 11299	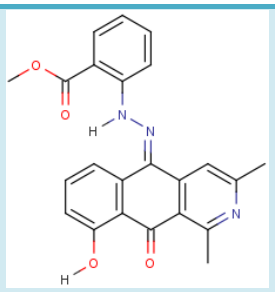	Katorazone (2012)
Fungi [10] *Penicillium minioluteum* F-4627	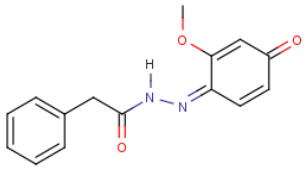	NG-061 (1999)
Plants [9] Thai plant *Wedelia biflora*	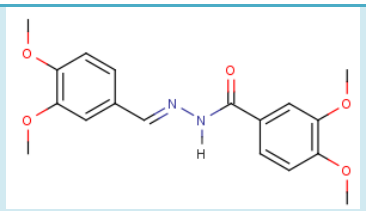	Veratrylidenehydrazide (1993)
Marine organisms Sponge [9] *Pseudoceratina purpurea*	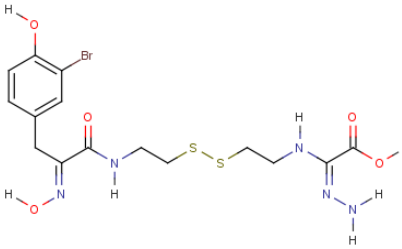	Psammaplin G (2003)

I.5. Semi-synthetic of hydrazones

The semi-synthesis of hydrazones was demonstrated by the administration of the antitubercular drug isoniazid (**INH)** by healthy human. Analysis of urine indicates the formation of hydrazones, which resulted from **INH** conjugation with endogen substances (amino acids) or theirs metabolites such as leucine and/or isoleucine, lysine, tyrosine, tryptophan, and phenylalanine. **Figure 3,** summarizes various hydrazones(**1-10**) formed by **INH** conjugation with various metabolites; 3-(1*H*-indol-3-yl)-2-oxopropanoic acid, 2-oxo-3-phenylpropanoic acid, 3-(4-hydroxyphenyl)-2-oxopropanoic acid, 2-oxohexanedioic acid, 4-methyl-2-oxopentanoic acid, 3-methyl-2-oxopentanoic acid, α-ketoglutaric acid, glycine, and glucose and 5-hydroxy-4-(hydroxymethyl)-6-methylpyridine-3-carbaldehyde [11].

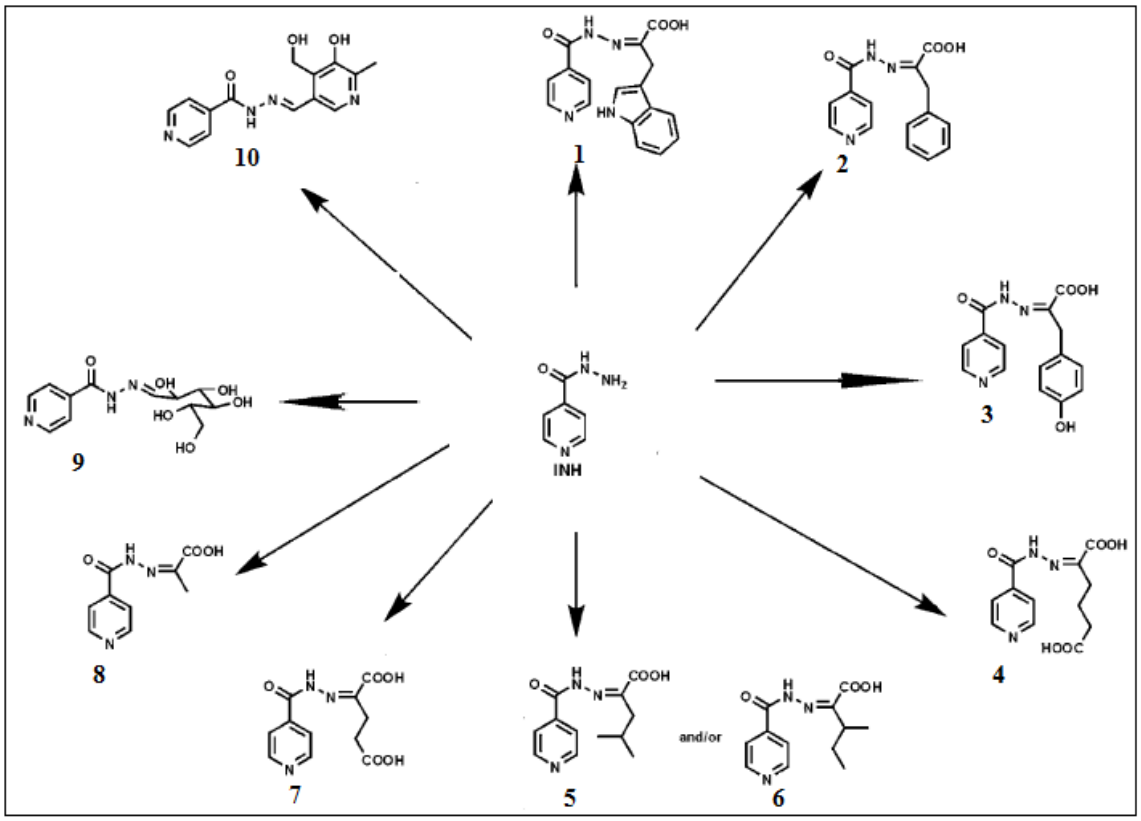

Figure 3. Semi-synthesis of hydrazones [11].

I.6. Reactivity of hydrazones

Hydrazones contain two connected nitrogen atoms of different nature and a carbon- nitrogen double bond that is conjugated with a lone electron pair of the terminal nitrogen atom. These structural fragments are mainly responsible for the physical and chemical properties of hydrazones. Both nitrogen atoms of the hydrazone group are nucleophilic, although the amino- type nitrogen is more reactive. The carbon atom of hydrazone group has both electrophilic and nucleophilic characters [12]. Shown in **Figure 4** are the active centers of N-monosubstitutedhydrazones (**A**), N,N-dialkylhydrazones (**B**), and N-acyl hydrazones **(C).**

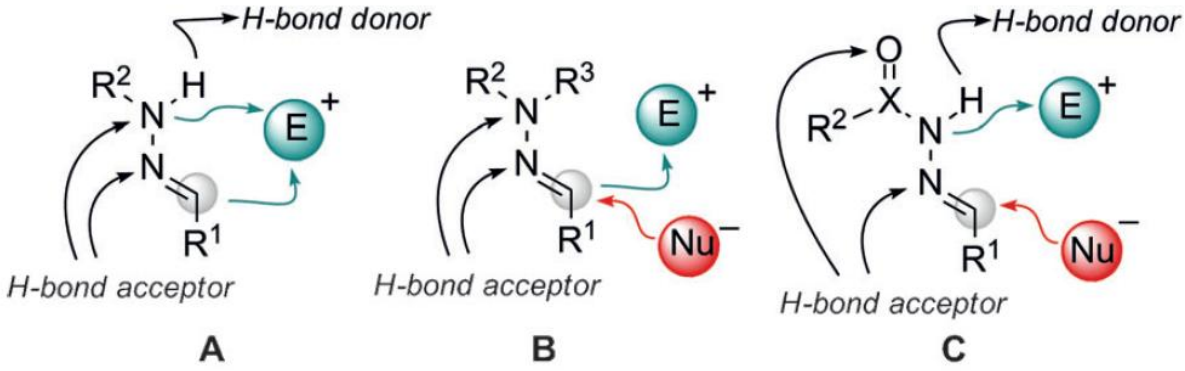

Figure 4. Active centers of hydrazones [12].

Hydrazones display diverse reactivity, taking part in reactions with nucleophiles, electrophiles, and other chemical reagents. Being a bidentate nucleophiles, hydrazones react with electrophilic reagents with participation of either nitrogen atom (compounds **1, 2**), or the carbon atom of the azomethine group (compounds **3**). Strong bases deprotonate hydrazones to form anions of types **4** and **5**, whereas nucleophiles attack the azomethine carbon atom to form products of both addition **6, 7** and substitution **8**. Furthermore, hydrazones can be reduced to amines **9** or oxidized to diazo compounds **10** [13] (**Figure 5**).

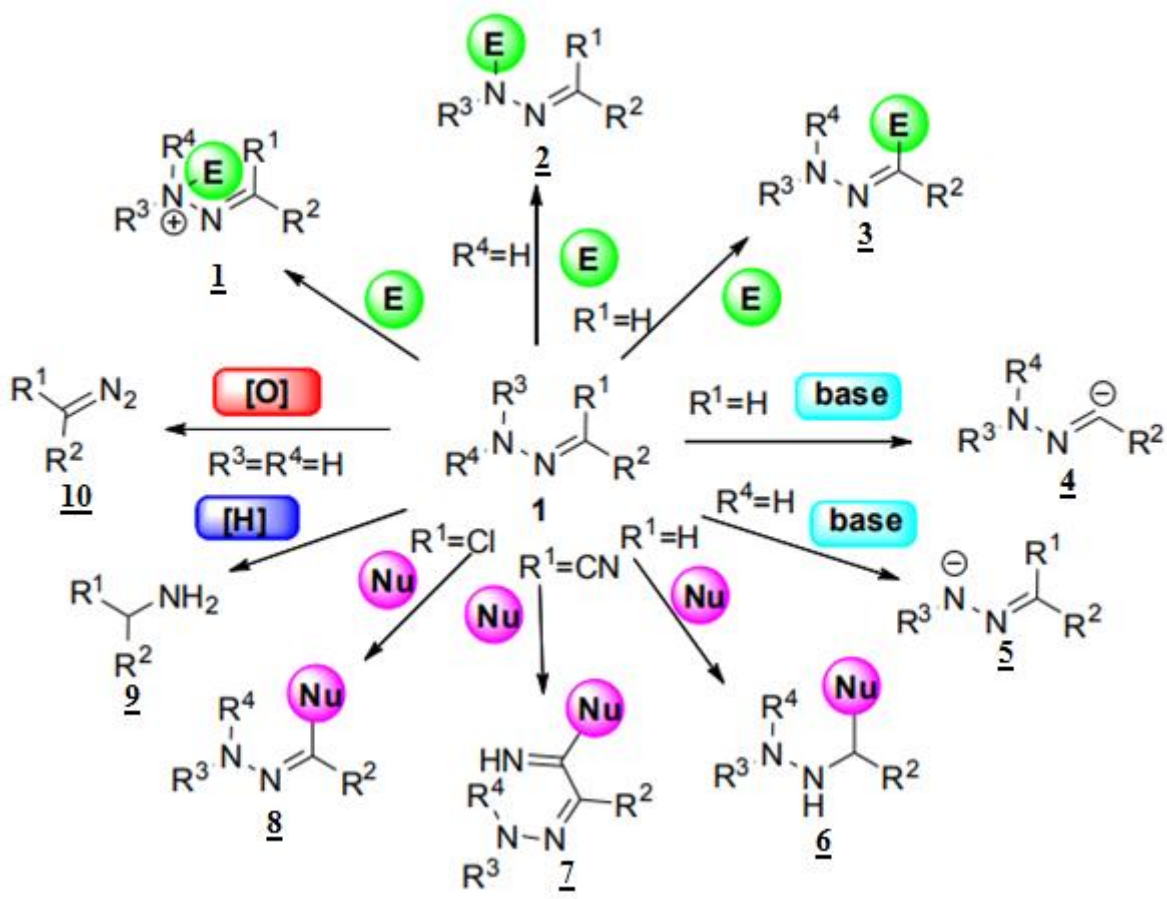

Figure 5. Reactions of hydrazones with different types of reagents [13].

I.7. Heterocyclization of hydrazide-hydrazones

Hydrazide-hydrazones are very effective organic compounds. Several researchers reported on the synthesis of heterocyclic compounds from these compounds. Rollas et al. [14] prepared four substituted 1,3,4-oxadiazolines from 4-fluorobenzoic acid (substituted methylene) hydrazides and acetic anhydride. In addition, Thomas et al. [15] synthesized a series of 2-azetidinones from the reaction of N'-[(1Z)-(substituted aromatic) methylidene]pyridine-4-carbohydrazides and chloroacetylchloride, bynovel methods; microwave irradiation and stirring/sonication. Furthermore, Patel et al. [16] prepared a series of 4-thiazolidinones from

the cyclocondensation of hydrazide-hydrazones with thioglycolic acid in dry 1,4-dioxane. These reactions are shown in **Figure 6**.

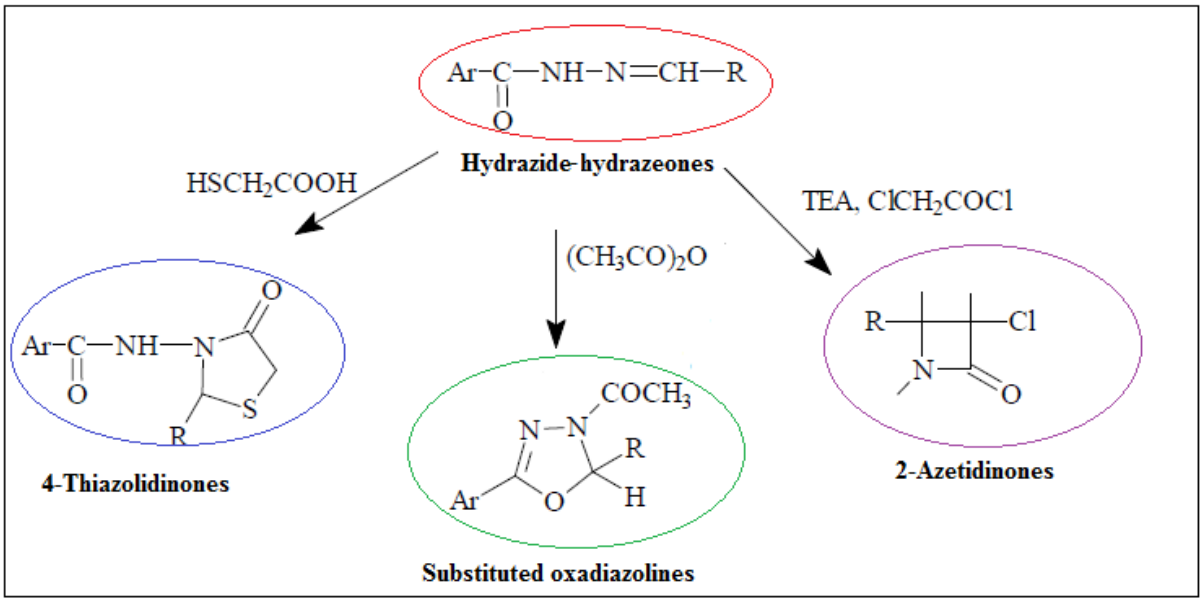

Figure 6. Heterocyclic compounds formed from hydrazide-hydrazones.

I.8. Biological activity of hydrazones

Hydrazones are a bioactive compounds with clinical and pharmacological proprieties. Nifuroxazide is an oral nitrofuran antibiotic used in anti-dehydration and colitis treatment. It neutralizes microbacterials in diarrhea, and has "a spectrum which covers most enteropathogenic microbacterials, *Shigella, Escherichia coli, Salmonella, Staphylococci, Klebsiella,* and *Yersinia* (**Figure 7**) [17].



Figure 7. Structure of nifuroxazide [17].

I.8.1. Anti-mycobacterial activity

Due to the increasing number of drug resistant *Mycobacterium tuberculosis* strains, there is an urgent need for new anti-tubercular drugs, capable of overcoming the resistance mechanisms. Along this line, some new 3,4-disubstituted thiazolylidene-isonicotino hydrazide derivatives were synthesized and tested *in vitro* against *Mycobacterium tuberculosis* H37Ra 7131 strains. Among the potential compounds, N'-(4-(4-chlorophenyl)-3-phenylthiazol-2(3H)-ylidene) isonicotinohydrazide (**1**), which exhibited MIC value of 1.99 µg/mL [18]. In addition, hydrazone derived from thriazol-1-yl ethoxy phenyl, compound (**2**), has a potential anti-tubercular effect with MIC values ranging from 0.09 to 0.19 µg/mL (**Figure 8**) [19].

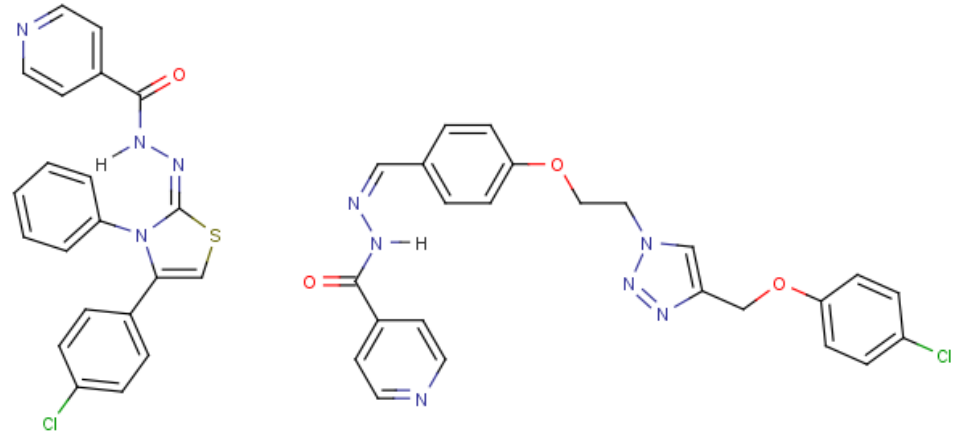

Figure 8. Structures of thiazolylidene-isonicotino hydrazide derivatives [18][19].

I.8.2. Anticancer activity

Structure-activity relationship (SAR) study of thirty-two isoniazid derivatives, demonstrated that the presence of a hydroxyl group on the aromatic ring, especially the *ortho*-position, plays an important role in the anticancer activity against human cancer cell lines: OVCAR-8 (ovary), SF-295 (glioblastoma), HCT-116 (colon), and HL-60 (leukemia). Shown in **Figure 9** are the structures of three compounds that exhibited good cytotoxic activity when compared to the reference drug doxorubicin; these compounds are considered new anticancer agents [20].

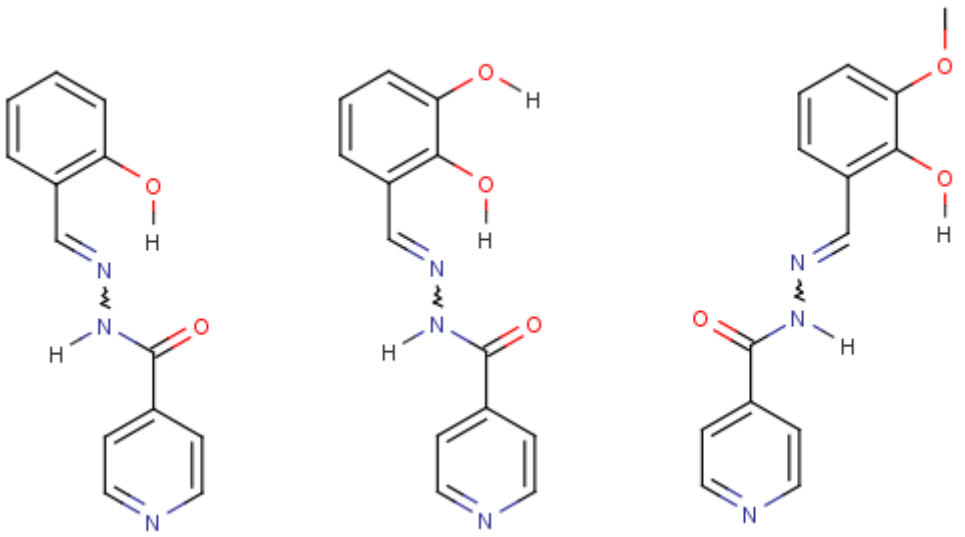

Figure 9. Structure of anticancer, monohydroxylated, dihydroxylated, and methoxylated hydrazones [20].

I.8.3. Leishmanicidal activity

Hydrazones and their thiosemicarbazone derivatives displayed antileishmanial effects. For this, **INH**-derivatives hydrazones (**HPAmIH** and **HPCIH**) were prepared and tested against intracellular amastigote form of *Leishmania (Viannia) braziliensis* strains and exhibited leishmanicidal effects (**Figure 10**) [21].

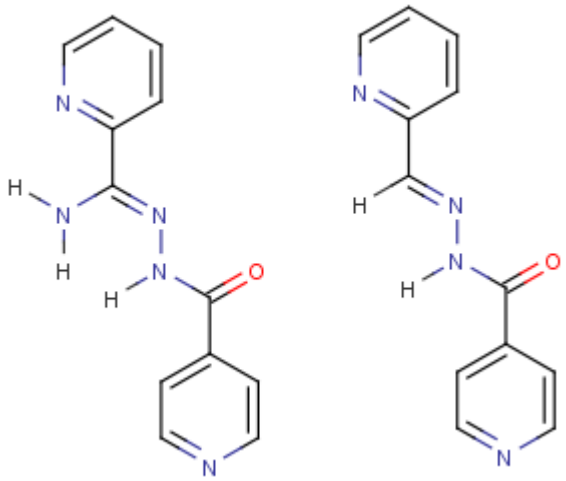

Figure 10. Structure of leishmanicidal hydrazones (**HPAmIH** and **HPCIH)** [21].

I.8.4. Antibacterial activity

Malhotra et al. [22] prepared a series of hydrazones by condensation of 2-ethoxybenzaldehyde with isoniazid. Aminomethylation of these hydrazones with formaldehyde and substituted secondary amines formed the new hydrazones, which were tested for their antimicrobial

activity. Results revealed that the compounds **3**, **4**, and **5** showed excellent effects against bacterial strains, such as *Bacillus subtilis*, *Staphylococcus aureus*, *Pseudomonas aeruginosa*, and *Escherichia coli* (**Figure 11**).

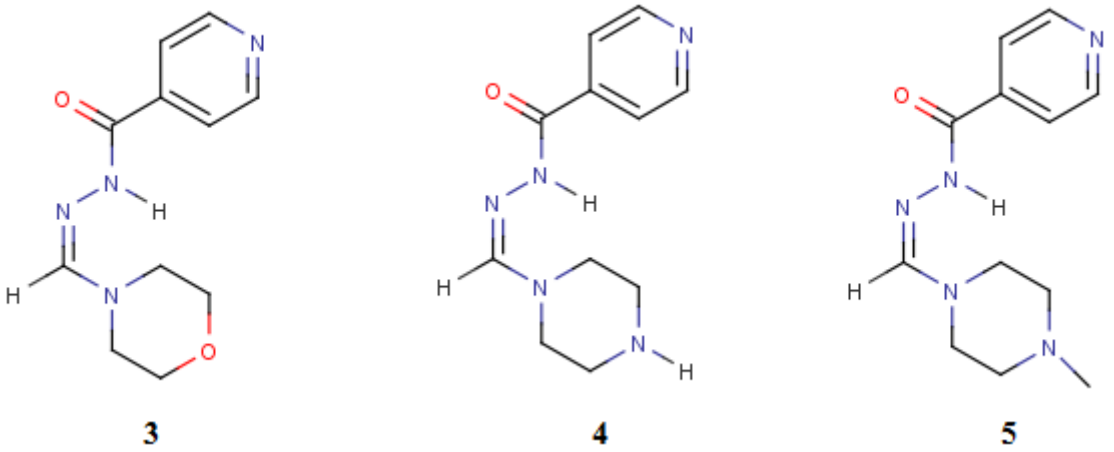

Figure 11. Structure of antibacterial hydrazones **3**, **4**, and **5** [22].

I.8.5. Antifungal activity

Cordeiro et al. [23] synthesized a series of hydrazones derived from **INH** and evaluated their antifungal activity against *Coccidioides posadasii*. Three compounds of the series, N'-[(E)-1-(4-methoxyphenyl)ethylidene]pyridine-4-carbohydrazide (**A**), N'-[(E)-1-(4-methylphenyl) ethylidene]pyridine-4-carbohydrazide (**B**), and N'-[(E)-1-(phenyl)ethylidene]pyridine-4-carbohydrazide (**C**) exhibited significant antifungal activity (**Figure 12**).

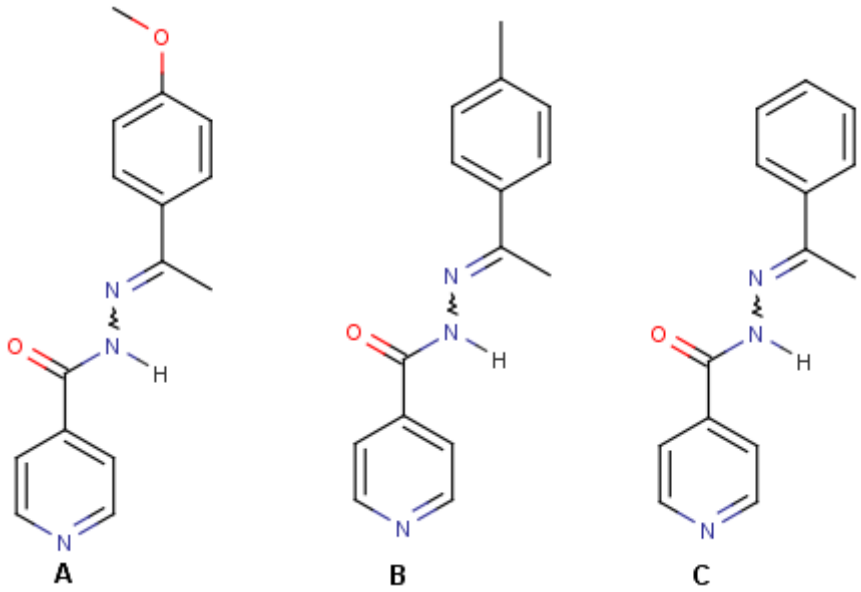

Figure 12. Structure of antifungal hydrazones (**A**, **B**, and **C**) [23].

Chapter II: Overview of Isoniazid and its hepatotoxicity

II. Hepatotoxicity

II.1. Liver

The liver is the largest solid organ in the body, weighing about 1.5 kg in an adult. It lies in the right upper quadrant of the abdomen completely protected by the thoracic rib cage (**Figure13**). The liver is connected to two large blood vessels, one called hepatic artery and the other the portal vein. The hepatic artery carries blood from the aorta whereas the portal vein carries blood containing digested food from the small intestine. The basic functional unit of the liver is the liver lobule; the human liver contains 50,000 to 100,000 individual lobules [24]

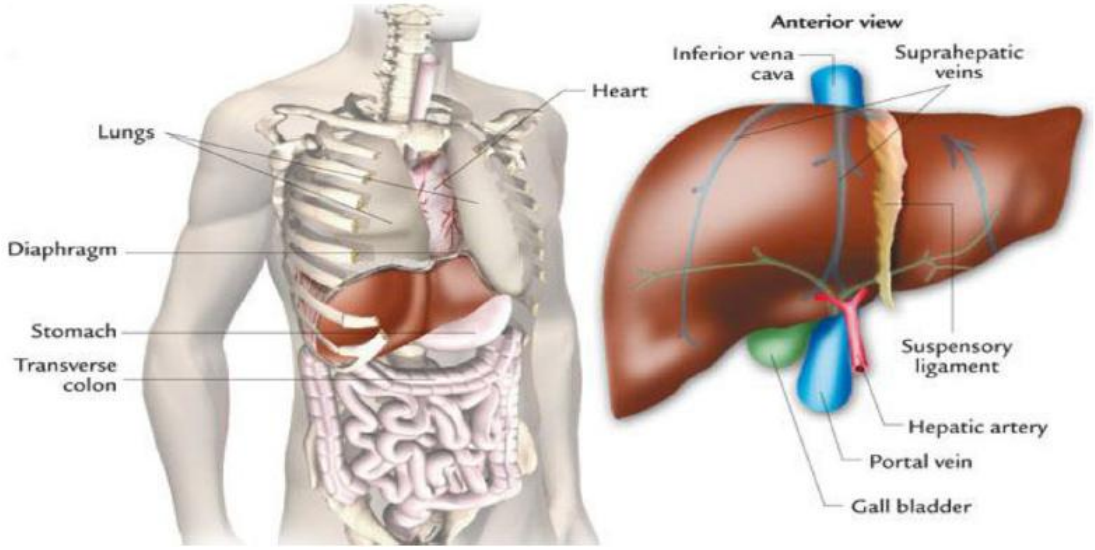

Figure 13. The liver [25]

The liver plays the central role in the body, which is the center for drug and xenobiotic metabolism [26] where phase 1 and phase 2 enzymes play the fundamental roles. Phase 1 reaction involves oxidation, reduction, hydrolysis, hydration and many other rare chemical reactions. These processes tend to increase water solubility of the drug and can generate metabolites that are more chemically active and potentially toxic. Most of phase 2 reactions take place in cytosol and involve conjugation with endogenous compounds *via* transferase enzymes. In addition, cytochrome P-450 is the most important family of metabolizing enzymes in the liver; six of them metabolize 90% of drugs [27].

II.2. Drug induced liver injury (DILI)

DILI or hepatotoxicity can be defined as liver injury caused by drugs used either in medical practice or herbal medicines resulting in persistent significant elevations in liver enzyme levels, abnormalities in liver test or liver dysfunction [28].

According to statistics, more than a thousand medicines and chemicals have been reported to cause liver injury [29]. Drug-induced liver injury is a relatively common cause of acute liver disease and carries a mortality of around 10% [30].

II.2.1. Types of DILI

Alkaline phosphatase (ALP), alanine transaminase (ALT), and aspartate transaminase (AST) are the useful biochemical markers in the evaluation and detection of DILI. DILI was classified by R value, (R= ALT/ALP) as hepatocellular, cholestatic, or mixed type injury [31] (**Table 2**).

Table 2. Types of DILI

Types of DILI	Definition	R value
Hepatocellular injury	Associated with the elevation of ALT	≥5
Cholestatic injury	Linked to an increase in ALP level	≤ 2
Mixed pattern of liver injury	Manifested when both ALT and ALP are elevated	2 < R < 5

II.2.2. Mechanism of DILI

Drugs and their metabolites may affect the hepatocytes in three steps [32]; for all mechanisms (**Figure14**), mitochondria play a central role in events leading to apoptotic vs. necrotic cell death.

II.2.2.1. First step, Initial injury is exerted through direct cell stress, direct mitochondrial inhibition and/or specific immune reactions:

- **Direct cell stress**

- Depletion of glutathione (GSH), or binding to enzymes, lipids, nucleic acids
- Disruption of bile excretion caused toxic bile acid accumulation

- **Direct mitochondrial inhibition**

Reactive metabolites or parent drugs inhibit the mitochondrial respiratory chain causing ATP depletion and increased concentrations of reactive oxygen species (ROS).

- **Specific immune reactions**

- Direct cytotoxic T cell by innate immune response
- Antibody-mediated cytotoxic response

II.2.2.2. Second step, Initial injury can lead to mitochondrial permeability transition (MPT).

Direct cell stress causes MPT *via* the intrinsic pathway. The intrinsic pathway involves activation of intracellular stressor cascades and pro-apoptotic proteins including Bax. MPT can be initiated through the death receptor-mediated extrinsic pathway that is activated by immune reactions and/or after sensitization to TNF and FasL binding to death receptors. Cytokines modulate the sensitivity of its activation.

II.2.2.3. Third step, MPT leads to necrosis or apoptosis depending on the availability of ATP.

In hepatocytes activation of initiator caspase 8 through the extrinsic pathway is not sufficient to directly activate apoptosis, but amplification through pro-apoptotic factors including Bid and ceramides lead to MPT, which will then lead to the apoptotic pathway that is activated in the presence of sufficient remaining ATP production. Necrosis occurs if there is no ATP available, which is required for energy-consuming apoptotic pathways.

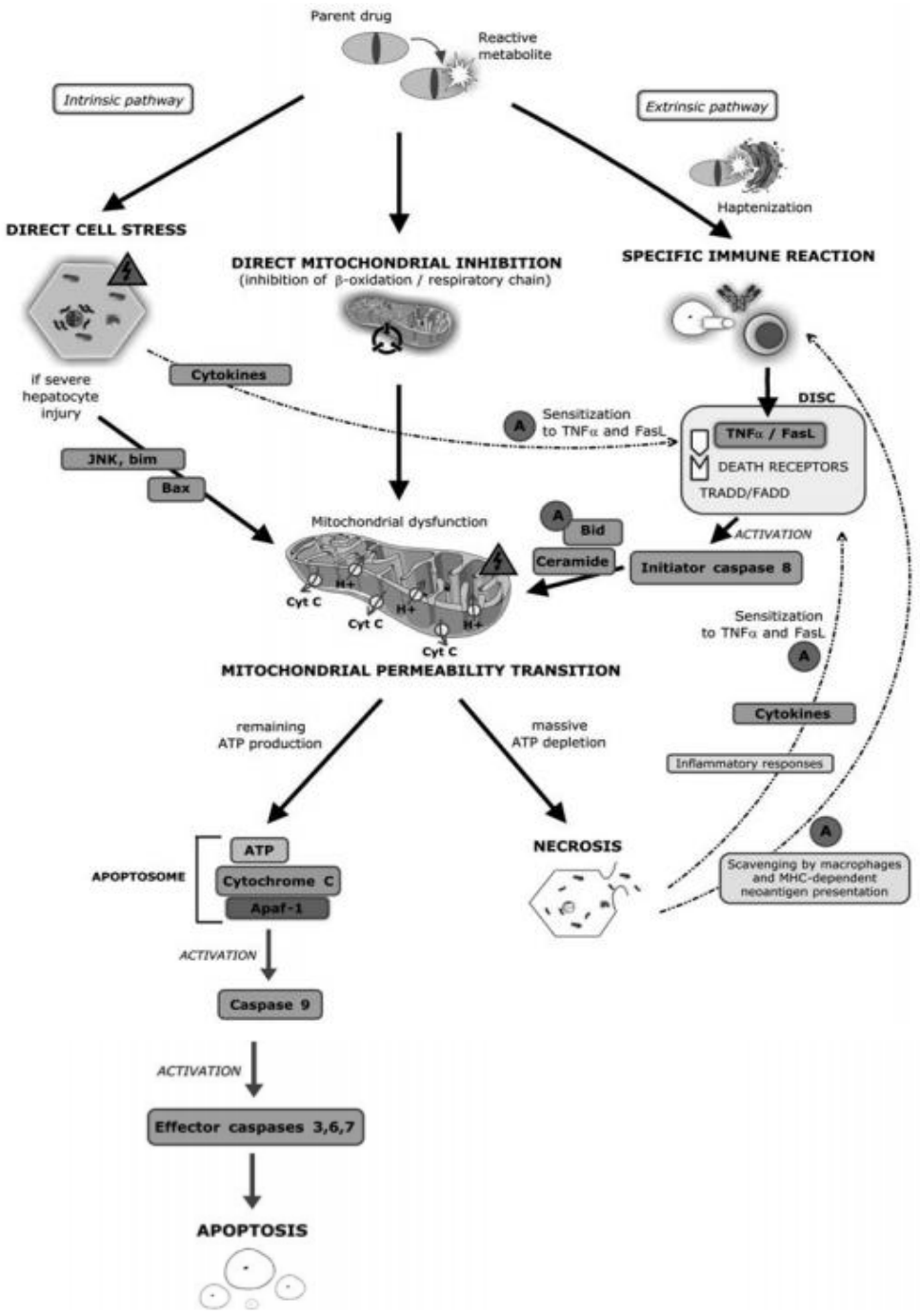

Figure 14. Mechanisms of DILI [32].

II.2.3. Factors affecting DILI

Several factors affect the heptotoxic effects of drugs, which enhance a person's susceptibility to a potentially hepatotoxic drug such as advancing age, gender, lifestyle factors, obesity, nutritional status, genetic background, dose, and duration of drugs may affect the risk of drug-mediated hepatotoxic reactions [33] (**Figure15**).

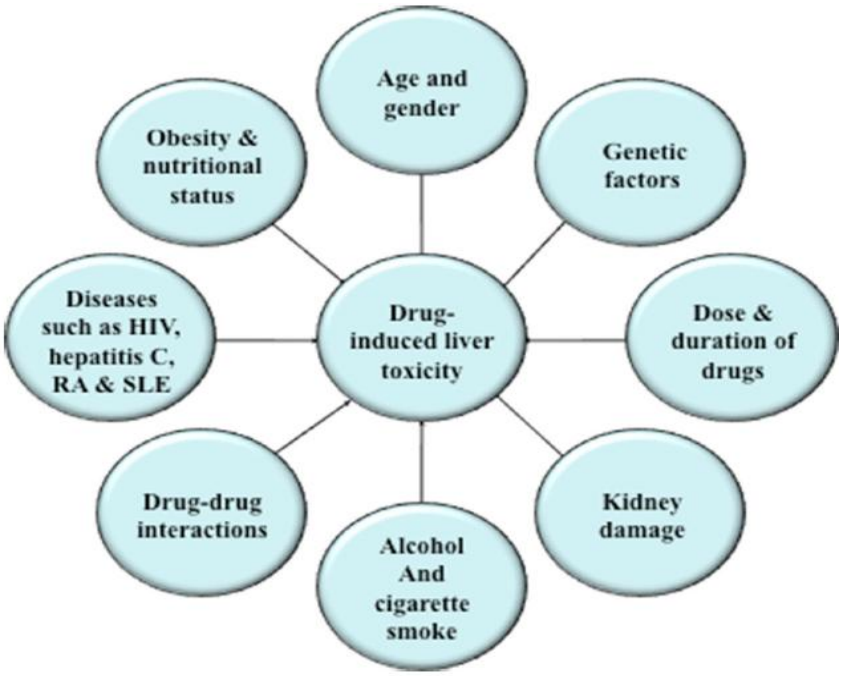

Figure 15. Factors affecting drug-induced hepatotoxicity [33].

II.2. Isoniazid induced oxidative stress and hepatotoxicity

II.2.1. Isoniazid proprieties

Isoniazid (**INH**), chemically known as isonicotinic acid hydrazide, is a low-molecular weight and water-soluble compound that can be rapidly absorbed from the gastrointestinal tract. **INH** has been a first-line drug for the treatment of tuberculosis for more than 50 years, with maximum doses for adult of 300 mg (**Figure 16**).



Figure 16. Structure of the anti-tubercular drug (isoniazid)

It inhibits bacterial cell wall synthesis, thus killing *Mycobacterium tuberculosis* organisms (**Figure 17**). Due to its low efficacy towards resistant tuberculosis, it is generally used in combination with other anti-tubercular drugs such as pyrazinamide, ethambutol, and/or rifampicin [34].

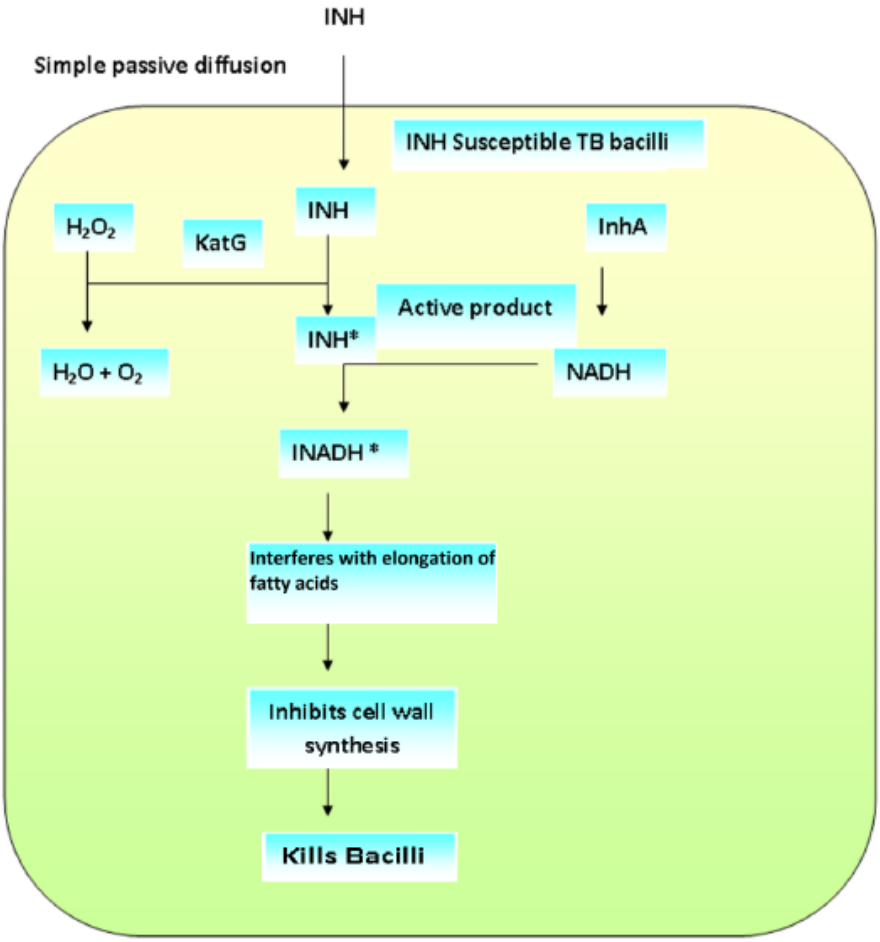

Figure 17. Mechanism of action of **INH** on susceptible bacilli [35].

II.2.2. Isoniazid-induced oxidative stress

Oxidative stress describes various harmful processes resulting from an imbalance between the formation of free radicals and limited antioxidant defenses [36]. Drug-induced oxidative stress is implicated as a mechanism of toxicity in numerous tissues and organ systems, including liver, kidney, ear, cardiovascular and nervous systems [37].

Three principal proposed mechanisms for the oxidative stress induced by **INH** (**Figure 18**);

1. Immune cell products (H_2O_2 and peroxidase) activate **INH** to pro-oxidant hydrazyl, inducing oxidative stress [38].
2. The damage of lysosomal membrane causes ROS formation *via* Fenton reaction, which induces oxidative stress and cytotoxicity
3. The oxidation of **INH** leads to the formation of nitric oxide radical, causing oxidative stress [39,40].

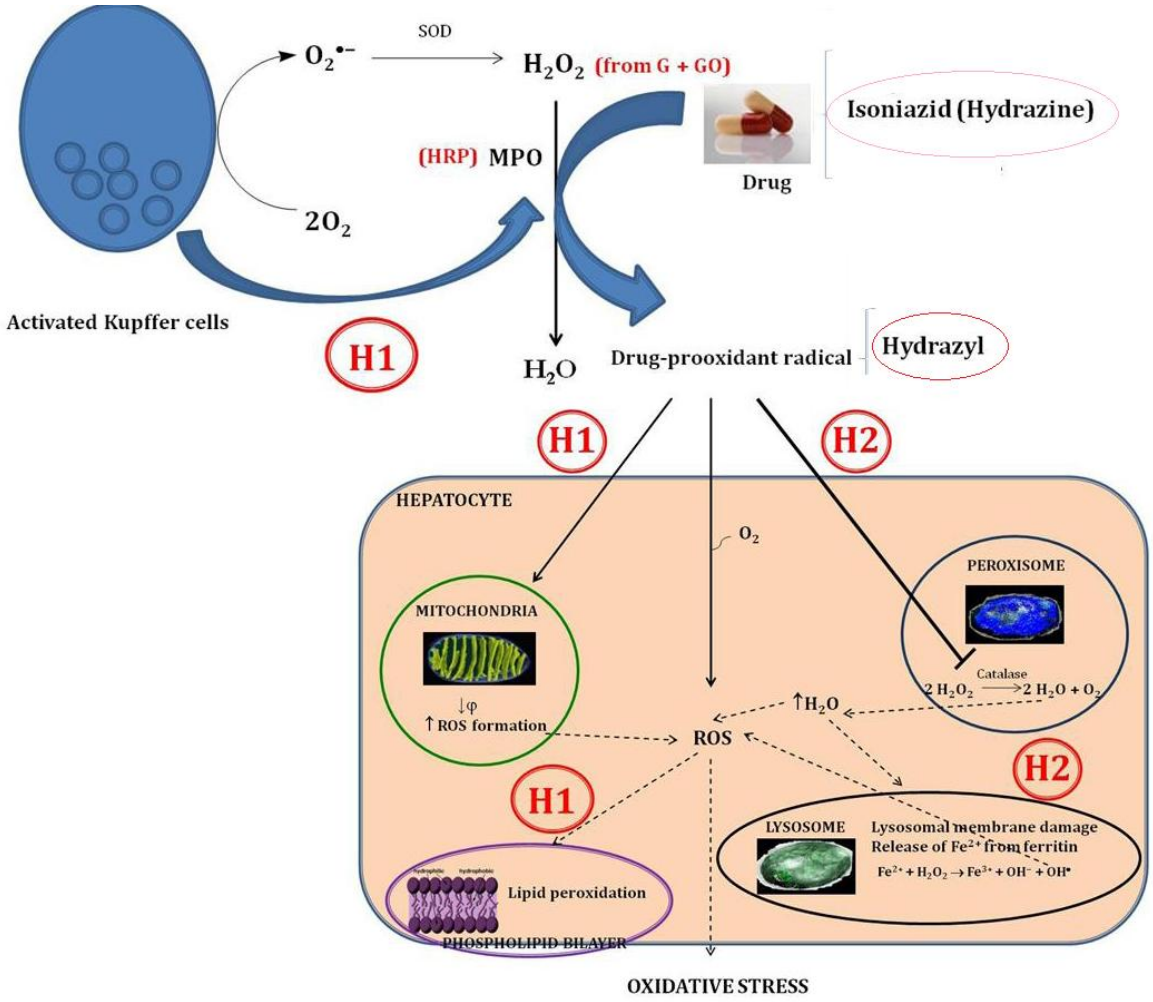

Figure 18. Isoniazid-induced oxidative stress in hepatocyte cell [38]

II.2.3. Isoniazid-induced hepatotoxicity

II.2.3.1. Isoniazid metabolism

INH is primarily cleared through acetylation by N-acetyltransferase 2 (NAT2) in the liver, resulting in acetylisonazid which is then hydrolyzed to isonicotinic acid and monoacetylhydrazine (MAH). **INH** also undergoes hydrolysis catalyzed by isoniazid hydrolase and forms hydrazine, which is then metabolized to MAH by NAT2. MAH can be acetylated to diacetylhydrazine which is non-toxic, or oxidized by cytochrome P4502E1 (CYP2E1) into hepatotoxic intermediates. Acetylhydrazine can be hydrolyzed to hydrazine which may further induce CYP2E1, increasing the production of toxic metabolites. Hydrazine, MAH, and isonicotinic acid are potentially hepatotoxic metabolites of **INH** and accumulation of these reactive metabolites in patients may cause serious adverse drug reactions (**Figure 19**) [41].

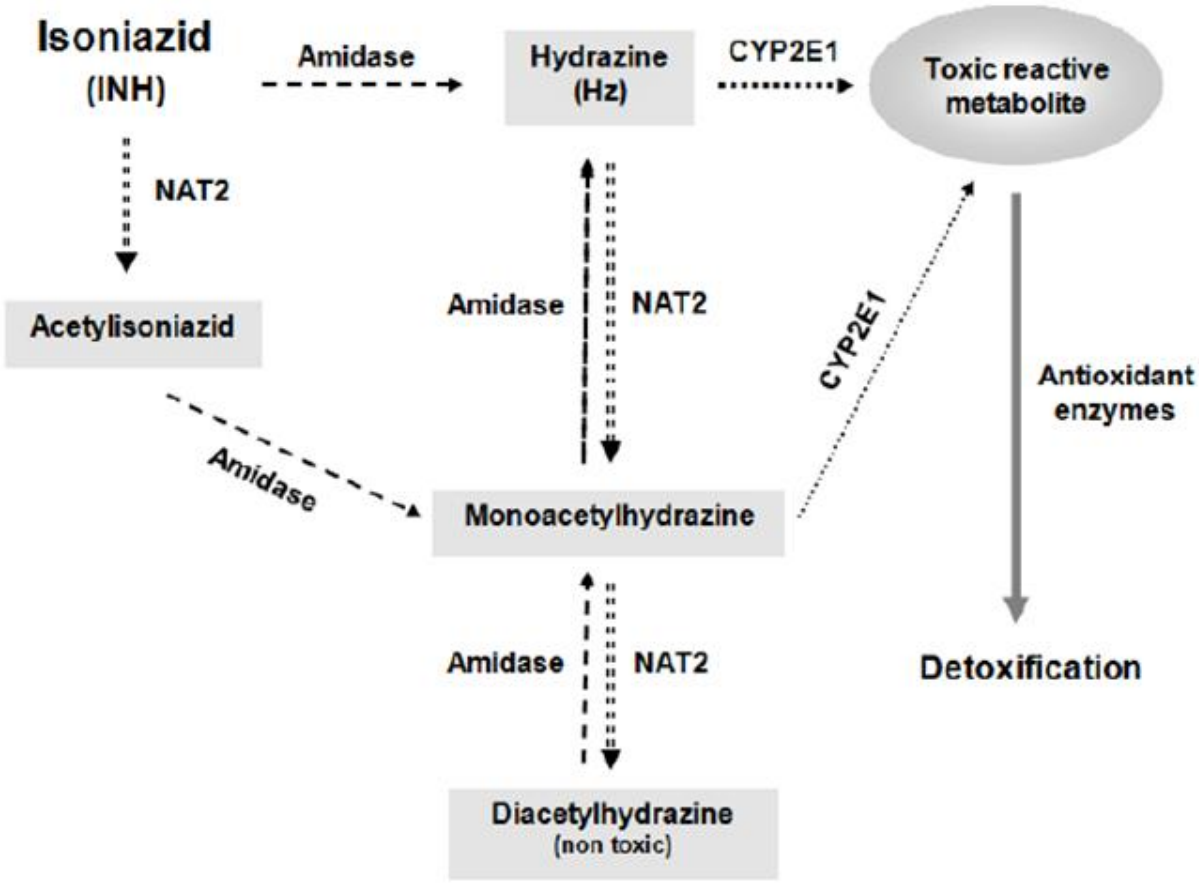

Figure 19. Isoniazid metabolic pathways [41].

II.2.3.2. Mechanisms of INH-hepatotoxicity

Recently, a number of *in vitro* and in *vivo* models have been used to investigate the possible mechanisms of **INH**-related hepatotoxicity. Among these are three principle mechanisms were reported:

1. Direct oxidation of **INH** to reactive metabolite (Diazohydroxide), which reacts with primary amine of proteins forming amide function, and causing hepatic necrosis and autoimmunity (**Figure 20**) [42].
2. **INH**-metabolites from **INH** hydrolysis, **INH**-enzymatic oxidation, **INH**-acylation, -**INH**-acetylation covalent binding to proteins leading to hepatotoxic effect (**Figure 21**) [43].
3. **INH** induced oxidative stress and decreased nuclear Nrf2 protein by the inhibition of Nrf2 translocation into the nucleus (inhibits transcription of cytoprotective genes) caused hepatocytes defenseless to oxidative stress, which lead to the apoptosis (**Figure 22**) [44].

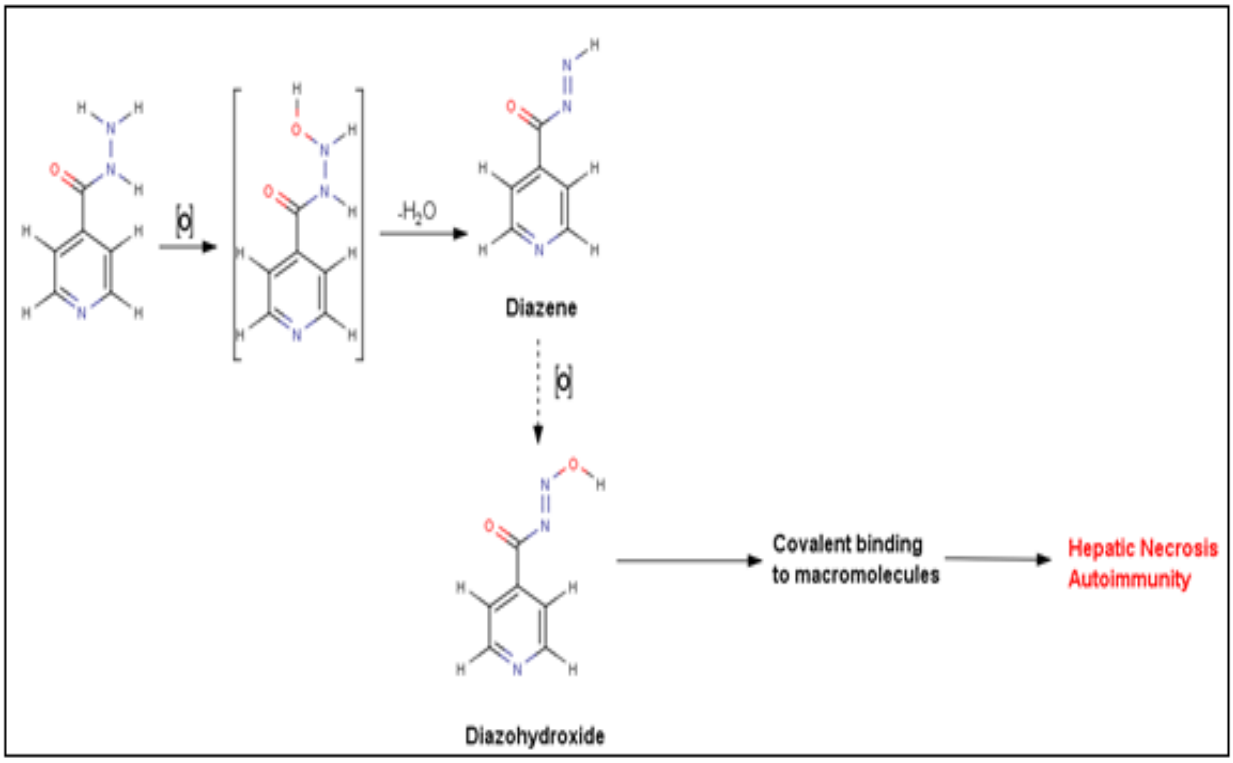

Figure 20. Direct oxidation of **INH** and covalent binding with macromolecules [42]

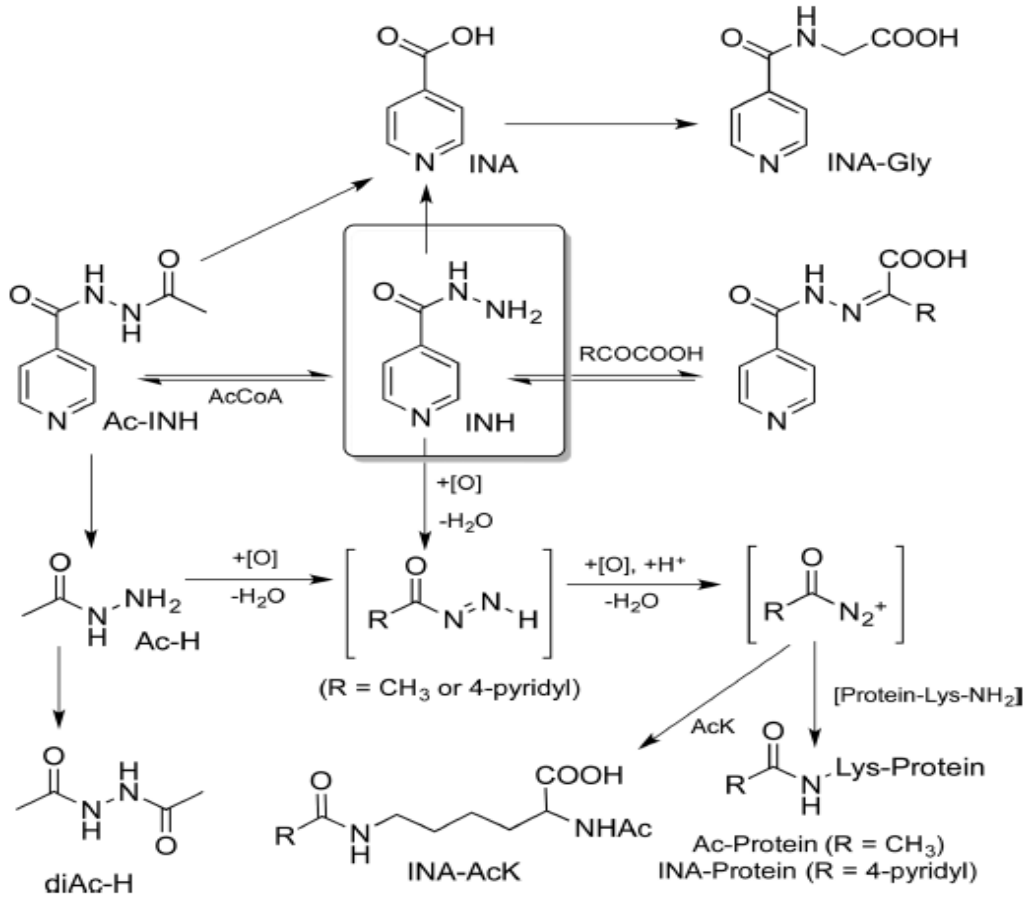

Figure 21. Biotransformation and bioactivation of **INH** [43].

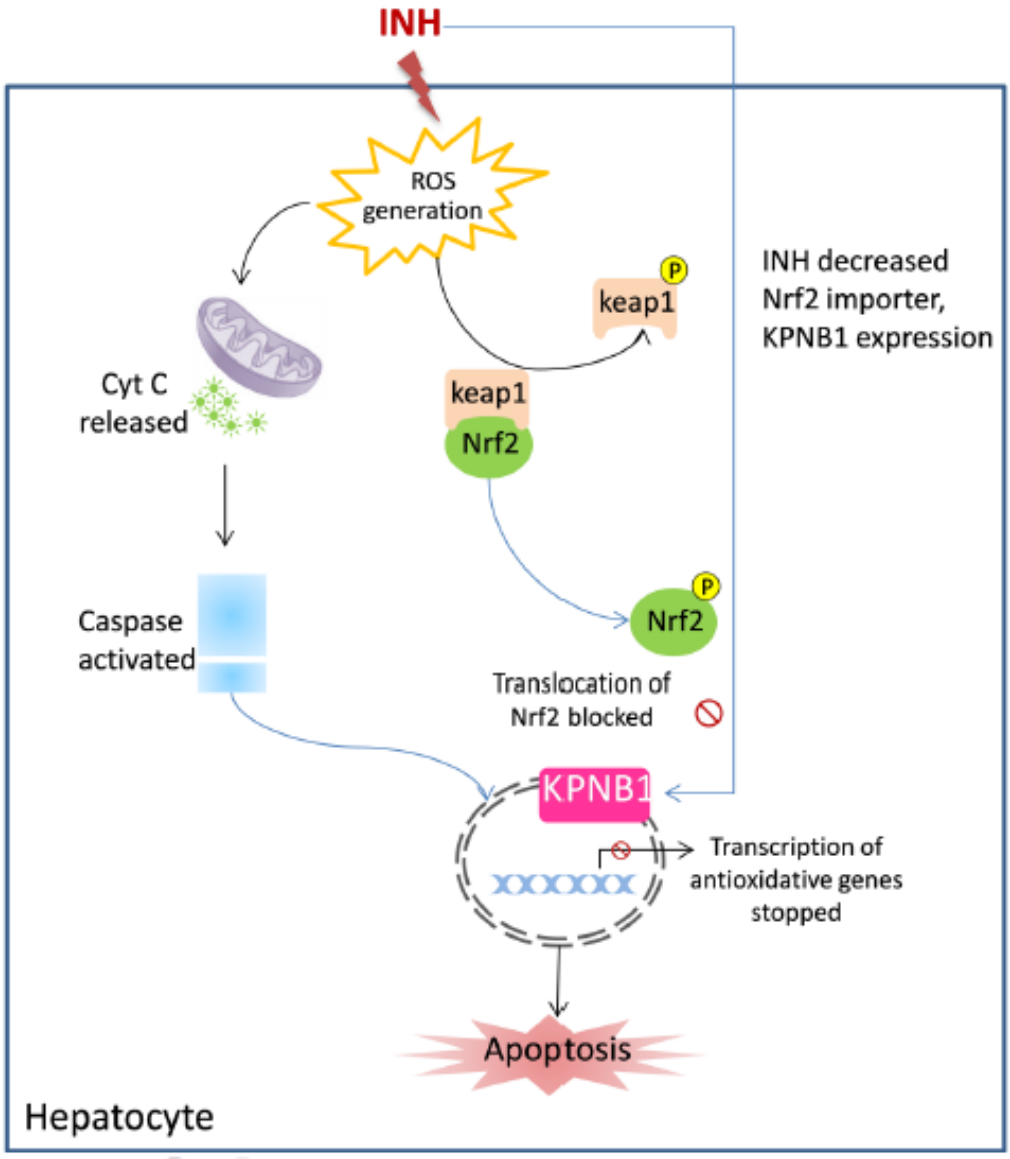

Figure 22. **INH**-induced oxidative stress and apoptosis in hepatocyte [44]

Chapter III: Materials and Methods

III.1. Computational methods

III.1.1. DFT study

Density functional theory (DFT) was employed for molecular analysis and calculations using Becke's three parameters hybrid exchange functional with Lee-Yang-Parr correlation functional (B3LYP) [45]. Quantum chemical calculations were performed using the Gaussian 09 program [46], where the following parameters: ionization potential (IP), electron affinities (EA) [47], electronegativity (χ), chemical potential (μ) [48], global hardness (η) [49], global softness (σ), and electrophilicity index (ω) [50] were calculated by using the following equations [51]:

$$IP = - E_{HOMO} \quad (1)$$

$$EA = -E_{LUMO} \quad (2)$$

$$\eta = E_{LUMO} - E_{HOMO} \quad (3)$$

$$\sigma = 1 / \eta \quad (4)$$

$$\chi = - (E_{HOMO} - E_{LUMO}) / 2 \quad (5)$$

$$\mu = (E_{HOMO} - E_{LUMO}) / 2 \quad (6)$$

$$\omega = \mu^2 / 2\eta \quad (7)$$

III.1.2. Physicochemical proprieties calculation

Each of the following parameters has been computed using the package MARVIN [52]: Partial atomic charge, protonation/deprotonation forms, lipophilicity descriptors, and topological surface area (TPSA).

III.1.3. Toxicity and bioactivity predictions

The online software programs used for toxicological and biological studies are summarized in the following **Table 3.**

Table 3. Online software programs for toxicity and bioactivity prediction of **INH**, **Hyd1** and **Hyd2**

Online software programs	**Toxicity/ Bioactivity prediction**
e-MolTOX [53] (http://xundrug.cn/moltox)	Toxic substructure predictions
ProToxII [54] (http://tox.charite.de/protox II)	Carcinogenicity, Hepatotoxicity, Mutagenicity, Immunotoxicity, and Cytotoxicity
Predskin [55] (http:// labmol.com.br/predskin/)	Skin sensitization
Pass online tool [56] (http://cactus.nci.nih.gov/ncidb2/)	Anti-tubercular activity

III.1.4. Biodegradability prediction

We employed the University of Minnesota Biocatalysis/Biodegradation Database (UM-BBD, http://umbbd.msi.umn.edu/) to predict microbial biocatalytic reactions and biodegradation pathways of synthesized compound [57].

III. 2. Experimental methods

III.2.1. Reagents

All chemicals and reagents used throughout this study were obtained from commercial sources and used without further purification; Isoniazid (BHD chemicals Ltd Poole England), 4-chloro-3-nitrobenzaldehyde 97% (Aldrich), nicotinamide (Sigma),6-bromoindoline-2,3-dione (Wako), indomethacin, nitroblue tetrazolium, ascorbic acid, and butylated hydroxy toluene (Sigma).

III.2.2. Equipments

III.2.2.1. Thin layer chromatography

Progress of reaction was monitored by thin layer chromatography (TLC), carried out on TLC sheets that were visualized under UV light.

III.2.2.2. Nuclear Magnetic Resonance (NMR)

^{1}H and^{13}C NMR spectra were recorded on a 500 MHz spectrometer (Bruker DPX-400, Germany) with TMS as internal standard and DMSO as a solvent. Chemical shifts are expressed in δ units whereas ^{1}H-^{1}H coupling constants (*J*-values) are given in Hertz.

III.2.2.3. High Resolution Mass Spectra (HRMS)

We acquired high resolution mass spectra (HRMS) by electrospray ionization (ESI) technique with the aid of a Bruker APEX IV mass spectrometer (Bremen, Germany). Samples were dissolved in acetonitrile, diluted in spray solution (methanol/ water 1:1 v/v þ 0.1% formic acid), and infused using a syringe pump with a flow rate of 2 mL/min. External calibration was conducted using arginine cluster in a mass range m/z 175-871.

III.2.2.4. Melting point (Mp°)

Melting point (uncorrected) was determined with a Stuart melting point apparatus.

III.2.2.5. Elemental analysis

Microanalyses (for C, H, and N) were conducted on a Euro Vector elemental analyzer, model EA 3000 (Milan, Italy), and results agreed with the calculated percentages to within the experimental error (±0.4%).

III.2.2.6. Fourier transform infrared (FT-IR) spectrum

Infrared spectra (IR) were obtained, as KBr disks, on a Schimadzu FTIR-8400S spectrophotometer.

III.2.2.7. Electronic absorption spectrum

The electronic absorption spectra in the 200–900 nm range were recorded on a UV-1800 Schimadzu UV–visible spectrophotometer

III.2.3. Animals

Experiments were performed using adult female *Swiss albino's* mice, weighing 20–30 g. They were obtained from Pasteur institut (Algeria) and housed in plastic cages under normal laboratory conditions (12 h light / dark cycle, 23 ± 2 °C) for an acclimatization period to the experiments. All animals were given food and water *ad libitum*.

III.2.4. Microbial strains and culture medium

Bacterial strains from the American Type Culture Collection (ATCC) were used in this study: *Lysteria monocytogenes* ATCC 15313, *Escherichia coli* ATCC 25922, *Bacillus cereus* ATCC 10876, *Pseudomonas aerogenose* ATCC 27553, *Staphylococcus aureus* ATCC 25923, *Klebsiella pneumonia* ATCC 700603. In addition, fungal strains; *Aspergillus flavus* NRRL 391 and *Aspergillus niger* 2CA 936 were used.

III.2.5. Synthesis

Both hydrazones were prepared according to a published procedure [58] using acetic acid as catalyst.

III.2.5.1. Synthesis of (N'-[(*E*)-(4-chloro-3-nitrophenyl)methylidene]pyridine-4-carbohydrazide (Hyd1)

Hyd1 was prepared according to the following procedure: An ethanolic solution (30 ml) of 4-chloro-3-nitrobenzaldehyde (0.9278 g, 0.005 mol) was added to 30 mL of isoniazid solution (0.6857 g, 0.005 mol) and a few drops of acetic acid were added with stirring, and the reaction mixture was refluxed for 3 h at 78 ºC (**Figure 23**). After cooling, the precipitated powder was filtered, washed several time with hot ethanol and diethyl ether, and recrystallized from hot ethanol. Yield: 85%

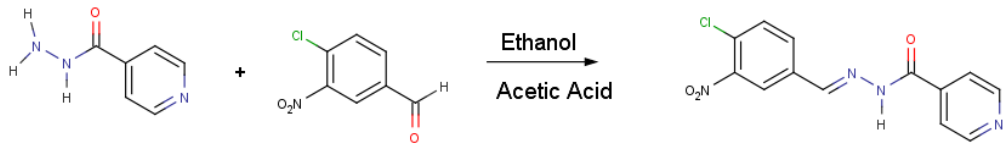

Figure 23. Pathway for preparation of **Hyd1**

III.2.5.2. Synthesis of N'-[(3*Z*)-6-bromo-2-oxo-2,3-dihydro-1*H*-indol-3-ylidene] pyridine-4-carbohydrazide (Hyd2)

An amount of 6-bromoindoline-2,3-dione (0.005 mole, 1.1301 g) was heated for 1 h in ethanol (30 mL), After dissolution, a hot solution of isoniazid (0.005 mole, 0.6857 g) and drops of acetic acid were added with stirring, the reaction mixture was refluxed at 78 ºC for 3 h. After cooling, the precipitate powder was filtered, washed several time with hot ethanol and diethyl ether, and recrystallized from hot ethanol. Yield: 81%. This reaction is shown in **Figure 24**.

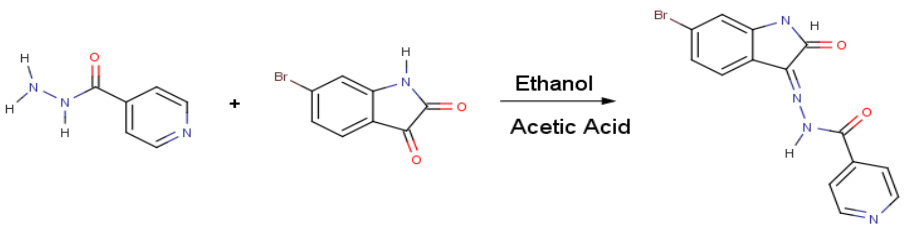

Figure 24. Pathway for preparation of **Hyd2**

III.2.6. Toxicological studies

III.2.6.1. *In vitro* evaluation using bacteria

In this experiment, the following strains of bacteria were used to evaluate the toxic effect of the tested compounds using a published procedure [59]: *Lysteria monocytogenes*, *Escherichia coli*, *Bacillus cereus*, *Pseudomonas aerogenose*, *Staphylococcus aureus*, and *Klebsiella pneumonia*. Bacterial strains were cultured overnight at 37 °C in Mueller Hinton agar (MHA). Suspensions of the bacterial strains tested were prepared in sterile saline (equivalent to 0.5 MacFarland or have Absorbance of 0.08 to 0.10). From these suspensions, strains were spread on the solid media plates (MHA). Filter paper discs (7 mm in diameter) were placed on the inoculated plates and impregnated with 15µL of the tested compounds (1000 and 2000 µg/mL in DMSO). The plates were incubated at 37 °C for 24 h, and the diameters of the inhibition zones were measured in millimeters.

III.2.6.2. *In vitro* evaluation using fungus

Fungal strains were activated on PDA plats (200 g potatoes, 10 g dextrose, and 15 g Agar in 1 L distilled water). The suspensions of the tested fungal strains were prepared in sterile saline. From these suspensions, strains were spread on the solid media plates (PDA). Filter paper discs (7 mm in diameter) were placed on the inoculated plates and impregnated with 15 µLof the tested compounds (1000 and 2000 µg / mL in DMSO). The plates were incubated at 28 °C for up to 72 h. The diameters of the inhibition zones were measured in millimeters every 48 h of incubation [59].

III.2.6.3. *In vivo* acute toxicity evaluation

Acute toxicity was evaluated using adult *Swiss albino* mice (25–30 g) [60]. The synthesized hydrazones **Hyd1** and **Hyd2** were suspended in 0.5% w/v solution of carboxyl methyl cellulose (CMC) and administered at 1000 mg/kg body weight. All mice were deprived of food for 24 h and water was withdrawn 2 h before start of the experiment. Mice were equally divided into three groups of five female mice each:

Group 1 (normal control) received vehicle (5 mL/kg CMC)

Group 2 received 1000 mg/kg **Hyd1**

Group3 received 1000 mg/kg **Hyd2**.

III.2.6.3.1. Observations

After 3 h of administration, mice were observed for abnormal behavior (sedation, convulsions, respiratory distress, salivation, changes in skin and fur) and mortality percent was calculated each 24 h during 14 days.

III.2.6.3.2. Animal weight

Body weights were recorded at the beginning, then once after every seven days during the study.

III.2.6.3.3. Biochemical analysis

At the end of the experiments period, animals were fasting 4 h and then sacrificed. Blood samples were collected in heparine-tubes and then centrifuged at 3000 rpm for 10 min. Plasma biochemical parameters were conducted, including urea, creatinine, albumine, calcium, protein, cholesterol, uric acid, aspartate aminotransferase (AST), alanine aminotransferase (ALT), and alkaline phosphatase (ALP), using Biolyser 100 analyticon and commercial kits (Spinreact, Spain and Cromatest react).

III.2.6.3.4. Histological analyses

Histopathological analyses of liver and kidneys were performed using a Leica DM-1000 microscope (10 and 40x) in order to verify alterations in the tissues. Digital images were obtained with the aid of a LEICA camera associated with the microscope, and all images were analyzed using the image processing software.

III.2.7. *In vitro* antioxidant activity evaluations

III.2.7.1. Superoxide anion scavenging activity

III.2.7.1.1. Chemical assay

Superoxide anion radical scavenging effect of **INH**, **Hyd1**, **Hyd2**, and ascorbic acid (**AA**) was evaluated according to a procedure outlined by Gowri and Madhavan [61]. Briefly, to a 50 µL solution of Nitoblue tetrazolium chloride, 200 µL of different concentrations of tested compounds and 500 µL of alkaline DMSO were added. The reaction mixture was incubated

for 5 min and absorbance measured at 560 nm [61]. Superoxide anion radical scavenging activity RSA % was calculated using the following equation:

$$\text{Superoxide anion radical scavenging}(\%) = 100\text{x}(\text{A0} - \text{A1})/\text{A0}$$

Where A_0: absorbance of the control and A_1: absorbance in the presence of the tested compound.

III.2.7.1.2. Electrochemical assay

Cyclic voltammetry was employed to examine the superoxide anion radical scavenging activity of synthesized hydrazone and ascorbic acid (**AA**) [62] based on oxygen reduction. In this experiment, we used an electrochemical cell containing an oxygen saturated solution of tetrabutylammoniumtetrafluoroborate (TBABF4) and DMSO. Tested compounds were added successively to the cell and cyclic voltammograms for reduction of oxygen were recorded. Superoxide anion radical scavenging activity (RSA %) was calculated using the following equation:

$$\text{RSA \%} = 100\ (I_o - I_t) / I_o$$

Where I_0 is the anodic peak current without the tested compounds and I_t is the anodic peak current in the presence of the tested compounds.

III.2.7.2. Hydrogen peroxide scavenging activity

In this assay,125 µL of ferrous ammonium sulphate (1 mM) were mixed with 750 µL of various concentrations of the tested compounds and 31.25 µL of hydrogen peroxide (5 mM) were added, the reaction mixture was incubated in the dark for 5 min, and then 750 µL of 1,10-phenanthroline (1 mM) were added. After incubation in the dark for 10 min, the absorbance was recorded at 510 nm [63]. Hydrogen peroxide-scavenging activity was calculated using the following equation:

$$\text{Hydrogen peroxide scavenging}\ (\%) = 100\text{x}(\text{A0} - \text{A1})/\text{A0}$$

A_0 is the absorbance of the control and A_1 the absorbance of the tested compounds

III.2.8. *In vivo* antioxidant activity evaluation

In this experiment, **INH** was used as an oxidizing agent that induces oxidative stress in mice. After an 18 h of fasting, **INH** was injected with intraperetenial route at 151 mg/kg [64]. The

tested compound (**Hyd2**) was administrated *via* oral route. The experimental mice were treated as followed:

Group I: control (untreated),
Group II: treated with INH,
Group III: treated with **INH** + **Hyd2** at 15 mg/kg,
Group IV: treated with **INH** + **Hyd2** at 30 mg/kg. After 4 h, animals were scarified.

III.2.8.1. Preparation of tissue homogenates

Liver samples were stored at –4 ºC until homogenation, then an amount of 500 mg of liver of the different groups was added to 5 mL of the ice KCl buffer (0.15 M). The mixture was homogenized at 1200 rpm using electric homogenizer.

III.2.8.2. Determination of CAT activity

The CAT activity was determined in supernatant, obtained after a 15 min centrifugation of liver homogenates at 4000–5000 rpm. The CAT activities were measured as follows: 30 mM hydrogen peroxide was used as a substrate. To each sample, 1.9 mL phosphate buffer (pH 7.2) and 1 mL 30 mM H_2O_2 were added. The decrease in H_2O_2 concentration at 25 ºC was spectrophotometrically determined at 240 nm. The extinction coefficient was read exactly 1 min after H_2O_2 addition. CAT activities presented as units permg protein (Units/mg Protein).

III.2.8.3. Estimation of GSH

The GSH levels were estimated in the homogenates of liver using (5,5'-dithiobis-(2-nitrobenzoic acid), (DTNB), in which 5 mL of sodium phosphate buffer (0.1 M, pH = 8) was added to 25 µL of supernatant homogenate, then 1.5 mL of the mixture was added to 10 µL of DTNB (0.01 M). Determination of GSH is based on the reaction of DTNB with GSH to yield a yellow colored chromophore with a maximum absorbance at 412 nm. The amount of GSH present in the tissue was calculated using its extinction coefficient (1.36×10^4 M^{-1} cm^{-1}) at 412 nm and expressed as µmoles/g tissue [65].

III.2.8.4. Estimation of MDA

The hepatic malondialdehyde (MDA) content was an indicator to determine hepatic lipid peroxidation levels. In this experiment, 125 µL of trichloric acid (TCA, 20%) and 250 µL of thiobarbituric acid (TBA, 0.67%) were added to 125 µL of tissue homogenate. The mixture was incubated at 100 °C during 20 min. After incubation, the sample was cooled. The MDA-TBA complex was extracted with 1 mL of butanol. The organic phase was separated by

centrifugation at 3000 rpm for 15 min. Absorbance was measured at 530 nm. The concentration of MDA was calculated using its extinction coefficient ($1.56\times105\ M^{-1}\ cm^{-1}$) at 530 nm and expressed as nanomoles MDA/g tissue [65].

III.2.9. Hepatoprotective activity evaluation

In this assay, **INH** was used as hepato-toxic agent in mice model. *Swiss albino* male mice (34-36 g) were divided into four groups containing five mice each:

Group 1: (standard control) received only vehicle (0.5 mL/kg/day);

Group 2: (control group) received (400 mg/kg/day) **INH**.

Group3: received **INH** and (25 mg/kg/day) **Hyd2**.

After 7 days, animals were scarified and blood samples were collected for biochemical assays including assessment of liver and kidney function. Liver and kidneys were conserved in 10% buffered formalin for 24 h for histological study [42].

III.2.9.1. Body weight estimation

The body weight of animals was measured in all 7 days of experiment.

III.2.9.2. Organs weight estimation

At the end of experiment, and after the sacrifice of animals, the weight of the organs such as liver and kidney was measured and compared with the control group.

III.2.9.3. Biochemical parameters

Blood samples were collected in heparine-tubes and then centrifuged at 3000 rpm for 10 min. Plasma biochemical parameters were conducted, including urea, creatinine, albumine, calcium, protein, cholesterol, uric acid, aspartate aminotransferase (AST), alanine aminotransferase (ALT), and alkaline phosphatase (ALP), using Biolyser 100 analyticon and commercial kits (Spinreact, Spain and Cromatest react).

III.2.9.4. Histological analysis

Histopathological analyses of liver and kidneys were performed using a Leica DM-1000 microscope (10 and 40x) in order to verify alterations in the tissues. Digital images were obtained with the aid of a LEICA camera connected with the microscope, and all images were analyzed using the image processing software.

III.2.10. *In vitro* biodegradability evaluations

In Petri dishes containing a mineral medium (NH_4NO_3 1.0 g, KH_2PO_4 0.7 g, K_2HPO_4 0.7 g, MgSO4·$7H_2O$ 0.7 g, NaCl 0.005 g, $FeSO_4·7H_2O$ 0.002 g, $ZnSO_4·7H_2O$ 0.02 g, $MnSO_4·7H_2O$ 0.001 g, water 1000 mL) and the tested compounds **INH, Hyd1, Hyd2** and Nicotinamide as sources of carbon and energy [66], filter paper discs (7 mm) were impregnated with 15 µL of *Aspargillus niger* strains. Plates were then incubated at 27 ºC for seven days, and the diameter of fungi growth was measured each 24 h.

III.3. Statistical analysis

The *in vitro* experimental results are expressed as mean ± SD of triplicate. Data were analyzed by Student's *t*-test to determine statistical significance. *p* values less than 0.05 ($p < 0.05$) were considered as indicative of significance. IC_{50} values were calculated from linear regression analysis. On the other hand, *in vivo* experimental results are expressed as mean ± SEM. Statistical analysis of data was accomplished using one-way analysis of variance (ANOVA; $p < 0.05$) and "Dunnett's multiple comparison tests" was used to compare with control group. The $p < 0.05$ was considered as indicative of significance. All statistical analysis and graphing of data were performed using Graph pad prism 5 Demo.

Chapter IV: Results and Discussion

Part 1 : *Computational Chemistry*

IV.1. Computational chemistry

IV.1.1. DFT study

IV.1.1.1. Structures optimization

Geometry optimization of **INH**, **Hyd1**, and **Hyd2** was accomplished using the DFT/B3LYP method with 6-31G (d,p) basis set of calculations. Optimized structures are shown in **Figure 25**.

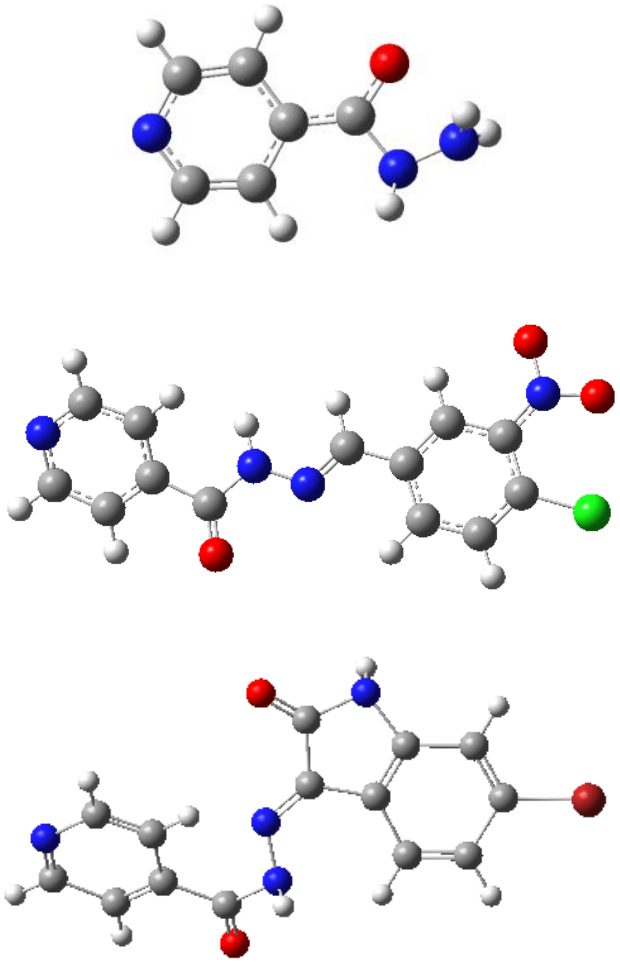

Figure 25. Optimized molecular structures of **INH**, **Hyd1**, and **Hyd2**

IV.1.1.2. HOMO and LUMO analysis

Molecular energy, electron donor distribution in the highest occupied molecular orbital (HOMO), and electron acceptor distribution in the lowest unoccupied molecular orbital (LUMO) are depicted in **Figure 26**. Molecular orbital calculations present a full description of orbitals as well as spatial characteristics, nodal patterns, and individual atom contributions. For **INH**, the LUMO orbitals are positioned on the whole molecule, and the HOMO orbitals are localized on the hydrazide group. In addition, LUMO orbitals of **Hyd1** are located on the C_6H_5, Cl, and NO_2 moieties, whereas the HOMO orbitals are poisoned on NO_2 and Cl, both of

which are electron-withdrawing. Furthermore, LUMO orbitals of **Hyd2** are positioned on the whole molecule, and the HOMO orbitals are localized on the azomethine and the heterocyclic moiety; bromoindoline 2,3-one. Energies of HOMO and LUMO are –0.2159 and –0.0696 a.u for **INH**,–0.2516 and –0.1152 a.u for **Hyd1**, and –0.2297 and –0.0941 a.u for **Hyd2** (in DMSO). In the gas phase, energies of HOMO and LUMO for **INH** are –0.2174 and –0.1045 a.u, respectively, whereas for **Hyd1** are –0.2613 and –0.1393 a.u, respectively, and –0.2365 and –0.1004 a.u for **Hyd2**.

HOMO-LUMO energy gap (ΔE_{gap}) which represents the lowest energy electronic transition is an important parameter for determining the molecular reactivity and stability, where molecules with a small ΔE_{gap} have a high chemical reactivity, low stability [67], and high bioactivity [68]. As shown in **Table 4**, ΔE_{gap} (in DMSO) of **INH**, **Hyd1**, and **Hyd2** are 0.1463, 0.1364, and 0.1356 a.u, respectively. In addition, other electronic properties indicate that **Hyd1** has lower LUMO energy (–0.1152 a.u), larger electron affinity (0.1152 a.u), and higher electronegativity (0.1834 a.u) than **INH** and **Hyd2**, which indicates that it is a better electron acceptor. Furthermore, **Hyd1** possesses a high value of electrophilicity (0.9863 a.u) which shows that this compound acts as a better electrophile than **Hyd2** and **INH**. **INH**, on the other hand, possesses a lower ionization potential (0.2159 a.u) which indicates the electron donating ability of this compound. For hardness and softness of molecules, results demonstrate that **Hyd2** has more chemical reactivity than **Hyd1** and **INH** with calculated values of 0.0678 and 0.0339 a.u, respectively.

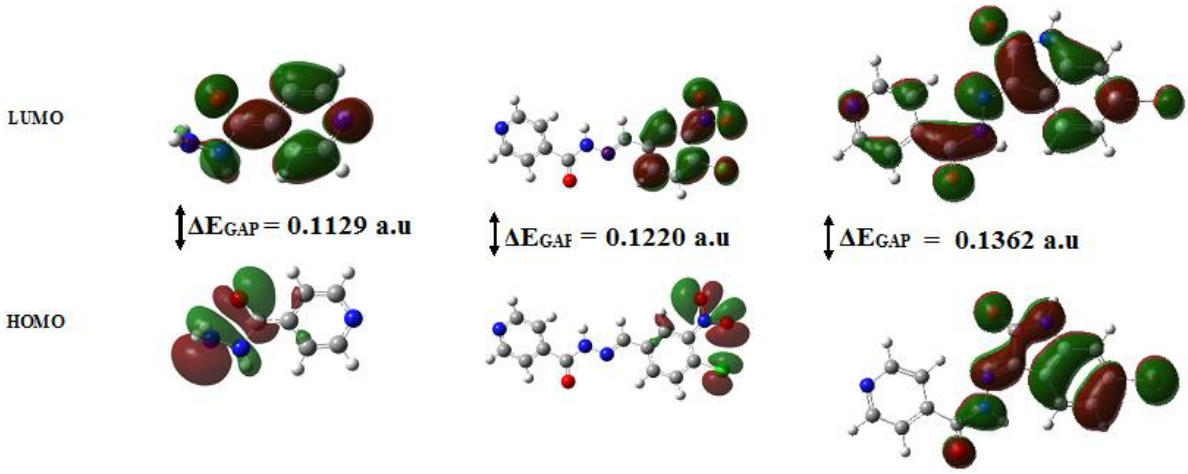

Figure 26. Frontier molecular orbitals of **INH**, **Hyd1**, and **Hyd2**; ΔE_{gap} in gas phase.

Table 4. Comparison of HOMO, LUMO, related molecular properties of **INH**, **Hyd1**, and **Hyd2** in DMSO and in gas state

B3LYP/6-31G (d,p)						
	In gas state			In DMSO		
Molecular energy (a.u)	**INH**	**Hyd1**	**Hyd2**	**INH**	**Hyd1**	**Hyd2**
E(B3LYP)	–472.2814	–1405.4900	–3480.074	–472.3384	–1391.6815	–3480.091
E_{LUMO}	–0.1045	–0.1393	–0.1004	–0.0696	–0.1152	–0.0941
E_{HOMO}	–0.2174	–0.2613	–0.2366	–0.2159	–0.2516	–0.2297
Energy gap (Δ)	0.1129	0.1220	0.1362	0.1463	0.1364	0.1356
Ionization potential (I)	0.2174	0.2613	0.2366	0.2159	0.2516	0.2297
Electron affinity (A)	0.1045	0.1393	0.1004	0.0696	0.1152	0.0941
Global hardness (η)	0.05645	0.0610	0.0681	0.07315	0.0682	0.0678
Global softness (S)	0.02822	0.0305	0.0340	0.03657	0.0341	0.0339
Chemical potential (μ)	–0.3219	–0.4006	–0.3370	–0.2855	–0.3668	–0.3238
Electophilicity (ω)	0.9177	1.3154	0.8338	0.5571	0.9863	0.7732
Electronegativity (χ)	0.1609	0.2003	0.1685	0.1427	0.1834	0.1619

IV.1.2. Physicochemical properties calculation

IV.1.2.1. Protonation/deprotonation forms

Chemical properties of organic compounds depend essentially on whether they are ionized or not, explained by gaining and/or losing a proton in aqueous solutions [69]. From statistics, 95% of drugs are ionizable [70]. In drug development, pka value influences the biopharmaceutical profile of the compounds, in biochemical properties, and pharmacokinetics. The progress of new methods for pka determination is a sign of the importance of this parameter in the development and the selection of new drugs [71]. It is evident from **Figure 27**, that each one of the synthesized hydrazones has ionization centers. **Hyd1** has two proton-accepting atoms; the nitrogen atom of azomethine group and nitrogen of the hetero-aromatic ring (pyridine) with pKa values of –0.002 and 3.033, respectively, in addition to one proton-donating atom, nitrogen of the amide group with a pKa value of 9.878. Similarly, **Hyd2** has three ionization centers; N of indoline ring, N of amide group, and N of pyridine ring with pka values of 11.81, 9.50, and 3.02, respectively.

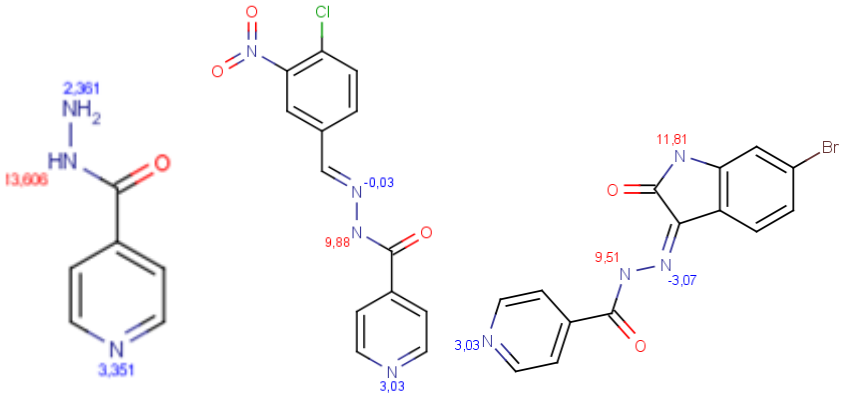

Figure 27. Ionization centers of **INH**, **Hyd1**, and **Hyd2**

On the other hand, results shown in **Figure 28** shed some light on the species of **Hyd1** present in solution at the pH range of 0.2–14. Five species from **Hyd1** were predicted: a **neutral** with a charge 0 (red color), two **cationic** each with a total charge of +1 (green and blue), one **anionic** with total charge of –1 (marron), and one **dicationic** with a total charge of +2 (violet). It is clear from **Figure 28**, that the unionized form **1** is the major species in solution in the pH range of 3.2–8.6. In addition, **3** and **4** are the major ionized forms in the pH range from 0.2–4 and 10.2–14.0, respectively, whereas species **2** and **5** are present in negligible amounts.

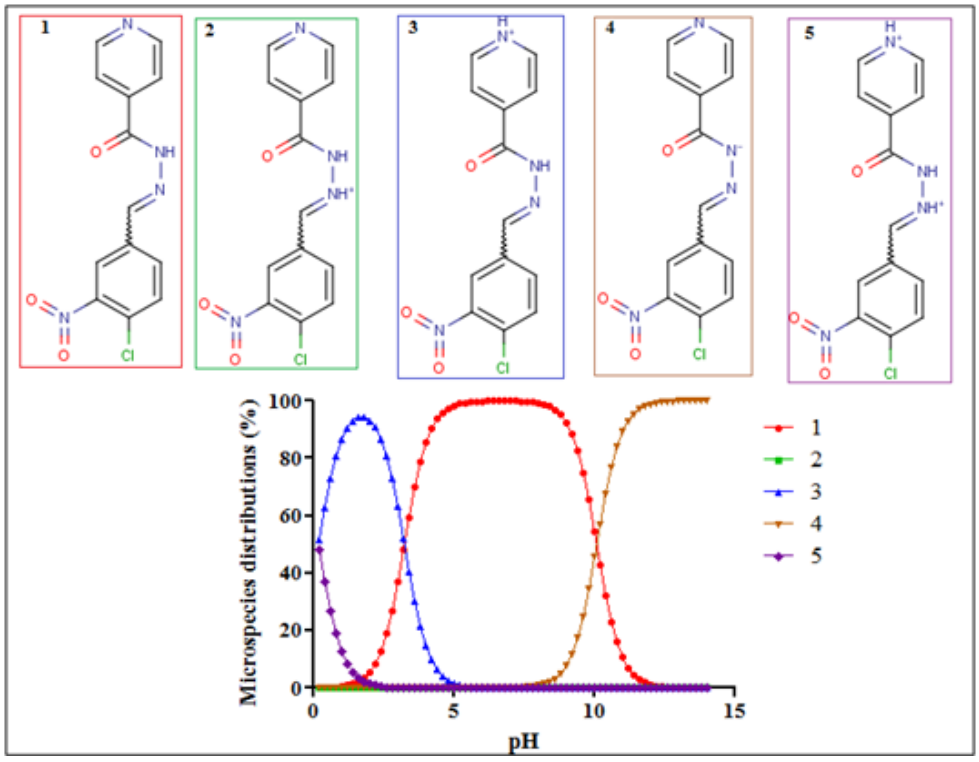

Figure 28. pH-dependent distribution of species derived from **Hyd1**.

Similarly, **Figure 29** illustrates the change of **Hyd2** ionic forms with pH. Results indicate that **Hyd2** has five forms in solution at the pH range 0–14; **neutral** form presents at the pH range 1–11 which represents the most abundant form (red), **cationic** form at pH 0–4 (green), two **anionic** forms (black and maron), and **dianionic** form at pH 8.3–13.7 (bleu).

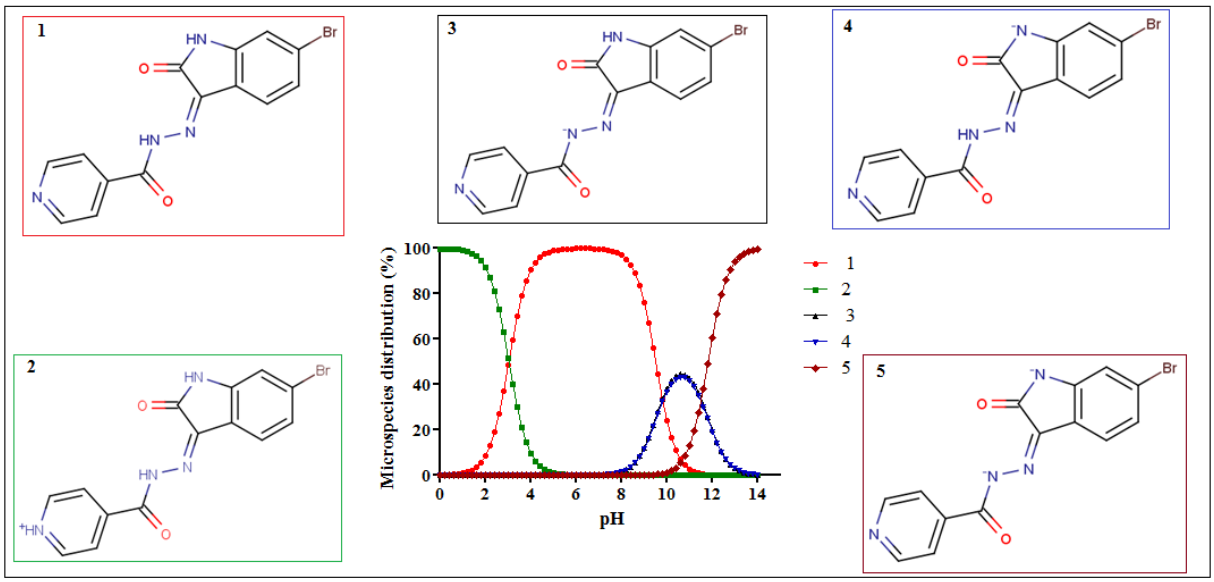

Figure 29. pH-dependent distribution of species derived from **Hyd2**.

IV.1.2.2. H-bond donor/acceptor centers and number of rotatable bonds

In a solvated environment, the number of hydrogen bond donors and acceptors was calculated. Results displayed in **Figure 30**, indicate that **Hyd1** has a number of hydrogen bond donors (= 1), and the number of hydrogen bond acceptors (=5). In a similar fashion, **Hyd2** has a number of hydrogen bond donors (= 1), and the number of hydrogen bond acceptors (=5). These results are in agreement with Lipinski rule [72] that (HBD< 5 and HBA <10).

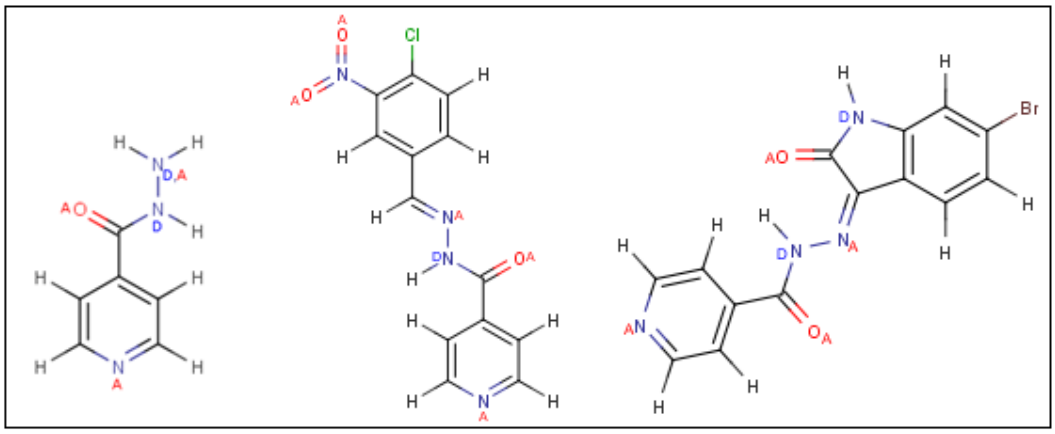

Figure 30. H-bond donor/acceptor centers of **INH, Hyd1**, and **Hyd2**

Additionlly, the rotatable bonds which allow free rotation around themselves, give information about the compound's conformational space and expresses its flexibility [73]. Both synthesized hydrazones have a number of rotatable bonds < 9, NRB=4 for **Hyd1** and 2 for **Hyd2**.

IV.1.2.3. Partial atomic charges

In quantum chemistry, the atomic charge is an important factor to understand molecular properties [74]. Atomic charges affect the molecular system in acid-base behavior, electronic structure, polarizability, and dipole moment [75]. Additionally, several physicochemical proprieties of molecules can be affected by partial charge, such as pka, molecular activity, and pharmacophore profiles. Partial charge distribution changes with active sites of ionization [68]. Partial atomic charges of both hydrazones are given in **Figure 31**. For **Hyd1**, high negative charges (red color) were found on O of the amide group, N of azomethine, N of the pyridine ring, and two O of the nitro group with values of –0.31, –0.29, –0.22, –0.15, and–0.15, respectively. On the other hand, the highest positive charges (blue color) were found on H and C of the amide group with values of 0.18 and 0.11, respectively.

In the partial charge distribution of **Hyd2**, a negative values in red color represents rich electron centers which are: O atoms of indoline ring, amide group, N atoms of azomethine group and pyridine ring with values of –0.35, –0.3, –0.26 and –0.22, respectively. These centers represent nucleophilic sites in **Hyd2**, probably binding with hydrogen atoms of macromolecules such as nucleic acid, peptides, and proteins. Furthermore, high positive values in blue color correspond to the dissociation of proton from indoline ring and the amide group with values of 0.16 and 0.19, respectively. In addition, other positive values from carbon of amide group with value of 0.12 represent poor electron center, correspond to electrophile site. These results explain the possibility to interact with receptors; the positive site of receptor interacts with negative-charged atoms of the synthesized hydrazones (O, N) whereas the positive part of receptor interacts with the negatives-charged atoms of hydrazones (H, N) [76].

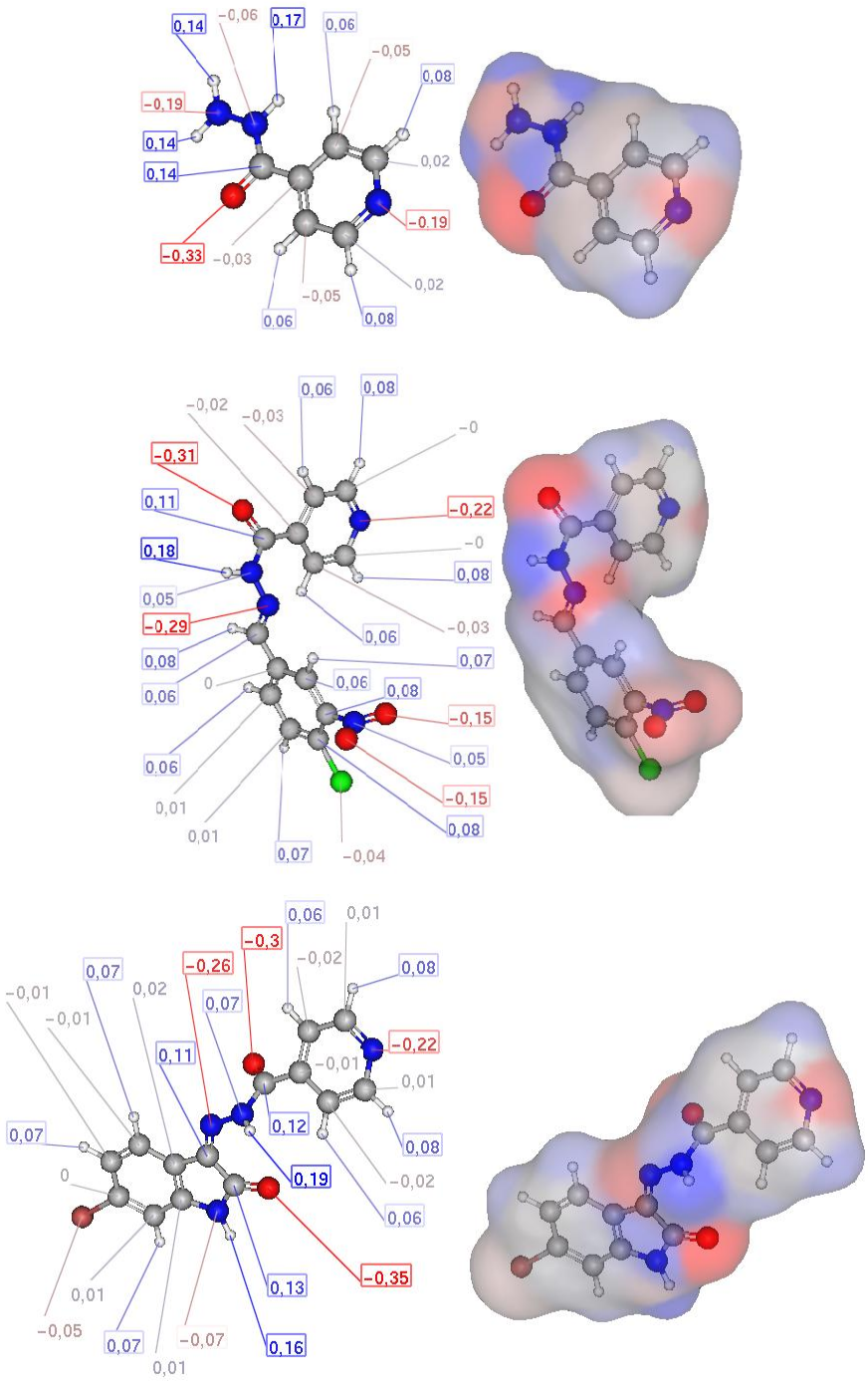

Figure 31. Partial atomic charges of **INH**, **Hyd1**, and **Hyd2**

IV.1.2.4. Steric hindrance

Steric hindrance is an important parameter in the molecule's stability and reactivity which can affect chemical reactions [77]. Results presented in **Figure 32,** show numerical values of each atom in molecules which predict steric effect. A-values (kcal mol^{-1}) ranging from 0.66 to 1.36 for **INH**, from 0.43 to 1.56 for **Hyd1**, and from 0.31 to 1.68 for **Hyd2**. These values

demonstrate an increase in steric hindrance of **INH** after condensation with 4-chloro-3-nitro benzaldehyde and 6-bromoindoline-2,3-dione in all atoms (**Hyd1** and **Hyd2**).

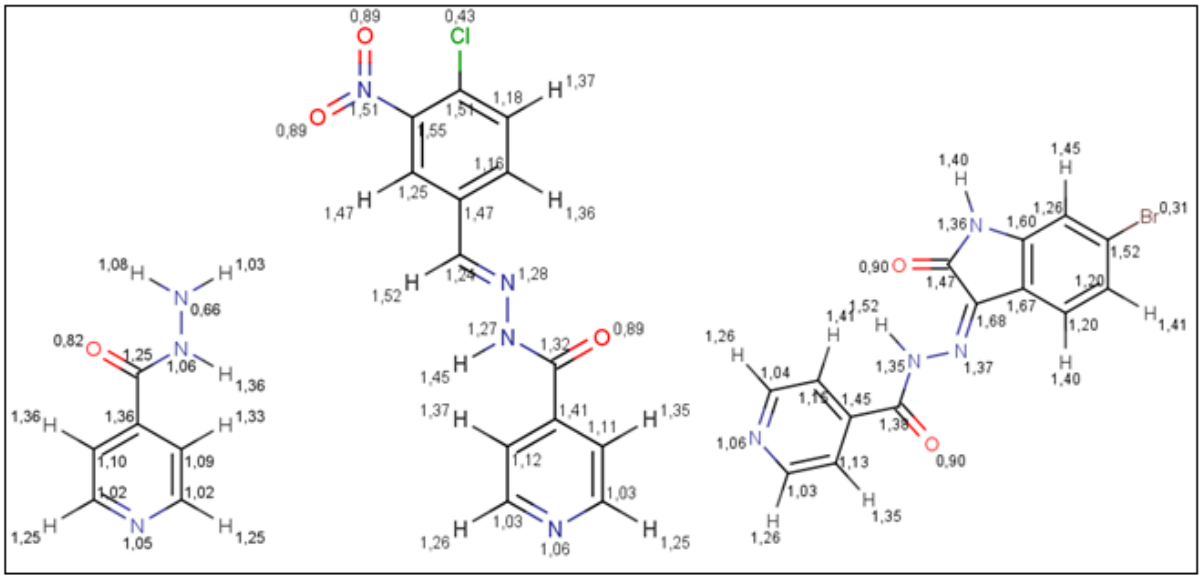

Figure 32. Steric hindrance of **INH, Hyd1** and **Hyd2**

IV.1.2.6. Lipophilicity descriptors

Lipophilicity is a significant function in drug candidate's absorption, distribution, metabolism, excretion, and toxicity, due to its contributions in the ability to penetrate through membranes, selectivity, efficiency, metabolism, and pharmacokinetics [78]. Research in drug design used 1-octanol/water partition coefficient (logP) for determining molecular lipophilicity [79]. Drugs with high partition coefficients have a preference to localize in hydrophobic parts of cells such as membranes' lipid, while drugs with low partition coefficients prefer to stay in hydrophilic liquids such as blood serum [80]. In this work, Chem Axon method was used to calculate logP of the investigated hydrazones. Results from **Figure 33** show that logP values distribution of each atom of the hydrazones indicate the lipophilic character of both hydrazones. From **Hyd1**, high positive values (blue color) were distributed on two oxygen atoms of the nitro group and in the chlorine atom with values of 1.01, 1.01, and 0.92 respectively, whereas high negative values (red color) were observed in N of nitro group, N of amide function and N of pyridine ring. In addition, logP distribution in each atom of **Hyd2**, values in red color with the negative values with –0.58, –0.36, –0.22, –0.14 and –0.05 correspond to N of amide function, N of pyridine ring, N of indoline ring, O (amide and indoline ring), C of carbonyl function respectively. On the other hand, bromine atom and the rest of carbons represent the positive values. Remarkably, nitrogen atoms with high negative values in both hydrazones are the ionization centers of these compounds. Sum of these

calculated values in each compound represent 1-octanol/water partition coefficient (logP); values are 2.29 for **Hyd1**, 1.78 for **Hyd2** and–0.69 for **INH**. These values demonstrate the good lipid solubility of these compounds. The obtained results are in good agreement with Lipinski rule [72] which stipulates that logP≤5. We conclude that the examined hydrazones are in the acceptable limit for the drugs to be able to penetrate through biomembranes.

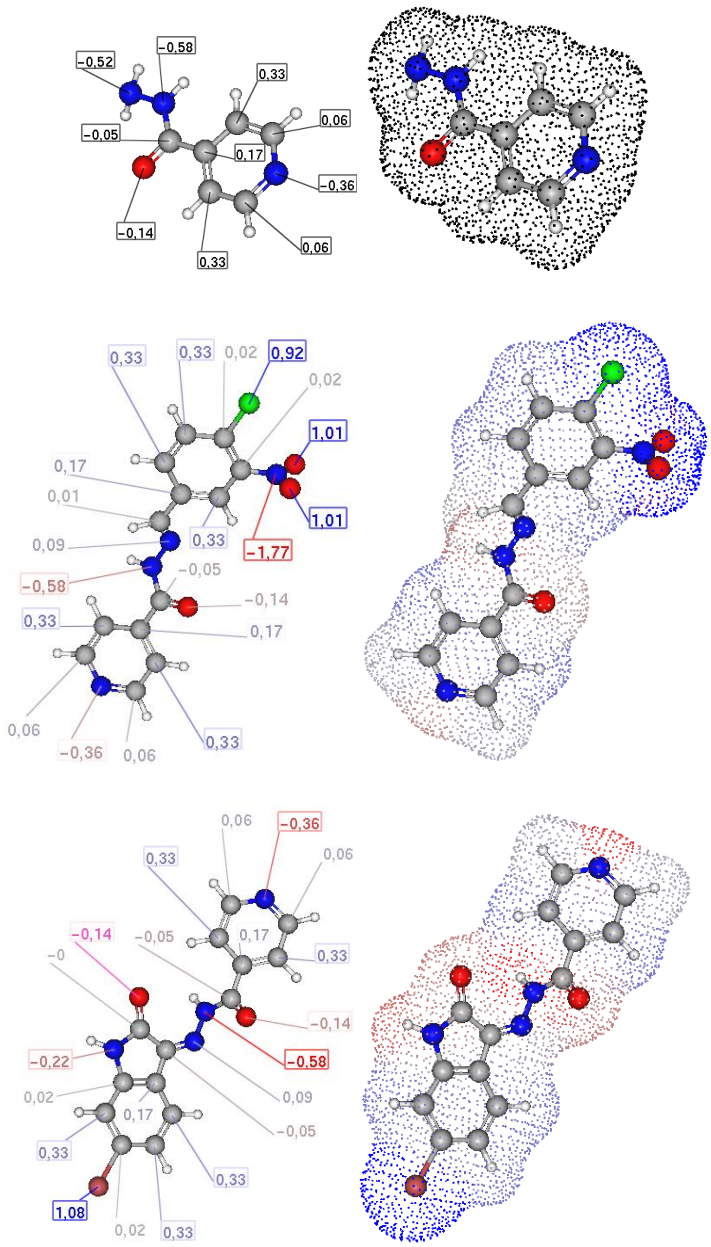

Figure 33. logP values distribution of **INH**, **Hyd1**, and **Hyd2**

In addition, the pH dependent distribution coefficient logD is a parameter for lipophilcity determination which represents the lipophilicity in all forms of the investigated compounds,

ionizable and neutral states and is correlated to logP through pka. Results depicted in **Figure 34**, show the pH dependent distribution coefficient logD of **INH**, **Hyd1**, and **Hyd2**.

For Hyd1 graph at pH 0.2 represents the lipophilic character with logD value of 1.01; this state is the dicationic form. In the pH range from 0.2 to 4, the graph represents an increase in lipophilicity with logD values from 1.01 to 2.25, which represents the cationic state. Additionally, in the pH range from 4 to 5, the graph shows an increase in lipophilicity with values ranging from 2.25 to 2.29, which represent both forms, cationic 50% and neutral 50%.

Similarly, in the pH range from 5 to 9, it shows a decrease in lipophilicity with logD values of 2.92 to 2.24, which represents the neutral form of **Hyd1**, whereas at pH 7.4, the partition coefficient logP as the pH dependent distribution coefficient logD, (logP= logD = 2.29). In the pH range from 9 to 12, it shows a decrease in lipophilicity with logD values of 2.24 to 1.37, which represent a mixture of neutral 50% and anionic 50%. Furthermore, the pH range from 12 to 14, represents the anionic state and characterizes stability in lipophilicity with logD value of 1.37.

For **Hyd2** graph, the pH range from 0.2 to 1, characterizes the cationic state and presents stability in lipophilicity with logD vale of 0.83, whereas pH range from 1 to 4, indicates that both states, cationic and neutral, and an increase in lipophilicity with logD increased from 0.83 to 1.74. On the other hand, in the pH range from 4 to 8.5, the neutral state, showed stability in lipophilicity with logD value of 1.74. At pH 7.4, partition coefficient logP as the pH dependent distribution coefficient logD, (logP = logD = 1.78). In the pH range from 8.5 to 12.5, the anionic form showed a decrease in lipophilicity with logD values vary from 1.74 to 0.06. Moreover, logD with negative values (–0.43 to 0.06) at the pH range from 12.5 to 14 indicate that **Hyd2** has lower lipophilicity and higher hydrophilicity.

The drug **INH** has negative values of logD, which confirm its hydrophilic character. From these results, we conclude that **Hyd1** has lipophilic character whereas **Hyd2** has lipophilic character in the pH range from 0.2 to 12.5 and hydrophilic character at pH greater than 12.5.

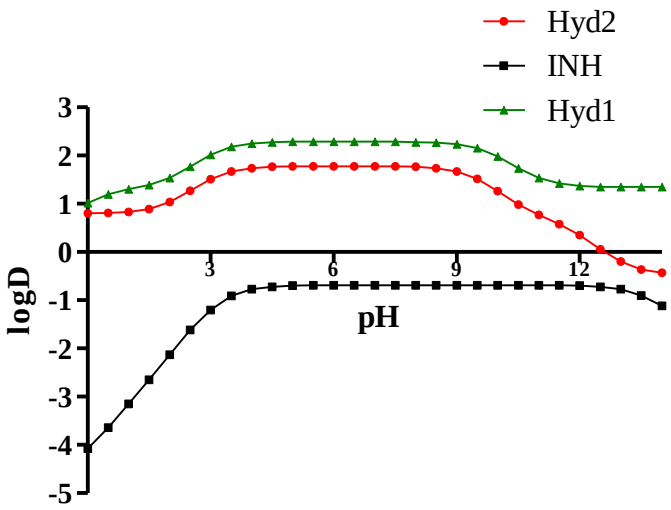

Figure 34. pH-dependent distribution coefficient, logD of **INH**, **Hyd1**, and **Hyd2**

IV.1.2.7. Topological polar surface area and absorption percentage

The polar surface area (TPSA) is defined as the surface sum above all polar atoms including, oxygen, nitrogen, and hydrogen attached to these polar atoms [81]. Pharmaceutical researchers used this parameter for the prediction of different drugs transport processes [82] in which TPSA was used for the drug-absorption percentage calculation, by using the formula; AB% = 109 – (0.345 x TPSA) [83]. Results presented in **Table 5**, show that the polar surface areas of **Hyd1** and **Hyd2** at pH 7.40 are 100.17 and 83.45Å^2, respectively. This is an indication that TPSA values of both hydrazones are in good agreement with Lipinski rule, where optimal TPSA ≤120 Å^2. This parameter influences lipophilicity in drugs absorption by passive diffusion, where optimal lipophilicity depends to low molecular mass and low TPSA [80]. Thus, high value of TPSA is associated with the high probability to be no permeable and no bioavailable [84]. For this reasons, results demonstrate an excellent oral absorption of **Hyd2** with high absorption percentage of 80.20 % comparable with the drug **INH**.

Table 5. Topological polar surface area and absorption parentage of **INH**, **Hyd1**, and **Hyd2**.

Compounds	**Topological Polar Surface Area (TPSA)** Å^2	**Absorption (%)**
INH	68.01	85.53
Hyd1	100.17	74.44
Hyd2	83.45	80.20

IV.1.3. *In Silico* Toxicological studies

Chemicals toxicity determination is the step to recognize their adverse effects on humans, animals, plants, or the environment. This step is important in the drug discovery processes [85]. For the protection of environmental and human health, all chemical compounds have to pass an acceptable toxicity test, which is the measure of any undesirable or bad effect of these chemicals. *In silico* toxicology (computational toxicology) is one type of toxicity assessment that uses computational resources (i.e., methods, algorithms, software, data, etc.) which can lead to screening of a large numbers of substances in a short time and low expenses [86].
To explore the toxicity effect of hydrazones**,** we use different online software programs with a variety of computational approaches.

IV.1.3.1. Toxic substructure prediction

Drug undesirables and toxic effects were traduced by unfavorable reactions affecting human organs, inducing harmful effects, are the principle problems in drug discovery and development [87]. These toxic actions can be related to chemical structures, or a part of the structures which defined by substructures or toxicophores, which could be an atom or fragments of chemical structure [88]. In order to predict the toxicity of **INH** and its derivatives **Hyd1** and **Hyd2**, **Table 6**, represents toxic substructures (in red color) and their adverse effects. The obtained results defined the toxic fragment in common of all investigated compounds; the hydrazine group (-NH-N-), predicted as responsible in hepatotoxicity effect induction. In addition to the hepatotoxic effect, the hydrazones have other toxic substructures: the nitro-aromatic part of **Hyd1**, presents the covalent bond with DNA, in the quaternary carbon atom, the nitro group bond with quaternary carbon, presents toxicity metabolic activation. From **Hyd2**, the C-N bond and the amide group of the indoline-2,3-one ring were predicted as being responsible for the covalent bond with proteins, the quaternary carbon of indoline ring was predicted as an inducer to covalent bond with DNA.

Table 6. Toxic substructure prediction of **INH**, **Hyd1**, and **Hyd2**.

Compounds	Toxic substructure	Alert name
INH	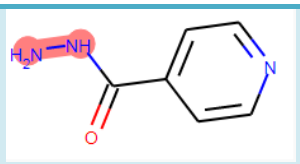	Covalent bind with DNA and Hepatotoxicity
Hyd1	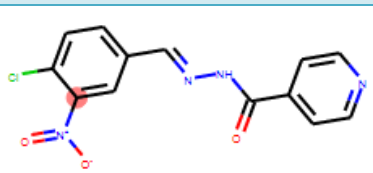	Covalent bind with DNA
	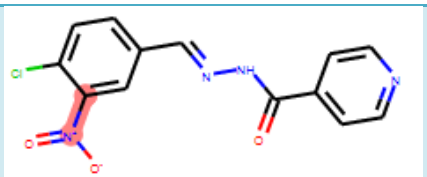	Idiosyncratic toxicity metabolic activation
	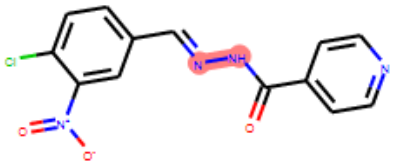	Hepatotoxicity
Hyd2	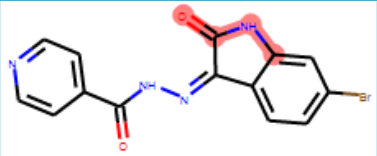	Covalent bind with protein
	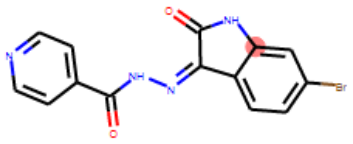	Covalent bind with DNA
	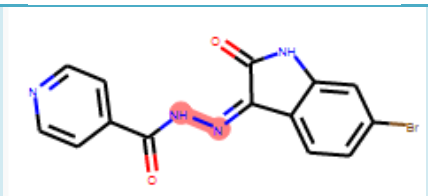	Hepatotoxicity

IV.1.3.2. Acute rat toxicity prediction

The major advantage of computational approaches for the acute toxicity and the toxicity classification of the investigated hydrazones, is to give important information before they are synthesized. Additionally, due to the ethical consideration, the time consumption and the high cost in animal models, the computational methods were used as a substitute in the *in vivo* toxicological studies.

LD_{50} values and the predicted toxicity class of the **INH** and its derivatives were predicted by GUSAR software in rodent with different administration routes (intraperitoneal, intravenous, oral and subcutaneous). Results in **Table 7** show non toxic effect of **Hyd2** in subcutaneous administration with high LD_{50} value of 4999.00 mg/kg, which is classified in the non toxic class. Additionally, intraperitoneal and intravenous routes were classified in the fifth class with LD_{50} values of 1179 and 426 mg/kg, respectively. Whereas intraperitoneal route was the low toxic way of **Hyd1** with LD_{50} value of 1086 mg/kg, classified in the class 5, the LD_{50} of both compounds in oral administration route were 1816 mg/kg for **Hyd1** and 984.60 mg/kg for **Hyd2**.

Table 7. Acute rat toxicity prediction of **INH**, **Hyd1**, and **Hyd2**.

Compounds	Administration route	LD50 log10(mmol/kg)	LD50 (mg/kg)	Predicted toxicity class
INH	**Intraperitoneal (IP)**	0.354	309.600	**4**
	Intravenous (IV)	0.271	256.100	**4**
	Oral administration	0.817	899.70	**4**
	Subcutaneous (SC)	0.326	290.20	**4**
Hyd1	**Intraperitoneal (IP)**	0.552	1086.00	**5**
	Intravenous (IV)	-0.096	244.00	**4**
	Oral administration	0.775	1816.00	**4**
	Subcutaneous (SC)	0.432	823.40	**4**
Hyd2	**Intraperitoneal (IP)**	0.533	1179.00	**5**
	Intravenous (IV)	0.092	426.00	**5**
	Oral administration	0.455	984.60	**4**
	Subcutaneous (SC)	1.161	4999.00	**Non Toxic**

IV.1.3.3. Carcinogenicity prediction

One of the strategies for human health protection is the study and evaluation of chemicals carcinogenicity [89]. For this reason, the prediction of carcinogenicity has been discussed for a long time [90]. In order to predict the carcinogenicity of **INH** and its derivatives, results displayed in **Table 8**, reveal the carcinogenicity of **INH** with high active probability of 93%, whereas **Hyd1** exhibited inactive action with probability of 50%, **Hyd2** was predicted as active carcinogen with probability of 52%. From these results, it's remarkable the reduction in

the carcinogenicity when INH reacts with our carbonyl compounds. For **Hyd1**, predicted results indicate the absence of the carcinogenicity, and in **Hyd2**, reduction from 81% to 52% with a high difference of 31%.This indicates the importance of the condensation reaction of carbonyl compounds with INH. These results suggest that **INH** derivatives could be no or low carcinogens. From these results, it's clear that we introduce important modifications in the anti-tubercular drug **INH** structure.

Table 8. Carcinogenicity prediction of **INH**, **Hyd1**, and **Hyd2**.

Compounds	Prediction	Probability %
INH	**Active**	81
Hyd1	**Inactive**	50
Hyd2	**Active**	52

IV.1.3.4. Hepatotoxicity prediction

Drug induced hepatotoxicity is a fundamental problem in human health and drug development [91]. This adverse effect could be introduced directly by the drug or by their reactive metabolites [92]. Several studies indicated that **INH** metabolites are responsible for its hepatotoxicity [93]. Our results from hepatotoxicity prediction of the drug **INH** and its derivatives, demonstrate the high hepatotoxic effect of this drug with probability of 93%, whereas the derivatives **Hyd1** and **Hyd2** have low toxic effects, with probabilities of 51 and 61%, respectively. These results indicate reduction in the hepatotoxic effect of **INH** from 93% to 51% in **Hyd1**, with a considerable difference of 42% and from 93% to 61% in **Hyd2** with a difference of 32%. These results are given in **Table 9**.

Table 9. Hepatotoxicity prediction of **INH**, **Hyd1**, and **Hyd2**.

Compounds	Prediction	Probability %
INH	**Active**	93
Hyd1	**Active**	51
Hyd2	**Active**	61

IV.1.3.5. Mutagenicity prediction

Mutagenicity is defined as the induction of changes in genes and/or chromosomes that are permanent or transmissible in cells or organisms [94]. Probability of **INH** and its derivatives to introduce genetic changes showed total mutagenic effect of **INH** with probability of 100%. From **Hyd1** and **Hyd2**, the predicted results depicted in **Table 10** indicate inactivity of **Hyd2**

with probability of 56%, and reduction in the mutagenic effect from 100% to 71% in **Hyd1**. In the literature, studies indicated that the hepatotoxic effect of **INH** can lead to the genetic variations in enzymes in Asian populations (Caucasian population) [95]. These variations could be attributed to the interaction between **INH**-reactive metabolites with DNA.

Table 10. Mutagenicity prediction of **INH**, **Hyd1**, and **Hyd2**.

Compounds	Prediction	Probability %
INH	**Active**	100
Hyd1	**Active**	71
Hyd2	**Inactive**	56

The high mutagenic effect of **Hyd1** when it was detected in substructure prediction could be explained by the presence of nitro-aromatic fragment in the structure. In the biotransformation, aromatic nitro group is involved in enzymatic reduction, catalyzed by both cytosolic and microsomal enzymes, leading to the formation of aromatic hydroxylamine intermediate. Then, this intermediate is activated to nitronium ion intermediate that covalently bind to DNA and as a result causes mutation (**Figure 35**) [88].

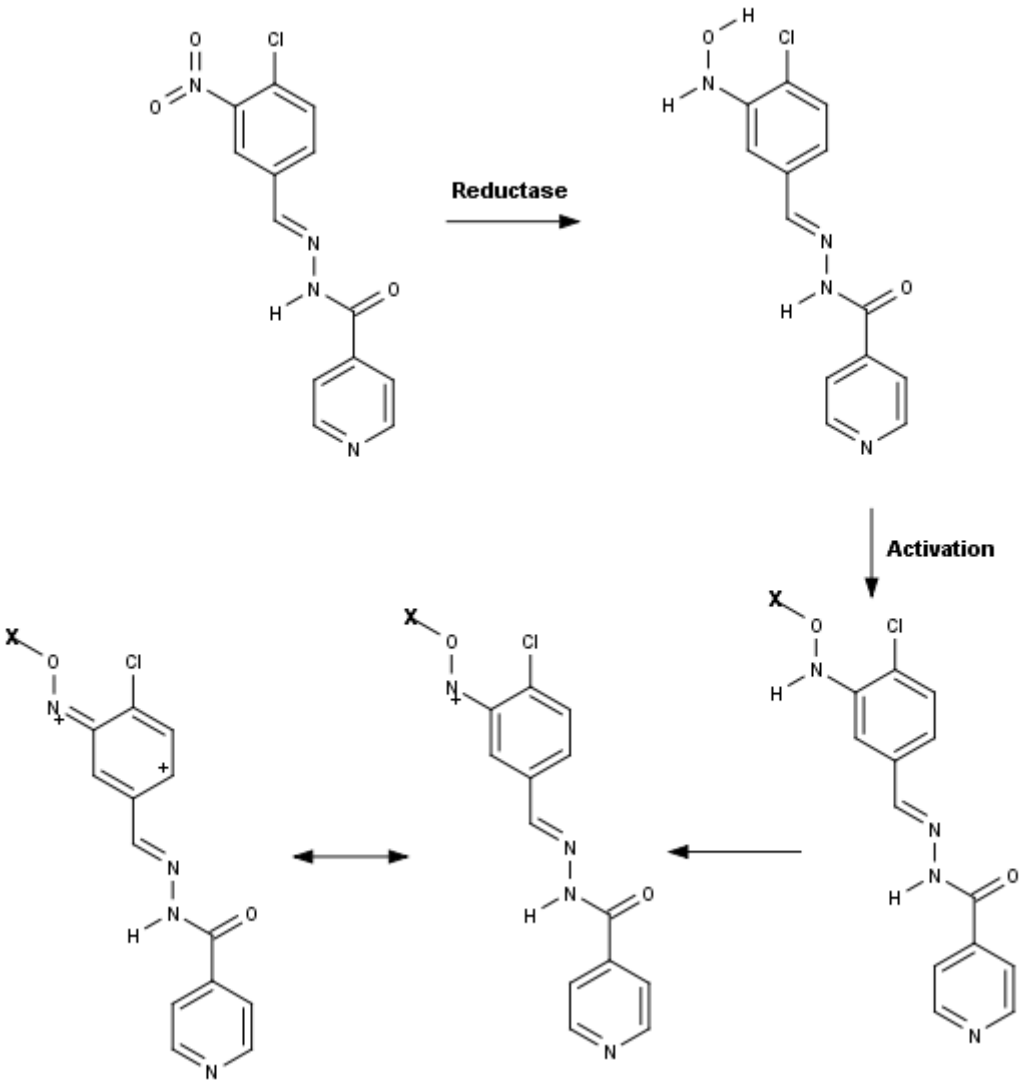

Figure 35. Proposed mechanism of **Hyd1** biotransformations to their reactive metabolite, nitrenium ion intermediate [88].

IV.1.3.6. Immunotoxicity prediction

Immunotoxicity, defined as the adverse effects of xenobiotics (immunotoxicants) on the immune system includes two main types: immunosuppression (decreased immuno competence) and inappropriate immunostimulation [96]. From the obtained results (**Table11**), **INH** and **Hyd2** don't have any toxic effect to the immune system with probability of 98 and 93%, respectively. Whereas, **Hyd1** has high immunotoxic effect with probability of 80%. This adverse effect could be due to the chemical structure of **Hyd1** and the presence of nitro group and chlorine atom attached to the aromatic ring, similar to *p*-chloronitrobenzene structure that reduces the numbers of NK, T, and B cells in spleen of mice and induces an increase of macrophage and nucleated erythrocyte numbers [97].

Table 11. Immunotoicity prediction of **INH, Hyd1** and **Hyd2**

Compounds	Prediction	Probability %
INH	**Inactive**	98
Hyd1	**Active**	80
Hyd2	**Inactive**	93

IV.1.3.7. Cytotoxicity prediction

In drug development, the cytotoxicity was estimated by the concentration of a drug that induces the death of half of cells in culture (LC_{50}) [98]. This type of toxicity was widely employed for testing the pharmaceutical formulations developed for gastrointestinal absorption and permeability of drugs [99]. The drug **INH** and its derivatives **Hyd1** and **Hyd2** were investigated for the cytotoxicity prediction; results in **Table 12** reveal the absence of cytotoxic effect of these compounds with inactivity percentage of 93.79 and 71%, respectively.

Table 12. Cytotoxicity prediction of **INH**, **Hyd1**, and **Hyd2**

Compounds	Prediction	Probability %
INH	**Inactive**	93
Hyd1	**Inactive**	79
Hyd2	**Inactive**	71

IV.1.3.8. Skin sensitization prediction

Reactivity profiles of chemical substances play an important role in their tendency to be allergic agents [100], and Skin sensitization is mainly steps in the inflammation process in allergic contact dermatitis [101]. Skin sensitization effect of **INH**, **Hyd1**, and **Hyd2** was predicted and compared with that of **AA** [102]. At first, skin sensitization was predicted by P value calculation using E_{HOMO} (Hartree). These results, listed in **Table 13**, show low sensitizer effect of both **Hyd1** and **Hyd2** with P values of 1.2305 and 1.5655, respectively, when compared with **AA** which has a P value of 0.4301.

Table 13. P values and predicted sensitization effect of **INH**, **Hyd1**, **Hyd2**, and **AA**.

Compound	E_{HOMO}	P values	Skin sensitization
INH	–0.2159	1.7767	Sensitizer
Hyd1	–0.2516	1.2305	Sensitizer
Hyd2	–0.2297	1.5655	Sensitizer
AA	–8.270	0.4301	Non-Sensitizer

In addition, results from this investigation shown in **Table 14**, predict the effect of investigated compounds towards human skin, murine local lymph node, direct peptide, human cell line, and KeratinoSens™. These results reveal that **Hyd1** exhibits sensitizer effect on human skin, in murine local lymph node, direct peptide, human cell line and, KeratinoSens™ with probability of 70, 50, 90, 80, and 90%, respectively. Whereas, **Hyd2** and **INH** induce sensitizer effect in all tests except in murine local lymph node assay with probability of 60% and 50%, respectively. On the other hand, results displayed in **Figures 36, 37**, and **38** explain the results in **Table 14**. These Figures indicate the atoms or the fragments that contributed to the sensitizing effect.

Table 14. Skin sensitization predictions of **Hyd1**, **Hyd2**, **INH**, and **AA**.

Compounds	Human skin sensitization	Murine local lymph node assay (LLNA)	Direct peptide reactivity assay (DPRA)	Human cell line activation test (h-CLAT)	KeratinoSens™
Hyd1	Sensitizer 70%	Sensitizer 50%	Sensitizer 90%	Sensitizer 80%	Sensitizer 90%
Hyd2	Sensitizer 70%	Non-Sensitizer 60%	Sensitizer 90%	Sensitizer 80%	Sensitizer 80%
INH	Sensitizer 70%	Non-Sensitizer 50%	Sensitizer 80%	Sensitizer 80%	Sensitizer 80%
AA	Non-Sensitizer 50%	Non-Sensitizer 90%	Sensitizer 80%	Sensitizer 70%	Sensitizer 70%

In this respect, green atoms or fragments represent an increase in skin sensitization potential, pink fragments represent a decrease in skin sensitization potential, and gray fragments do not contribute to skin sensitization.

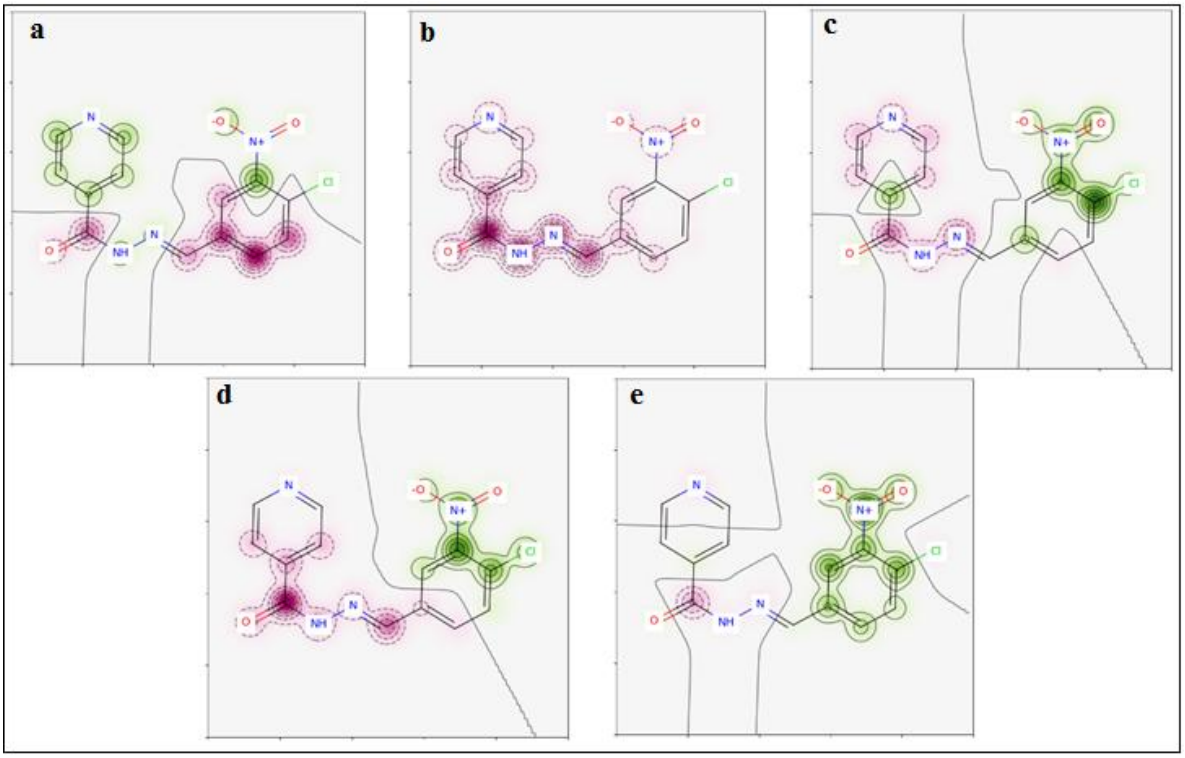

Figure 36. Effect of **Hyd1** on: **a**). Human skin sensitization**, b).** Murine local lymph node assay (LLNA)**, c).** Direct peptide reactivity assay (DPRA)**, d).** Human cell line activation test (h-CLAT), and **e).** KeratinoSens^{TM}.

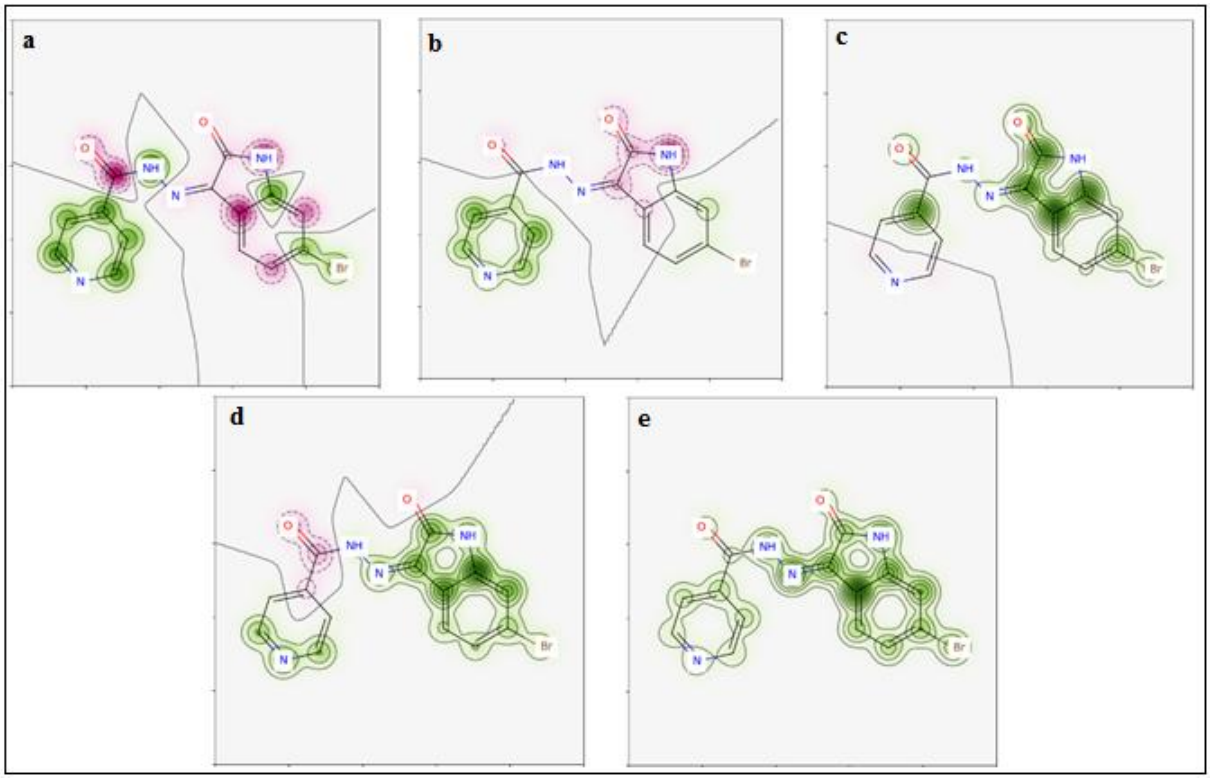

Figure 37. Effect of **Hyd2** on: **a**). Human skin sensitization, **b).** Murine local lymph node assay (LLNA), **c).** Direct peptide reactivity assay (DPRA), **d).** Human cell line activation test (h-CLAT), and **e).** KeratinoSens^{TM}.

Skin sensitization can be the result of electrophilic-nucleophilic reactions between chemicals and skin proteins [103], which permit chemicals to be incorporated in proteins structure. Electrophilic character of **Hyd1** was established by LUMO energy, electrophilicity index, and electron affinity; these parameters suggest that **Hyd1** acts as a Lewis acid [104], electron-acceptor, and as a sensitizer agent. **Hyd1** is more electrophilic than **Hyd2** and **INH** which explains the higher sensitizer effect. On the other hand, the reaction mechanism of skin sensitizers was classified as Michael acceptors (MA), S_N2 electrophiles, S_NAr electrophiles, Schiff base formers, or acylation agents [105]. From this classification, and due to the presence of an electron-withdrawing groups ($-NO_2$ and -Cl) attached to an aromatic ring, **Hyd1** can act as a S_NAr electrophile. Other results of **AA** and **INH**, which are a sensitizer to the direct peptide, Human cell line, and KeratinoSens™, as shown in **Figures 38** and **39.**

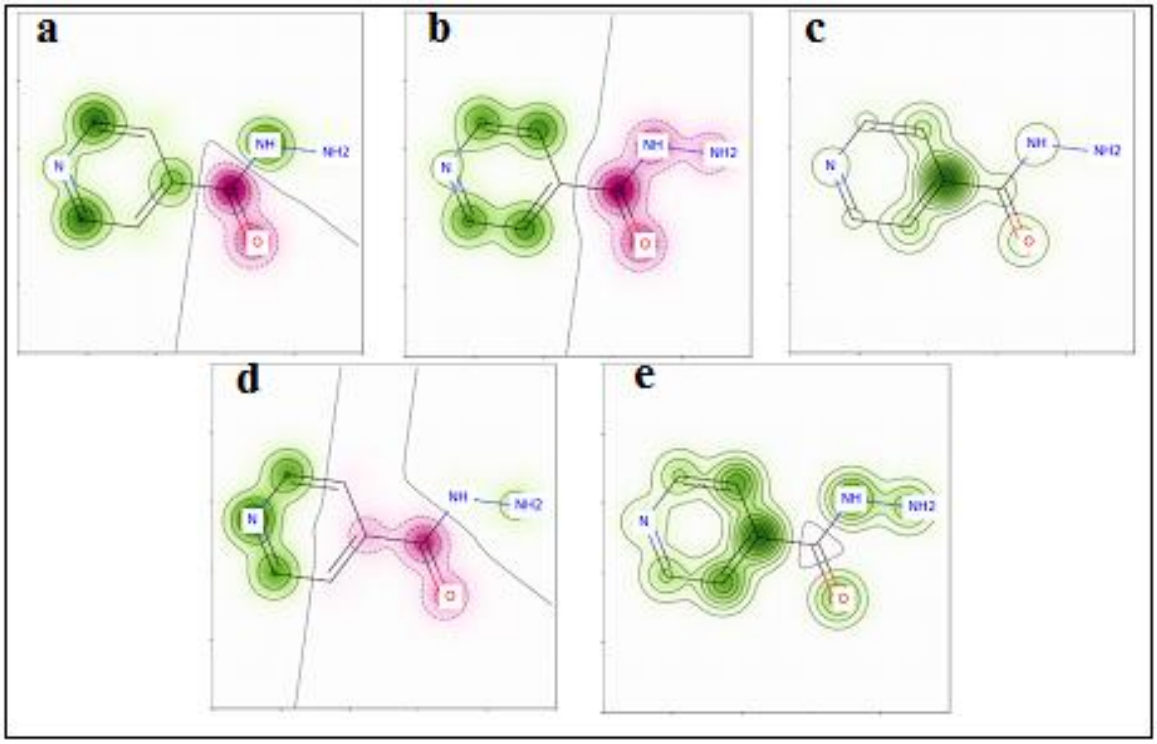

Figure 38. Effect of **INH** on: **a).** Human skin sensitization, **b).** Murine local lymph node assay (LLNA), **c).** Direct peptide reactivity assay (DPRA), **d).** Human cell line activation test (h-CLAT), and **e).** KeratinoSens™.

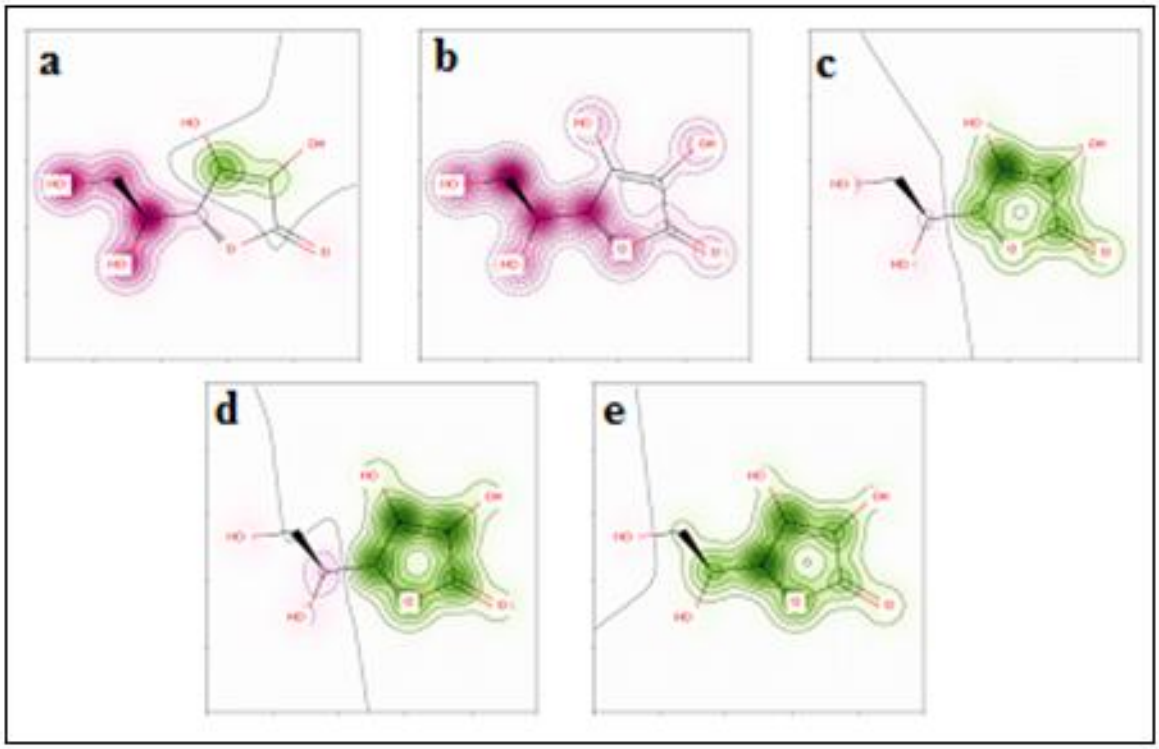

Figure39. Effect of **AA** on: **a).** Human skin sensitization**, b).** Murine local lymph node assay (LLNA**), c).** Direct peptide reactivity assay (DPRA), **d).** Human cell line activation test (h-CLAT), and **e).** KeratinoSens™.

IV.1.4. *In silico* anti-tubercular activity evaluation

According to World Health Organization statistics, tuberculosis is the principle infectious disease responsible of mortality in the word [106], which leads to search of potential anti-tubercular drugs [107]. In this context, the computational study is the essential step for the designing of new efficient drugs. The hydrazones **Hyd1** and **Hyd2** were investigated for these effects. The predicted results (**Figure 40**) were compared with the anti-tubercular drugs **INH**, and indicated excellent effects of both hydrazones with probabilities of anti-tubercular effects of 84.6 and 83.9% from **Hyd1** and **Hyd2**, respectively, while the standard anti-tubercular drug **INH** has the probability of 81.3 %. These results showed that the synthesized hydrazones have higher effect than **INH**. These results are in good agreement with the literature precedent investigations, which showed that hydrazones derived from **INH** have a similar or improved effect than the drug itself [108].

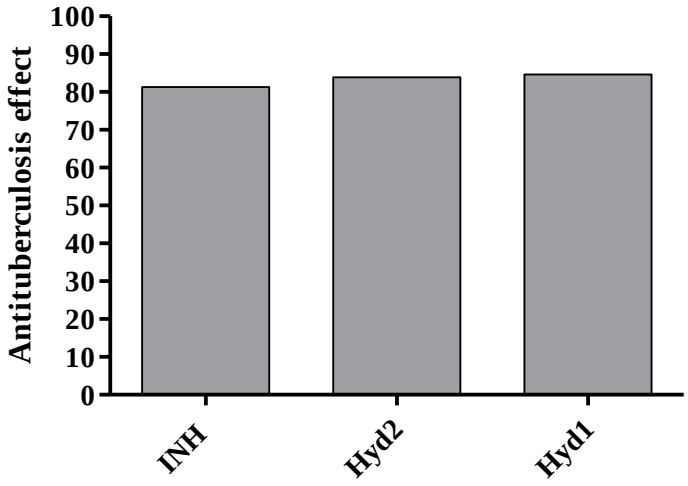

Figure 40. Anti-tubercular activity prediction of **Hyd1** and **Hyd2**

IV.1.4.1. Molecular docking

Molecular docking study was performed to predict the possible binding modes and to rationalize the observed biological activity [109]. In order to comprehend the mechanism of action of the new hydrazones, the active molecules were subjected to molecular docking studies against InhA which is considered as a promising target for the discovery of novel anti-tubercular drugs [110]. The molecular docking studies of active compounds were accomplished against the active site of InhA enzyme structure (PDB code: 4DRE) using SwissDock server. FullFitness and Gibbs free energy (ΔG) were evaluated. Favorable binding modes were scored based on FullFitness and cluster formation. Ranking of the cluster was accomplished using the value of FullFitness. As shown in **Table 15,** the clustering results obtained from the docking of the investigated hydrazones into InhA enzyme. **Hyd1** and **Hyd2** showed FullFitness values of –1084.565 and 1073.307 kcal/mol and estimated ΔG of –7.187 and –7.889 kcal/mol, respectively, for the most favorable interaction. While, **INH** showed FullFitness of –1088.536 kcal/mol and ΔG value of 6.458 kcal/mol. These results indicate that **Hyd2** had the highest anti-tubercular activity with the lowest energy ΔG.

The best poses obtained using SwissDock server for the synthesized compounds binding to enoyl ACP reductase (InhA) enzyme are presented in **Figure 41**, which showed different interactions traduced by H-bonds (green color). It's clear that **Hyd2** has the high number of H-bonds; O of the indoline ring, N of azomethine group, O of amide function and N of pyridine ring. **Hyd1**possess two centers of interaction; O of the amide and O of the nitro group.

Table 15. Clustering results obtained from the docking of **INH**, **Hyd1**, and **Hyd2** into InhA.

Compounds	Cluster rank	Fullfitness kcal/mol	Estimated ΔG kcal/mol
Hyd1	**1**	–1084.565	–7.187
	2	–1084.455	–7.141
	3	–1071.394	–7.142
	4	–1068.268	–7.138
	5	–1068.057	–6.999
Hyd2	**1**	–1073.307	–7.889
	2	–1072.840	–7.979
	3	–1069.943	-7.432
	4	–1069.051	–7.625
	5	–1068.451	–7.874
INH	**1**	–1088.536	–6.458
	2	–1086.227	–6.157
	3	–1083.790	–6.073
	4	–1083.735	–6.068
	5	–1079.096	–6.104

The standard drug **INH** has two interaction centers of H-bonds, O of amide and N of hydrazine function.

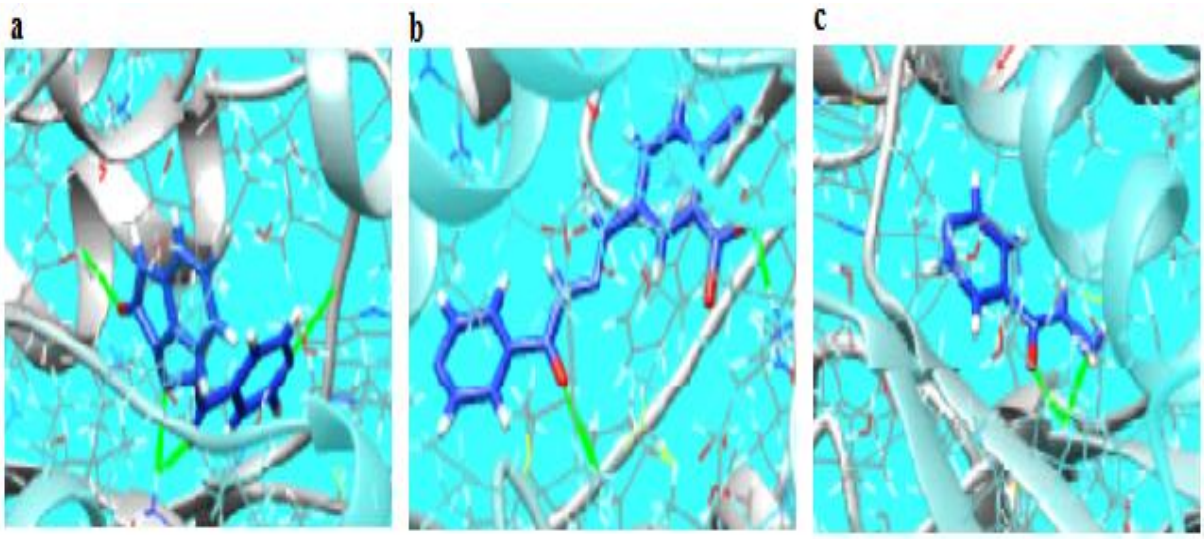

Figure 41. Visualization of binding of: **a**) **Hyd2**, **b**) **Hyd1**, **c**) **INH**, to enoyl ACP reductase (InhA) enzyme (PDB code: 4DRE), Visualization is performed using UCSF Chimera.

IV.1.5. *In silico* biodegradability prediction

Numerous chemicals in our lives can be considered as pollutants; these chemicals accumulate in the environment, interact with the biological systems, and can be harmful. In bioremediation, living organisms degrade hazards materials to less toxic compounds. In this context, the method of using fungi as a bioremediation method to clean up the environmental pollutants can be an option [111]. Another biodegradability method is the ability of soil bacteria to decompose organic matter by extracellular enzymes production, and can facilitate and accelerate the mineralization process [112], [113]. Presented in **Figure 42**, are molecules associated with the biodegradation and products [114].

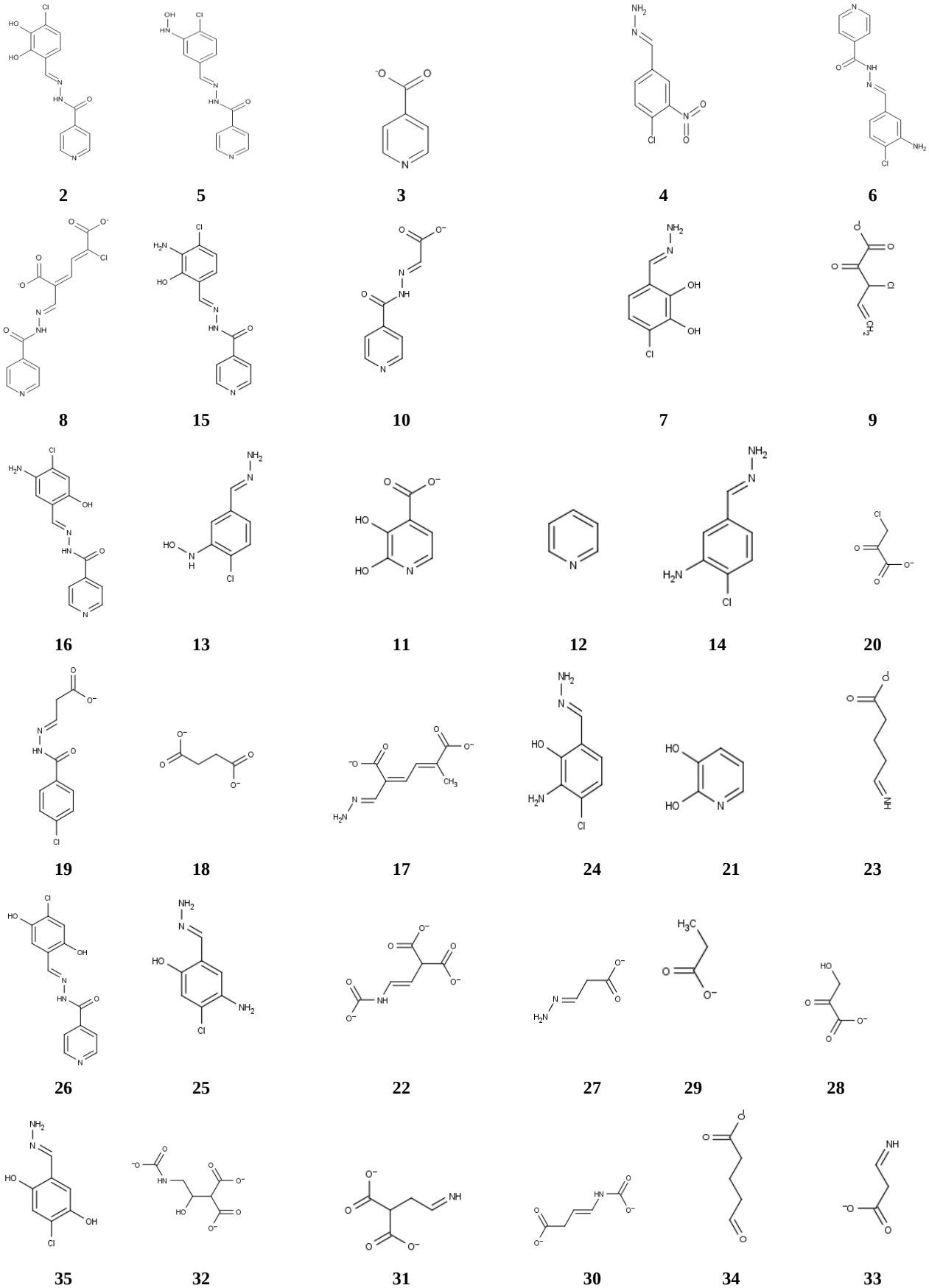

Figure 42. Biodegradation products of **Hyd1**

Part 2 : *Chemistry and Biological studies*

IV.2. Chemistry and biological studies

In this part, we are particularly interested in the synthesis and characterization of two hydrazones from the antitubercular drug **INH,** which are obtained by a simple reaction of condensation. These **INH**-derivatives are among the compounds that have various interests in the field of organic synthesis and in medicinal chemistry. For these reasons, the synthesized hydrazones were investigated for their toxicity twards microrganisms (bacteria and fungus) and animals (using mice), and for their antioxidant *in vitro* (against superoxide anion radical and hydrogene peroxide) and against oxidative stress *in vivo* (induced by **INH**). They were also investigated for their hepatoprotective effect (against **INH**-hepatotoxicity).

IV.2.1. Chemistry

Both hydrazones; (N'-[(*E*)-(4-chloro-3-nitrophenyl)methylidene] pyridine-4-carbohydrazide (**Hyd1**)**;** and N'-[(3*Z*)-6-bromo-2-oxo-2,3-dihydro-1*H*-indol-3-ylidene]pyridine-4-carbohydrazide (**Hyd2**); were prepared under glacial acetic acid catalysis, in a single step and in high yields, from the condensation reaction of **INH** with 4-chloro-3-nitrobenzaldehyde for **Hyd1** and with 6-bromoindoline-2,3-dione for **Hyd2**, respectively.

IV.2.1.1. Mechanisms of formation

Condensation reaction between hydrazine (**INH**) and aldehyde (4-chloro-3-nitrobenzaldehyde) or ketone (6-bromoindoline-2,3-dione) was catalyzed by acetic acid. Generally, reaction starts by a proton-catalyzed attack of the α-effect nucleophile (**INH**) on the carbonyl carbon atom of electrophile (4-chloro-3-nitrobenzaldehyde or 6-bromoindoline-2,3-dione). Upon proton transfer, tetrahedral intermediate (hemiaminal) was formed. This intermediate can undergo dehydration *via* protonation of the hydroxyl function and subsequent elimination of water. The resulting protonated intermediate is represented by two resonance forms. The final deprotonation yields both hydrazones [1]; **Hyd1 (Figure 43)** and **Hyd2 (Figure 44)**.

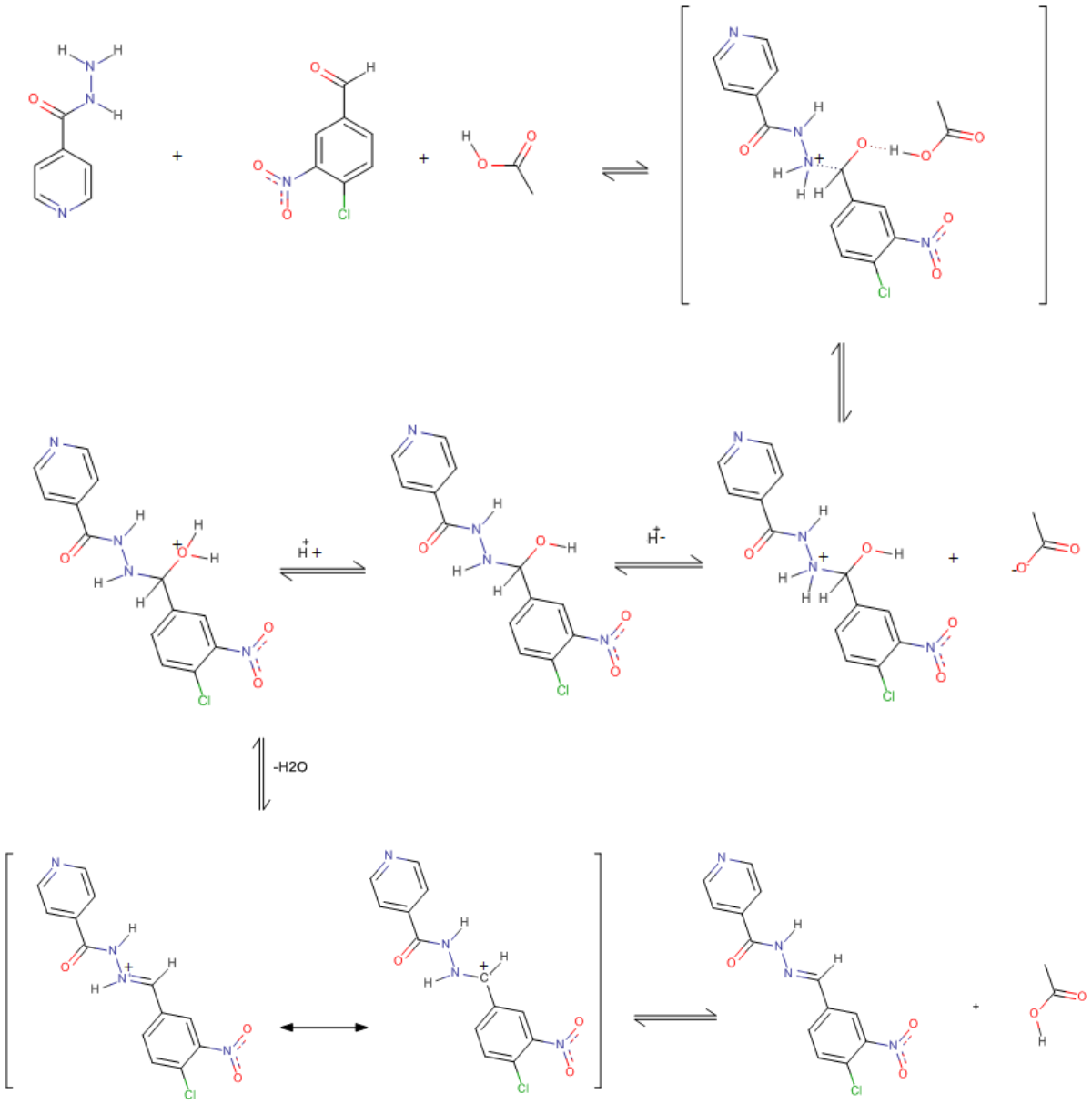

Figure 43. Proposed mechanism of formation of **Hyd1** [1]

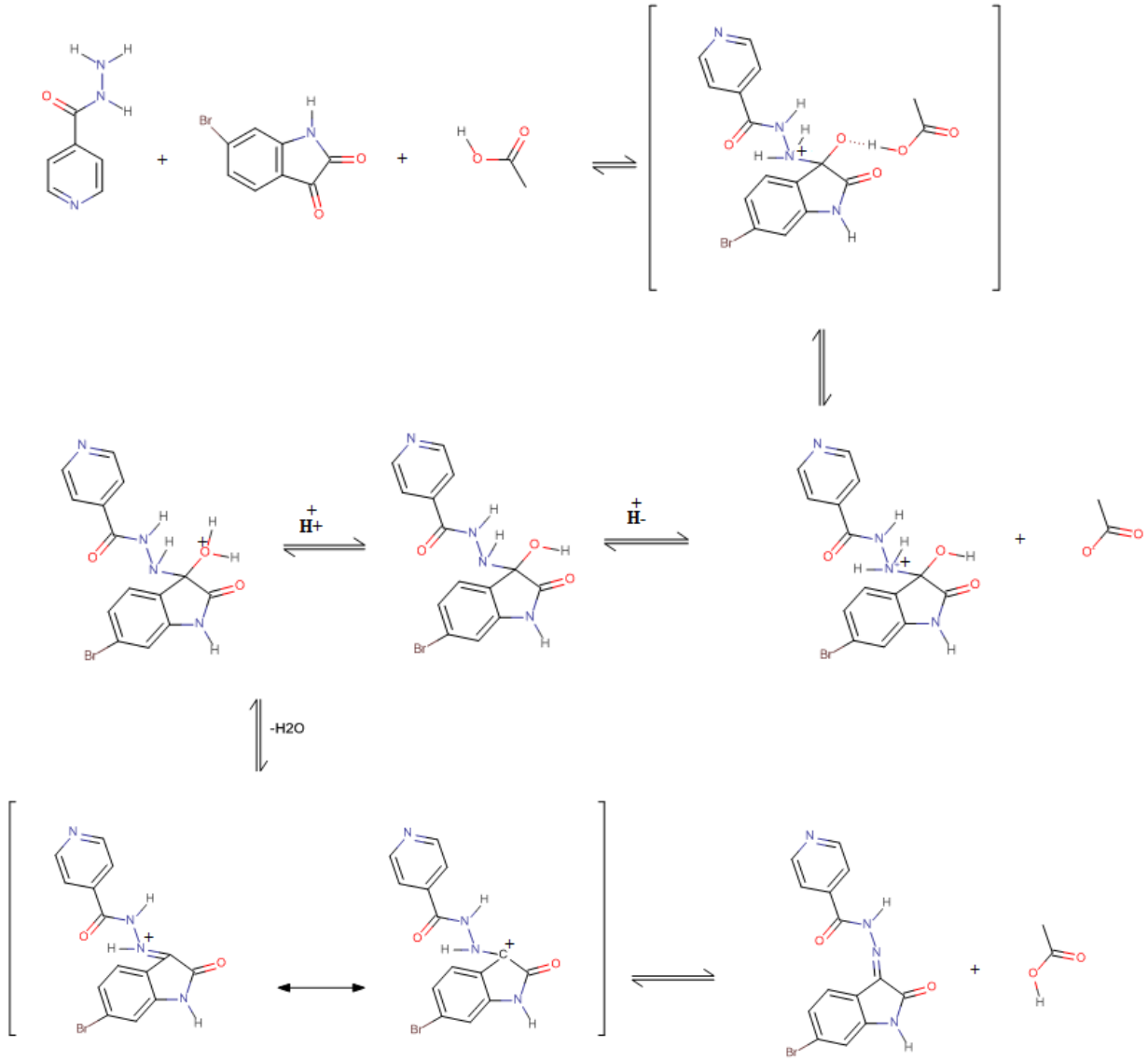

Figure 44. Proposed mechanism of the formation of **Hyd2** [1]

IV.2.1.2. Identification and characterizations

IV.2.1.2.1. Melting point determination

Melting points are listed with the physical appearance and the yields of the synthesized hydrazones in **Table 16**. These data confirm the purity of the investigated compounds.

IV.2.1.2.2. Thin layer chromatography (TLC)

TLC has been employed using the system (ethyl acetate/n-hexane: 9/1) to check the progress of reaction and purity of prepared compounds. The recorded Rf values of the synthesized compounds are listed in **Table 16**.

Table 16. Yields, physical appearance, uncorrected melting points, and Rf values **Hyd1** and **Hyd2**.

Compounds	Physical appearance	Yield (%)	Melting point (°C)	R_f
Hyd1	Yellowish crystals	85	234–235	0.63
Hyd2	Red powder	81	309–310	0.57

IV.2.1.2.3. Infrared spectra

The Fourier transform infrared (FT-IR) spectra of the synthesized hydrazones demonstrated the characteristic absorption bands of the functional groups present in each compound as shown in **Figures 45** and **46.** The observed values of the characteristic absorption bands of these spectra and their interpretation are checked and discussed according to Silverstein [115] and Shriner [116] (**Table 17**).

For **Hyd1**, the strong absorption bands at 1523 and 1681 cm^{-1} are assigned to the azomethine (-C=N-NH) and the carbonyl groups of amide function (O=C-NH), respectively. The band at 3013 cm^{-1} is attributed to the aromatic (C-H) stretching vibration, whereas the one at 3196 cm^{-1} is due to (N-H) symmetrical stretching vibration of secondary amide. For **Hyd2** the strong absorption band at1590–1525 cm^{-1} is assigned to the azomethine group (-C=N-NH), whereas the band at 1700–1671 cm^{-1} is ascribed to (C=O) stretching vibration of amide function (O=C-NH). On the other hand, the absorption peaks at 3010 and 3161cm^{-1} are attributed to the aromatic (C-H) stretching vibration and the amine group (N-H) symmetrical stretching vibration of secondary amide, respectively.

Table 17. Characteristic IR bands of **Hyd1** and **Hyd2**

Compounds	IR (KBr cm^{-1})				
	N-H	$C-H_{aromatic}$	C-N	O=C-NH	-C=N-NH
Hyd1	3196	3013	1473	1681	1523
Hyd2	3161	3010	1473	1700-1671	1590-1525

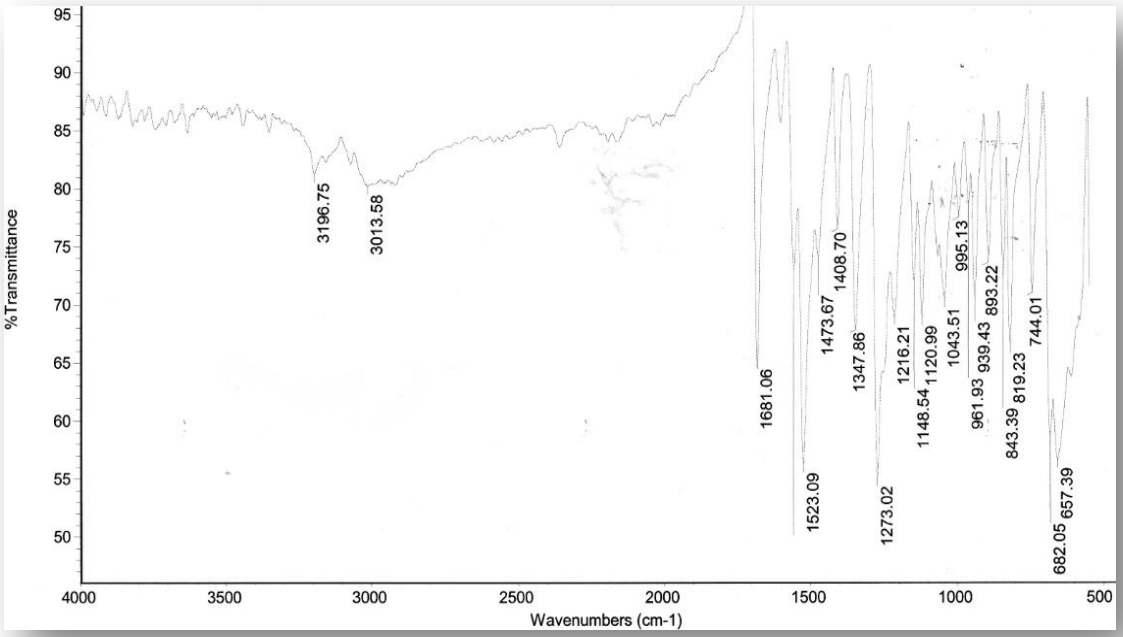

Figure 45. FT-IR spectrum of **Hyd1**

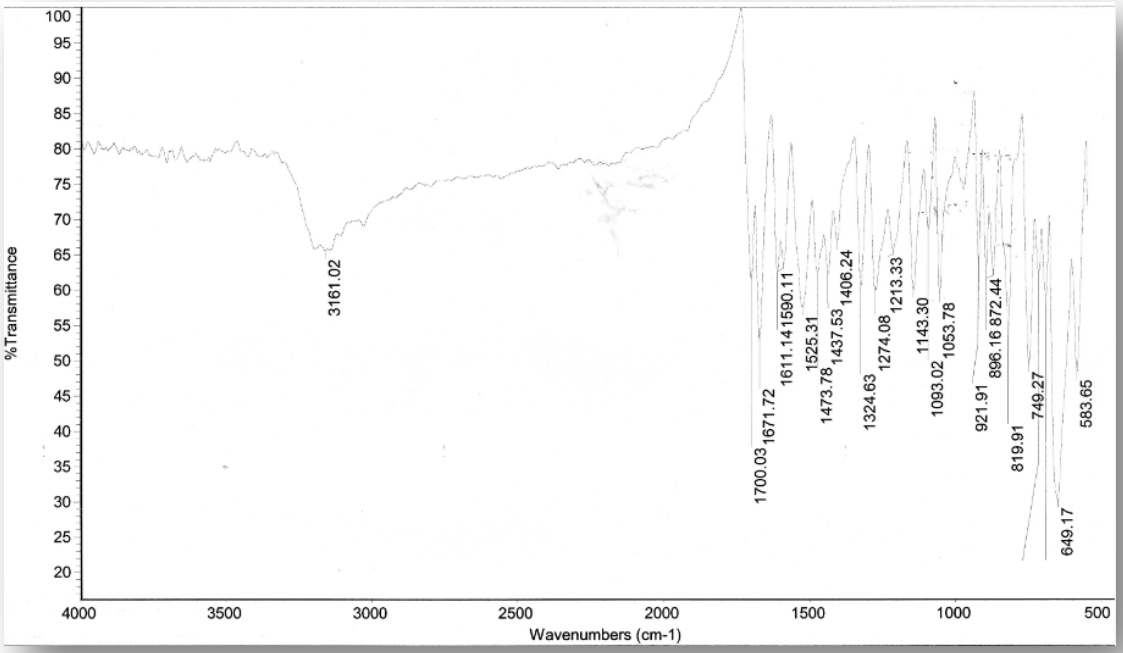

Figure 46. FT-IR spectrum of **Hyd2**

IV.2.1.2.4. Electronic spectra

The UV-visible spectrum (**Figure 47**) of **Hyd1** recorded in DMF shows two bands at 277 and 335 nm. The first band can be attributed to π-π* transition within the aromatic ring, whereas the second band could be due to n-π* transition within -C=N-N-H group. In addition, the UV-

visible spectrum of **Hyd2** (**Figure 47**) recorded in DMF, showed two bands at 275 and 305 nm. The first band can be ascribed to π-π* transition within the aromatic ring, whereas the second band could be due to n-π* transition within -C=N-N-H group.

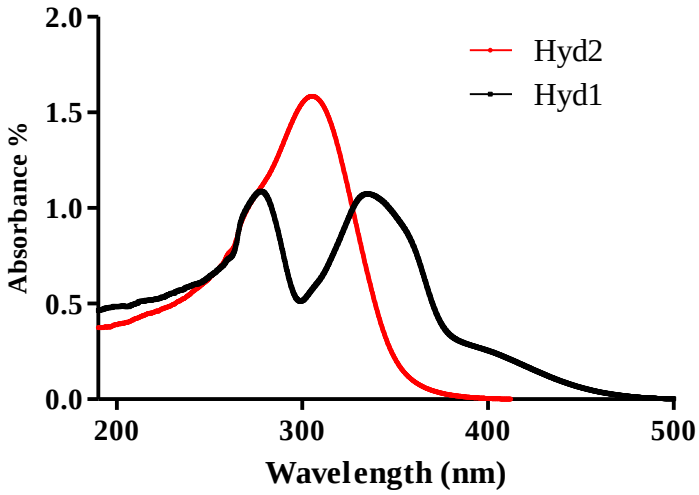

Figure 47. Electronic spectra of **Hyd1** and **Hyd2** in DMF

IV.2.1.2.5. Elemental analysis

Elemental analyses of the synthesized hydrazones were performed to confirm their molecular weights. The obtained results are presented in the **Table 18**, which are in excellent agreement with the calculated molecular weights.

Table 18. Elemental analyses of **Hyd1** and **Hyd2**

Compounds	Molecular formula	Molecular weight (g/mol)	Value type	C %	H %	N %
Hyd1	$C_{13}H_9ClN_4O_3$	304.03	**Calculated**	51.25	2.98	18.39
			Found	51.11	2.94	18.27
Hyd2	$C_{14}H_9BrN_4O_2$	343.99	**Calculated**	48.72	2.63	16.23
			Found	48.18	2.59	16.13

IV.2.1.2.6. NMR spectrum

a. NMR spectrum of Hyd1

The ^{1}H-NMR spectrum of the **Hyd1** (**Figure 48, 49**) shows a multiplet at 7.84–8.52 ppm, corresponding to the aromatic ring protons of the phenyl and pyridine moieties[117], a singlet at 8.42 ppm attributed to the proton (H_6) of the azomethine group, a singlet at 12.33 ppm due to the amide proton (H_5), a doublet at 7.84 ppm (J = 9.0 Hz) attributed to the protons (H_3 and

H_4), a doublet at 7.87 ppm (J = 16.8 Hz) ascribed to the proton (H_7), a doublet at 8.08 ppm (J = 16.7 Hz) due to the proton (H_8), a singlet at 8.52 ppm s attributed to the proton (H_9), and a doublet at 8.81 ppm ascribed to the protons (H_1 and H_2).

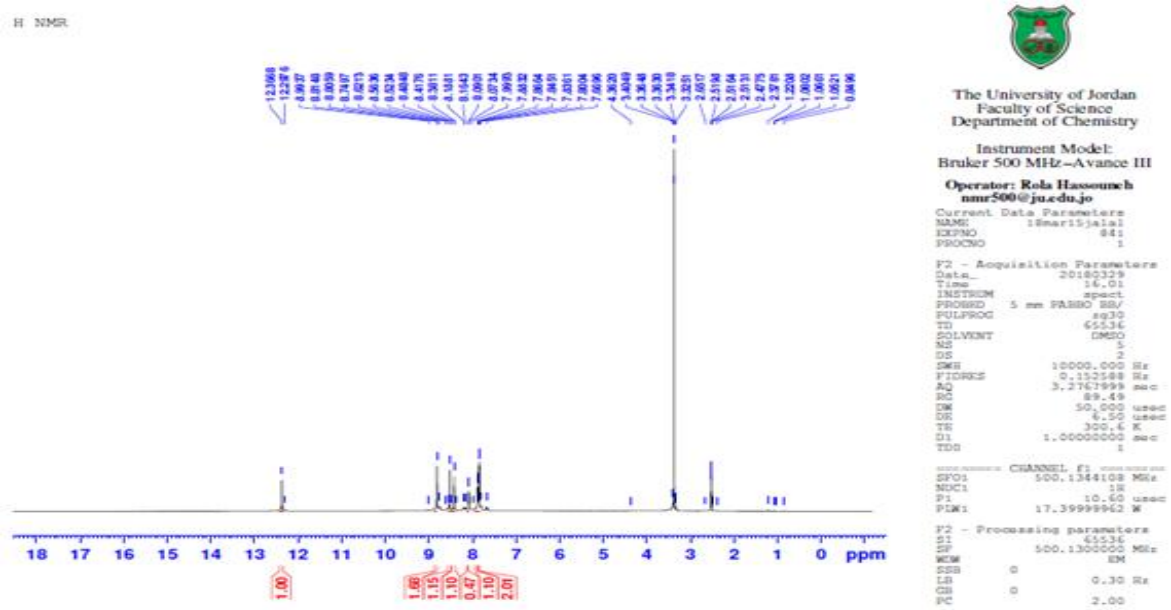

Figure 48. ^{1}H-NMR spectrum of **Hyd1;** (DMSO-d_6)

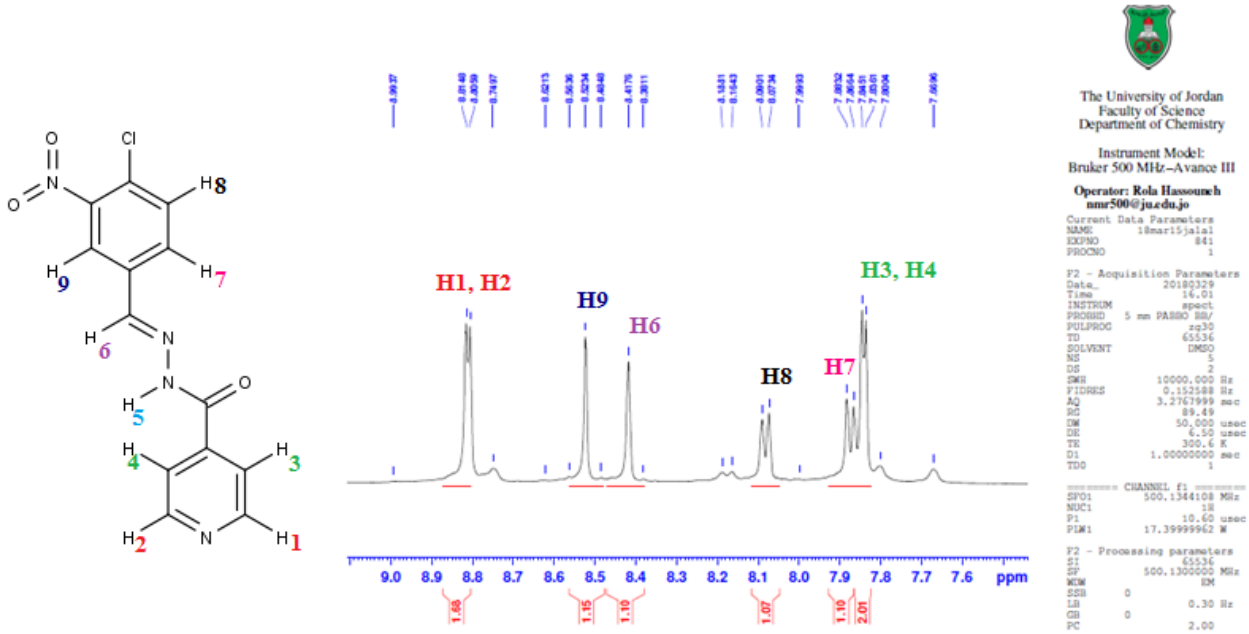

Figure 49. ^{1}H-NMR spectrum of **Hyd1** (7.6-8.9 ppm) (DMSO-d_6)

^{13}C-NMR chemical shifts of **Hyd1** are given in **Table 19**:

Table 19. ^{13}C-NMR of **Hyd1**

δ (ppm)	Attribution
162.4	Carbon (C_6) of the amide group
150.8	**Both carbon of pyridin ring (C_1 and C_2)**
148.4	Carbon (**C_5**)
146.0	**Carbon (C_7)**
140.6	Carbon (**C_{12}**)
135.2	Carbon (**C_8**)
132.7	**Carbon (C_9)**
132.1	**Carbon (C_{10})**
126.6	Carbon (**C_{11}**)
124.2	**Both carbon of pyridin ring (C_3 and C_4)**
122.0	**Carbon (C_{13})**

Bold values are of DEPT 135 (C-H) (**Figure 52**).

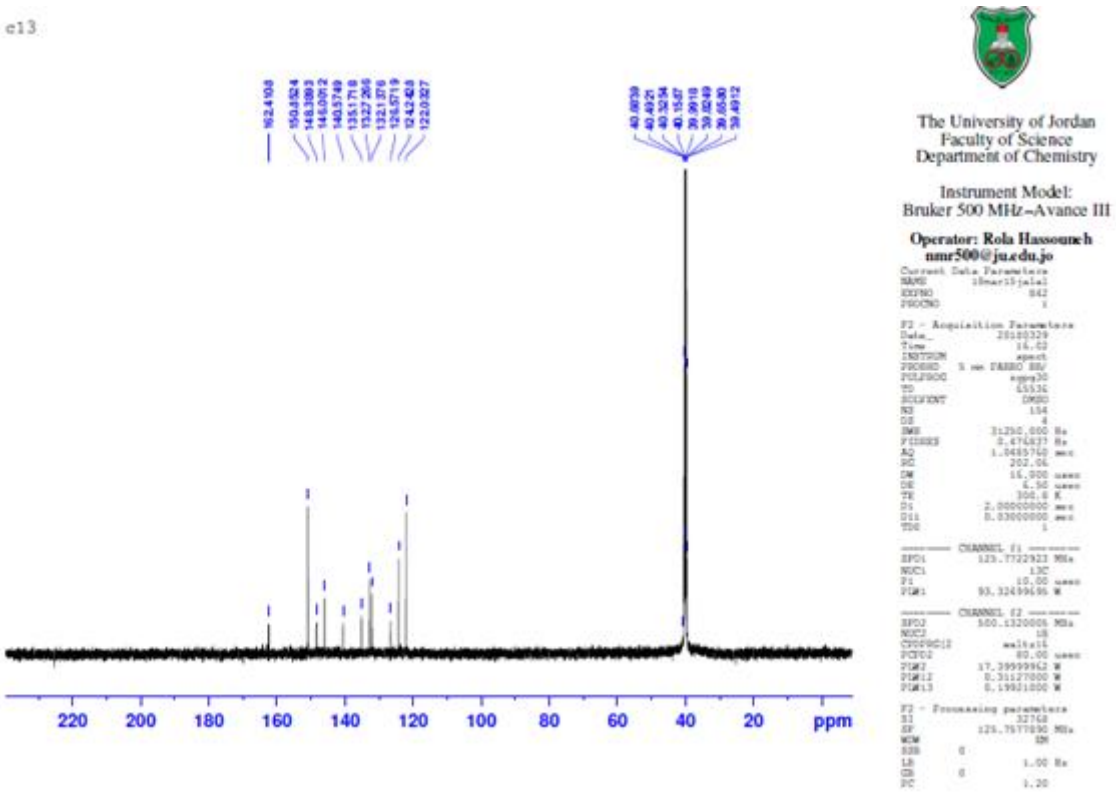

Figure 50. ^{13}C-NMR spectrum of **Hyd1**(DMSO-d_6)

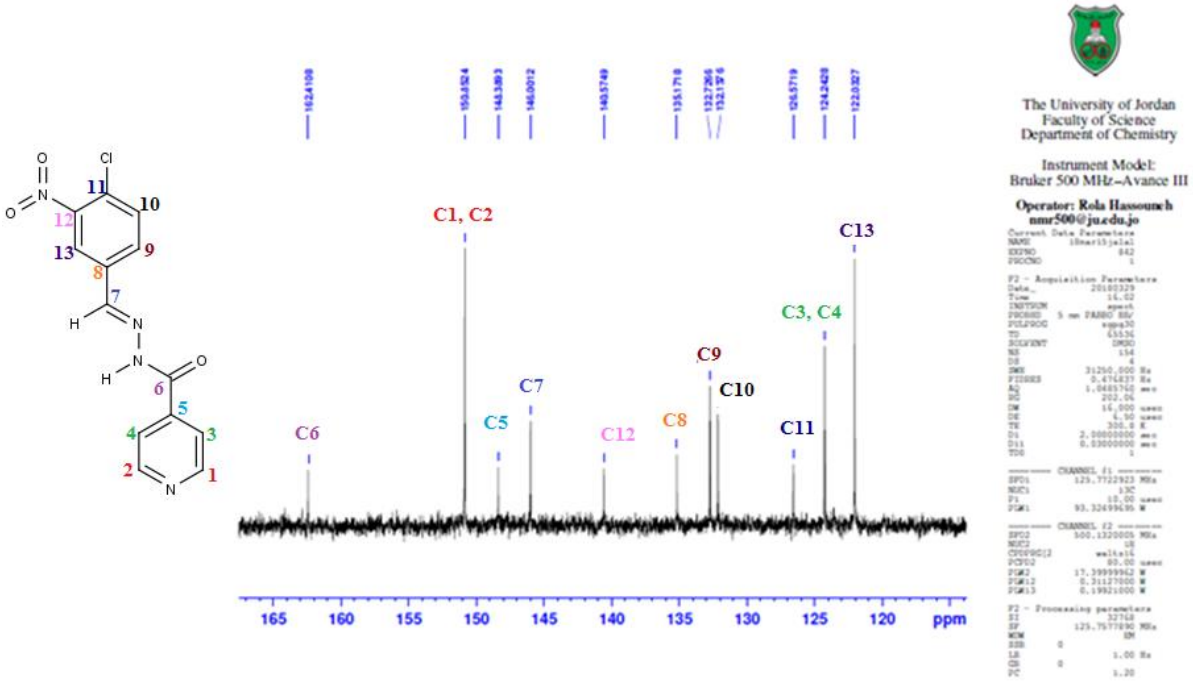

Figure 51. ^{13}C-NMR spectrum of **Hyd1** (120-165 ppm) (DMSO-d_6)

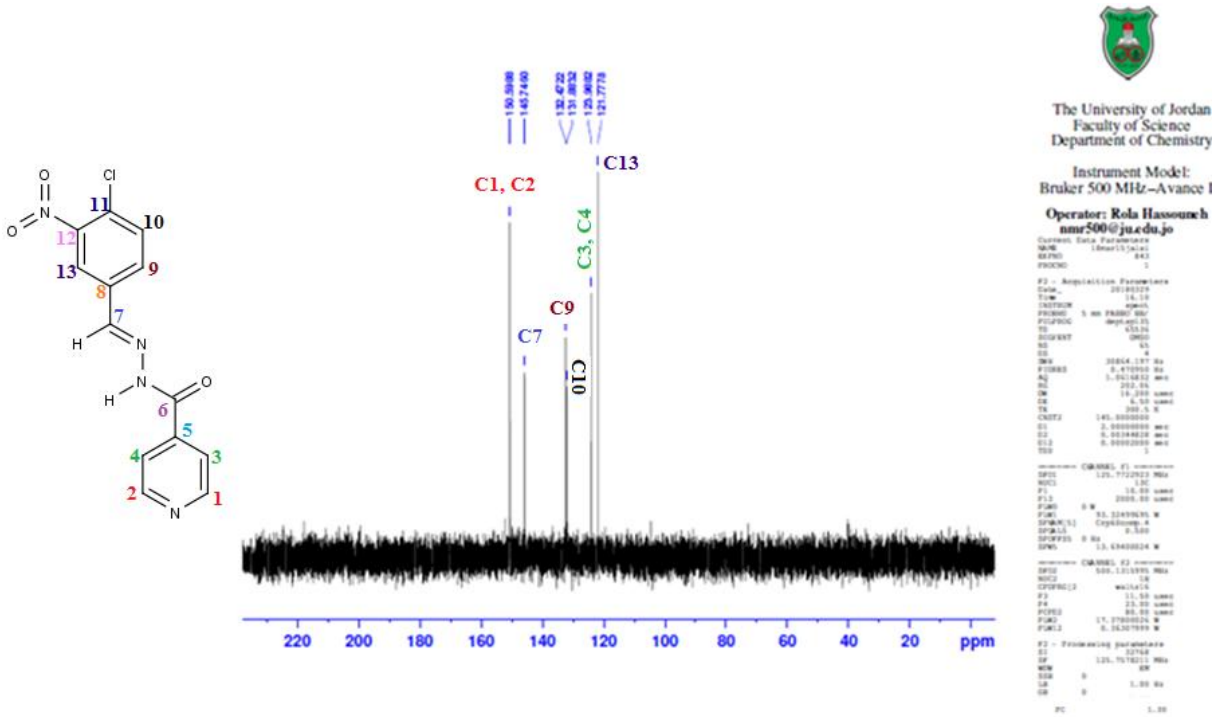

Figure 52. DEPT 135 spectrum of **Hyd1** (DMSO-d_6)

b. NMR spectrum of Hyd2

The ^{1}H-NMR spectrum of **Hyd2** (**Figure 53**) shows a multiplet at 7.12–8.85 ppm, corresponding to the aromatic ring protons of the phenyl and indoline 2,3-dione moieties [118]; a singlet at 13.74 ppm attributed to the proton (H_9) of the cyclic amide, a singlet at 11.44 ppm due to the aliphatic amide proton (H_5), a doublet of doublet at 8.85 ppm (J= 4.41,

1.63 Hz) attributed to the protons (H_1 and H_2), a doublet of doublet at 7.77 ppm (J = 4.39, 1.68 Hz) ascribed to the protons (H_3 and H_4), a doublet at 7.52 ppm (J = 8.03 Hz) due to the proton (H_6), a doublet at 7.12 ppm was attributed to the proton (H_7), and a doublet at 7.29 ppm ascribed to the protons (H_8).

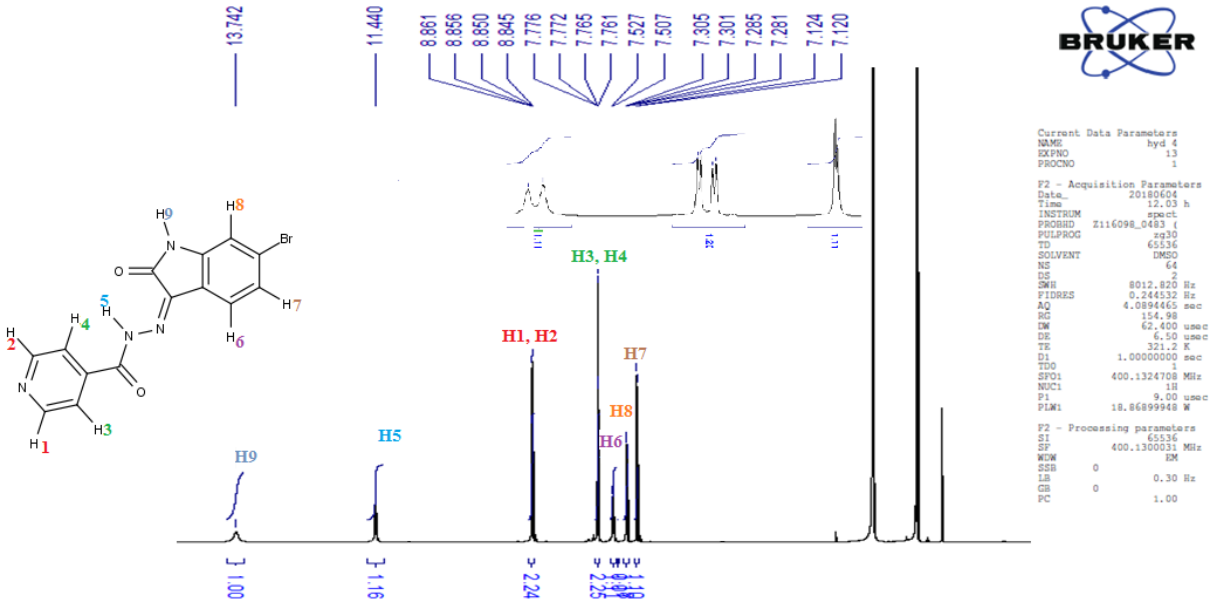

Figure 53. ^{1}H-NMR spectrum of **Hyd2** (DMSO-d_6)

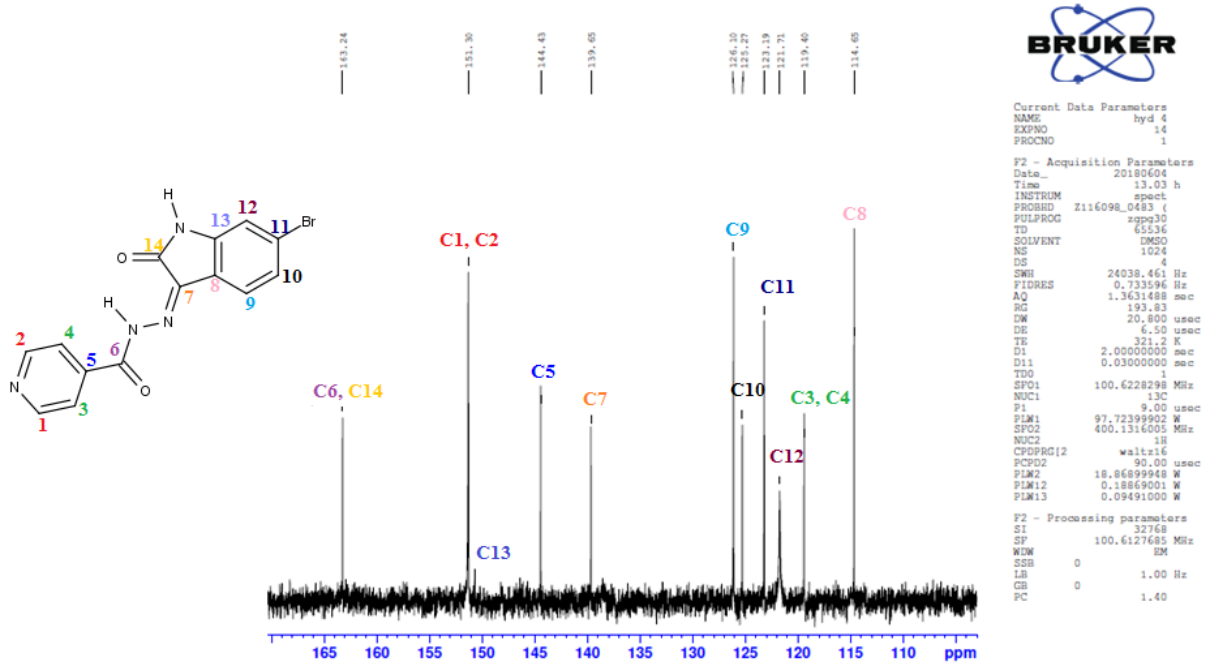

Figure 54. ^{13}C-NMR spectrum of **Hyd2** (114 to 165 ppm) (DMSO-d_6)

^{13}C-NMR chemical shift of **Hyd2** is summarized in **Table 20**.

Table 20. ^{13}C-NMR of **Hyd2**

δ (ppm)	Attribution
163.24	Both carbon of amides (**C_{14}**and **C_6**)
151.30	Both carbon of pyridin ring (**C_1**and **C_2**)
150.68	Carbon (**C_{13}**)
144.43	Carbon (**C_5**)
139.65	Carbon (**C_7**)
126.27	Carbon (**C_9**)
125.27	Carbon (**C_{10}**)
123.19	Carbon (**C_{11}**)
121.7	Carbon (**C_{12}**)
119.4	Both carbon of pyridin ring (**C_3**and **C_4**)
114.64	Carbon (**C_8**)

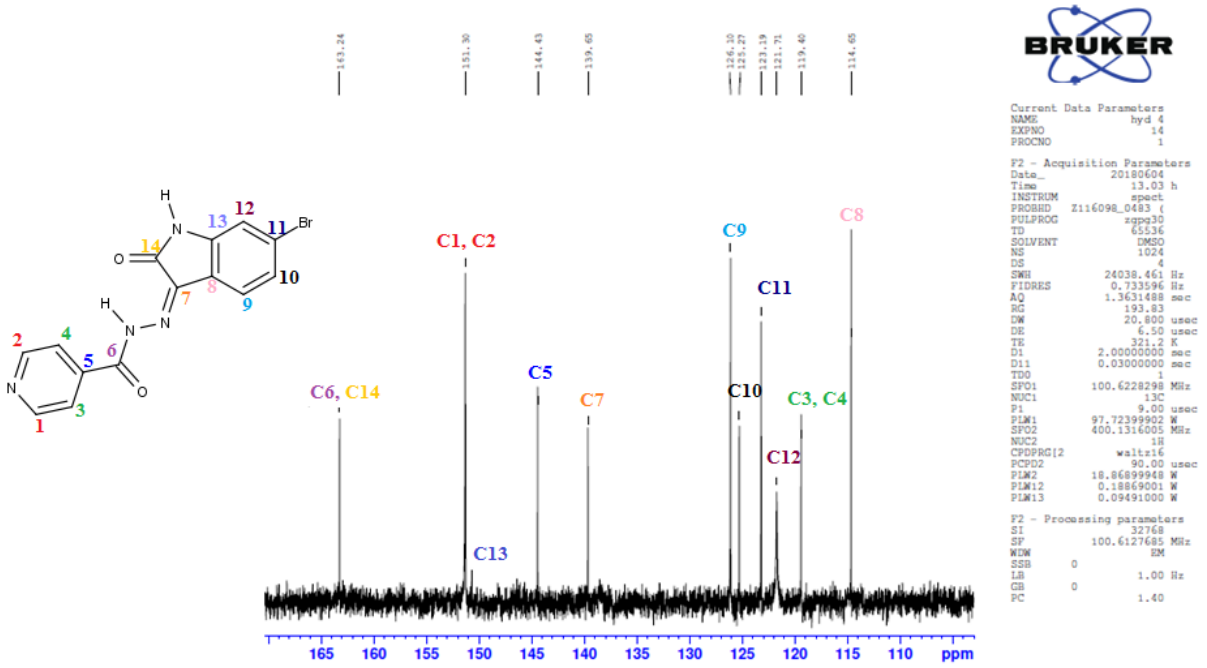

Figure 55. ^{13}C-NMR spectrum of **Hyd2** (114 to 165 ppm) (DMSO-d_6)

IV.2.1.2.7. Mass spectrometry

High resolution mass spectra were obtained for both hydrazones **Hyd1** and **Hyd2**, by electrospray ion source coupled mass spectrometry (SM □ ESI), followed by activation by the CID mode. Results obtained are depicted in **Figures 56** and **57**, which are in perfect

agreement with the molecular weights of these compounds. For **Hyd1**, HRMS (EIMS) m/z: calcd. for $C_{13}H_{10}ClN_4O_3$ $[M+H]^+$ 305.04414, 307.04119 found 305.04359, 307.04065.
For **Hyd2**, HRMS (EIMS) *m/z*: calcd. for $C_{14}H_{10}$ BrN_4O_2 $[M + H]^+$ 344.99871, 346.99667 found 344.99816, 346.99625.

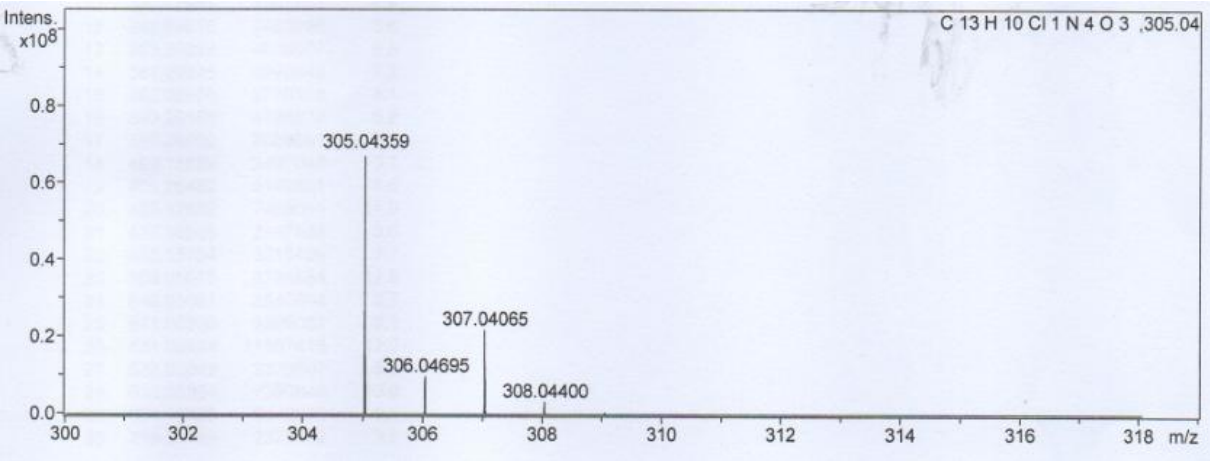

Figure 56. High resolution mass spectrum (HRMS) of **Hyd1**

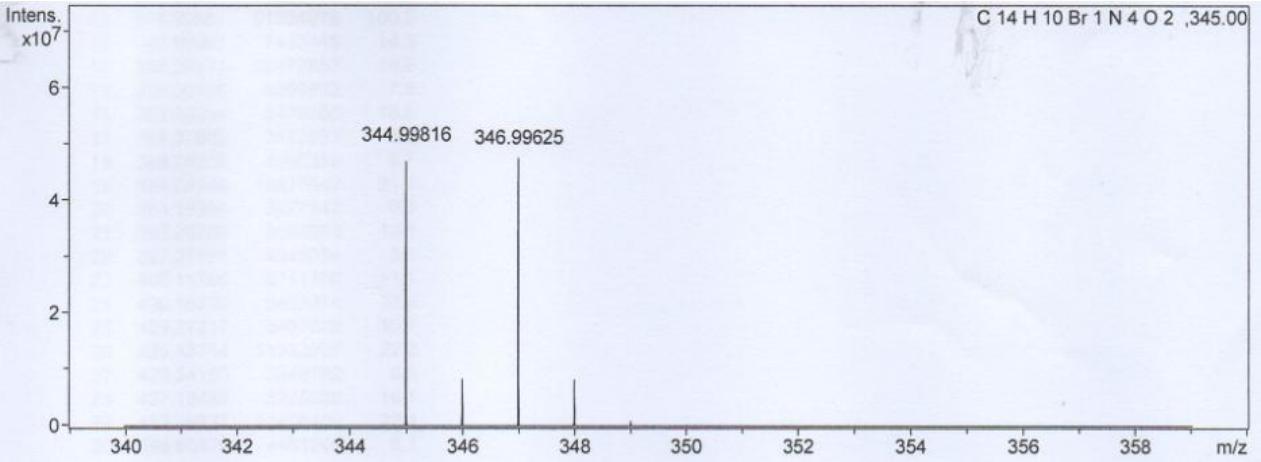

Figure 57. High resolution mass spectrum (HRMS) of **Hyd2**

IV.2.2. Biological studies

IV.2.2.1. *In vitro* toxicological evaluation

Toxicity effect of **INH**, **Hyd1**, and **Hyd2** was assessed by the use of microorganisms such as bacteria and fungus. Use of microorganism is a rapid and cost-effective method, and is valuable in bioassays for eco-toxicity assessment [119]. Our findings, listed in **Table 21**, indicate the absence of adverse effect of **INH**, **Hyd1**, and **Hyd2** against all tested microorganisms at the high concentration of 2000 µg/mL. These results reveal the absence of any risks to microorganisms, thus suggesting the tested compounds are not toxic.

Table 21. Effect of the **INH**, **Hyd1**, and **Hyd2**, gentamicine and econazol on bacteria and fungi.

Microorganisms	Zone of inhibition (mm)				
	Compounds (2000 µg/mL)			**Control positive**	
	Hyd1	**Hyd2**	**INH**	**Gent (10 µg/disc)**	**Eco (75 µg/mL)**
Lysteria monocytogenes	-	-	-	13.5	-
Escherichia coli	-	-	-	19.00	-
Pseudomonas aerogenose	-	-	-	27.00	-
Staphylococcus aureus	-	-	-	-	-
Klebsiella pneumoniae	-	-	-	-	-
Bacillus cereus	-	-	-	-	-
Aspergillus niger	-	-	-	-	35.00

IV.2.2.2. *In vivo* acute toxicity evaluation

Acute toxicity determination plays fundamental roles in drug design and in eco-toxicological studies [120]. In acute toxicological testing, the tested compounds were administered at different dose levels, and the effect was observed for 14 days [121]. According to acute toxicity prediction, oral administration was selected for *in vivo* acute toxicity determination of the synthesized hydrazones **Hyd1** and **Hyd2**. Due to the higher sensibility of rat than mice to the tested products in acute toxicity [122], this is an indication that experimental LD50 values of the synthesized compounds are more than the predicted values. For this reason, 1000 mg/kg was selected as the dose for in vivo acute toxicity evaluation.

IV.2.2.2.1. Behavioral observations and mortality patterns

In vivo acute toxicity evaluation of **Hyd1** and **Hyd2** demonstrated no mortality at the dose of 1000 mg/kg after 24 h of drug administration, and without abnormal actions over 14 days.

IV.2.2.2.2. Body weight estimation

Mice body weight was measured each seven days of experiment and results (**Figure 58**) indicate an increase in the body weight of both treated groups compared with the control.

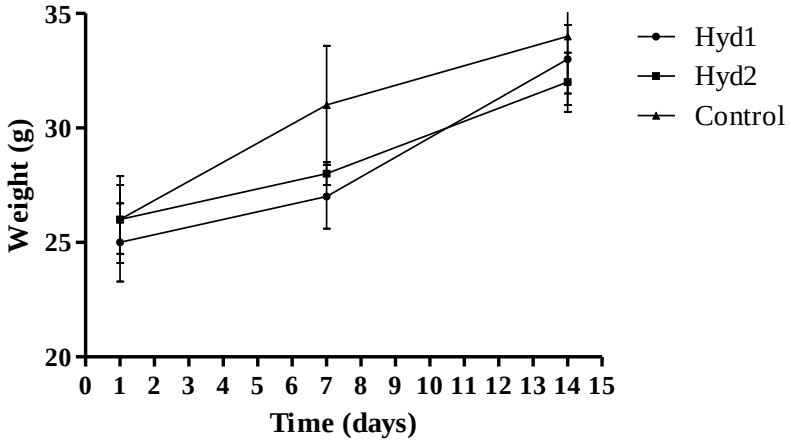

Figure 58. Development of mice body weight; Values expressed as mean ± SEM, n= 5 animals /group.

IV.2.2.2.3. Biochemical parameters

Biochemical analyses were conducted at the end of the experiments. Plasma biochemical parameters including urea, creatinine, albumin, calcium, protein, cholesterol, uric acid, AST, ALT, and ALP, results are given in **Table 22**. AST and ALT are the most commonly used biochemical markers of liver injury [123]. Results revealed that ALT increased significantly by 1.2 and 1.5 fold, respectively, compared to the control group when mice were treated with **Hyd1** and **Hyd2**. Similarly, levels of AST increased significantly by 1.3 and 1.2 fold, respectively, compared to that of the control group.

Table 22. Biochemical parameters of control and mice treated with **Hyd1** and **Hyd2**.

Parameters	Control	Hyd1	Hyd2
ALP (UI/L)	321.25 ± 0.32	380.9 ± 0.425***	215.9 ± 39.1***
AST (UI/L)	132.1 ± 0.520	179.7 ± 0.721***	159.70 ± 11.03***
ALT (UI/L)	34.55 ± 0.237	41.15 ± 0.139***	53.45 ± 3.5***
Urea (g/L)	0.69 ± 0.92	0.68 ± 0.541**ns**	0.82 ± 0.654***
Creatinine (mg/L)	21.95 ± 0.873	19.8 ± 0.675**ns**	18.71 ± 0.310**
Uric acid (mg/L)	13.20 ± 0.651	5.28 ± 0.547***	7.28 ± 0.815***
Cholesterol (g/L)	1.01 ± 0.751	1.52 ± 0.654***	2.53 ± 0.962***
Albumin (g/L)	18.96 ± 0.265	24.22 ± 0.478***	25.98 ± 0.230***
Protein (g/L)	58.44 ± 0.557	73.27 ± 0.783***	75.02 ± 0.364***
Calcium (mg/L)	1.67 ± 0.427	3.71 ± 0.865***	0.83 ± 0.453***

Values expressed as mean ± SEM, n= 5 animals /group;***: p<0.001, **: p < 0.01, **ns**: no significant differences.

IV.2.2.2.4. Histological analysis

The observation of histological sections of the liver and kidneys (**Figure 59**) showed the presence of some congestion in both organs of animals treated with **Hyd1**. However, a vascular congestion and inflammatory infiltrated were recorded in some hepatic tissues of animals treated with **Hyd2**. From the histological analysis and the enzymes levels, we can conclude the absence of hepatotoxic effect of **Hyd1** and the possibility of a hepatic disorder induced by **Hyd2**. Furthermore, kidneys' histological section did not show any structure modifications which demonstrate the absence of the nephrotxoic effects. These results are in good agreement with previous studies where **INH** hydrazone derivatives showed less toxicity in mice than **INH** [124]. This could be explained by the blockage of $-NH_2$ group by aldehydes or ketones.

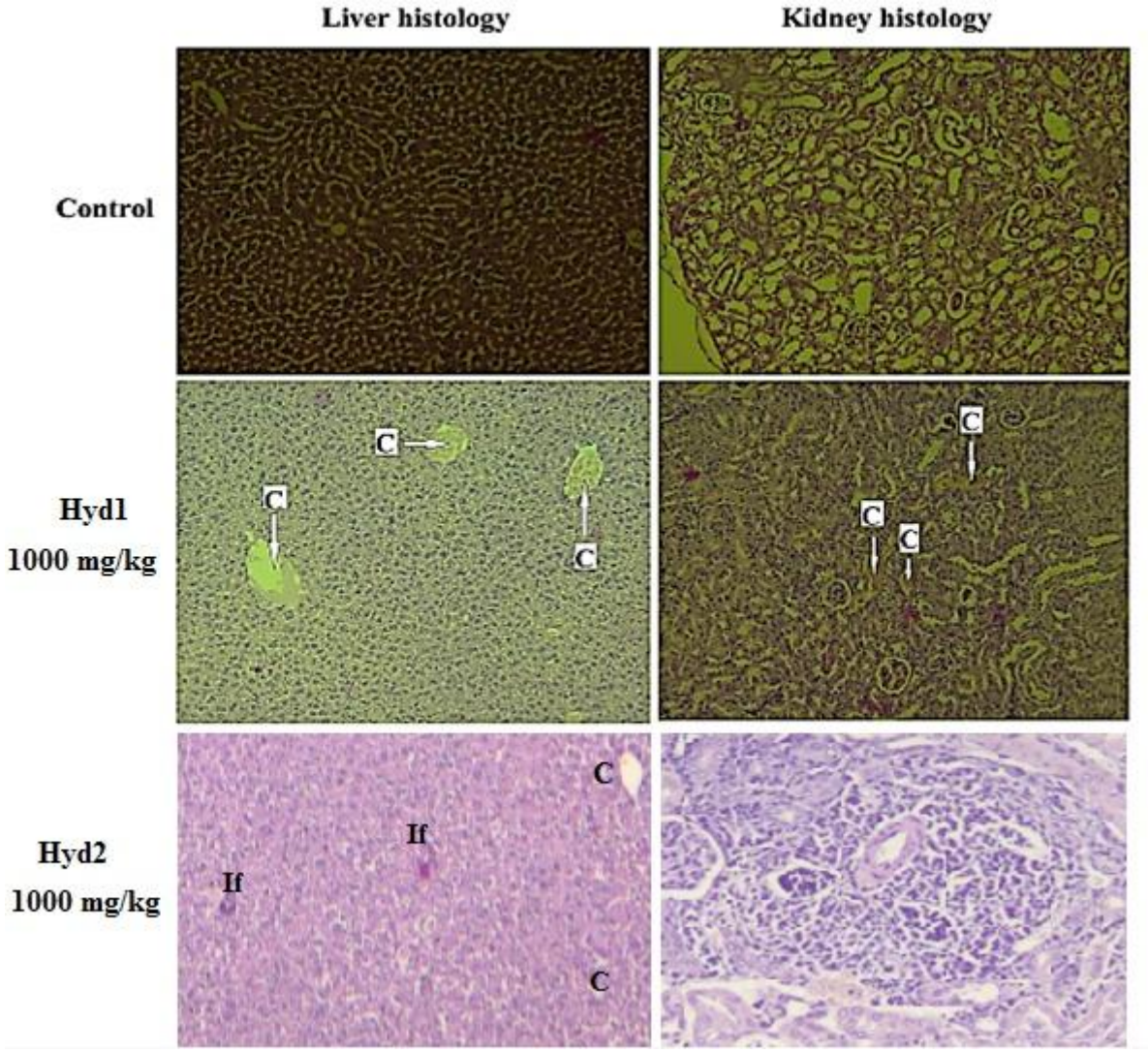

Figure 59. Histopathological analysis of mice females' liver and kidney treated with **Hyd1**and **Hyd2** in acute toxicity (x10 and x 40). **C**: congestion, **If**: inflammatory infiltrate.

IV.2.2.3. *In vitro* antioxidant activity evaluation

Free radicals are known as damaging species and cause cells injury which is considered a major source of numerous pathologies in human body [125]. These species are probably formed during inflammatory processes by special defenses cells [126]. In this study, **INH** and its derivatives were investigated for their antioxidant effects using superoxide anion and hydrogen peroxide scavenging assays.

IV.2.2.3.1. Superoxide Anion Radical Scavenging effect

Superoxide anion radical ($O_2^{\bullet -}$), is among the harmful reactive oxygen species (ROS), responsible for generation of strongest ROS such as hydrogen peroxide (H_2O_2), peroxynitrite ($ONOO^-$), and hydroxyl radicals ($HO^{\bullet}$) [127]. In this study, for the development of new free radical-scavengers, the synthesized hydrazones **Hyd1** and **Hyd2** were investigated *in vitro* against this radical which acts as a Brønsted base, an oxidant, a nucleophile, a one-electron reductant and a radical in aprotic media [128], by electrochemical and chemical methods.

Electrochemical experience was used as a qualitative assay, describes superoxide anion scavenging effect;

For **Hyd1**, results show a proportional decrease of the anodic current peak while the intensity of the cathodic current is not significantly modified, with inhibition effects of 50.3 ± 0.32 and 67.5 ± 0.67% at both solution volumes 0.2 and 0.4 mL, respectively (**Figure 60**). In a similar fashion, **Hyd2** exhibited an excellent effect by the decrease in both anodic and cathodic current peaks with inhibition percentages of 72.3 ± 0.93 and 88.4 ± 0.79 % at the added volumes of 0.2 and 0.4 mL, respectively (**Figure 61**).

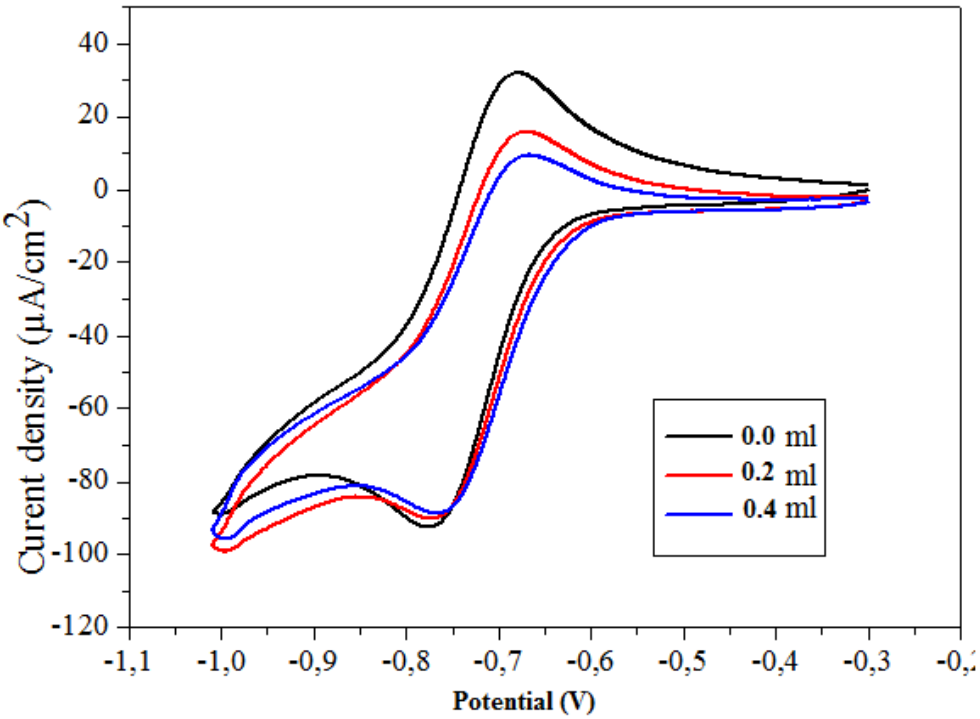

Figure 60. Cyclic voltammograms showing superoxide anion scavenging effect of **Hyd1**.

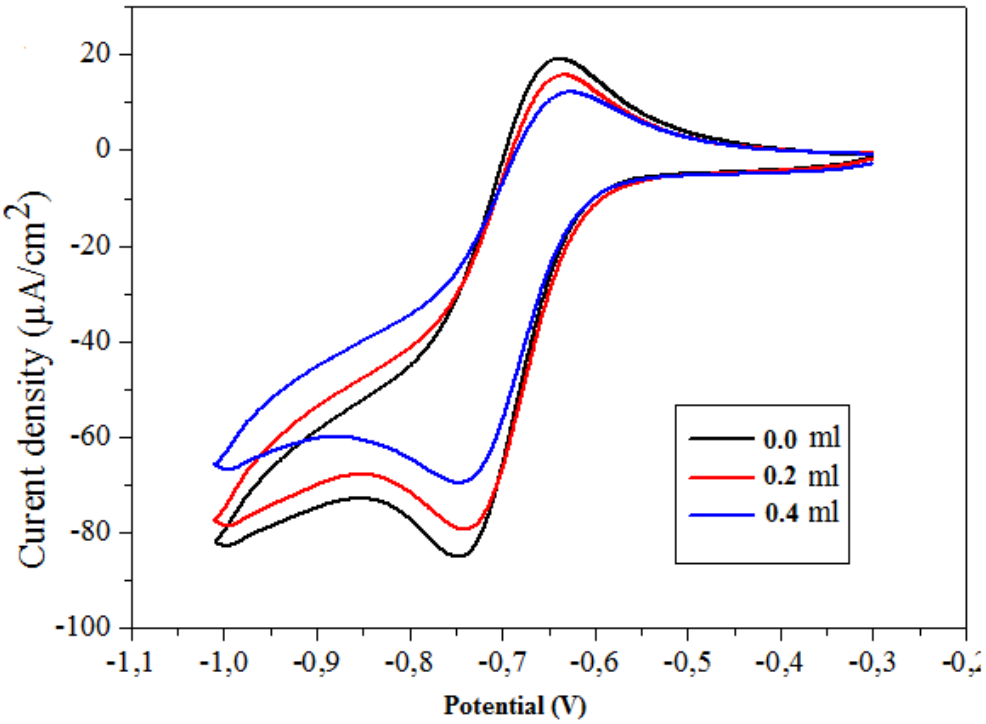

Figure 61. Cyclic voltammograms showing superoxide anion scavenging effect of **Hyd2**.

Results displayed in **Figures 62** and **63** show an excellent scavenging effect of **Hyd1**, which exhibits a good superoxide anion scavenging with an inhibition effect of 87.57 % ± 0.12 and IC_{50} value of 32.37 ± 0.45 µg/mL, comparable with ascorbic acid (**AA**) with inhibition effect of 85.40% ± 0.138 and IC_{50} value of 29.91 ± 0.17 µg/mL. In addition, results indicate

moderate effect of **Hyd2** with inhibition percentage of 53.5% and IC_{50} value of 125.66 µg/mL and an excellent effect of **IND** with percentage of 89.95% and IC_{50} value of 69.39 µg/mL.

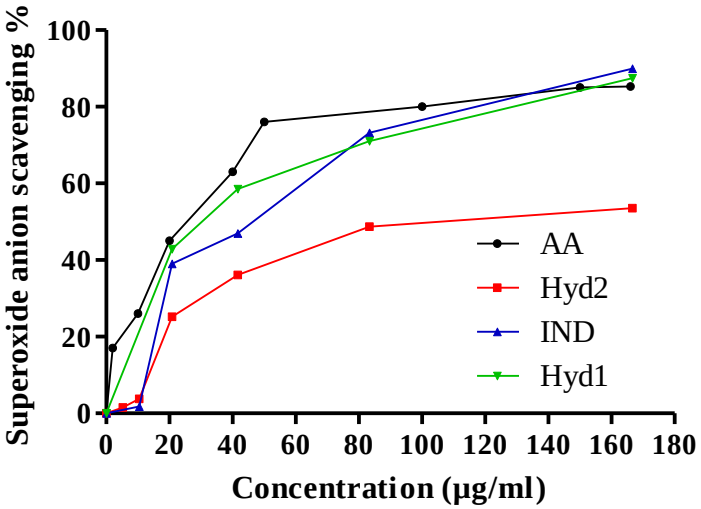

Figure 62. Superoxide anion scavenging effect of **Hyd1**, **Hyd2**, **IND**, and **AA**

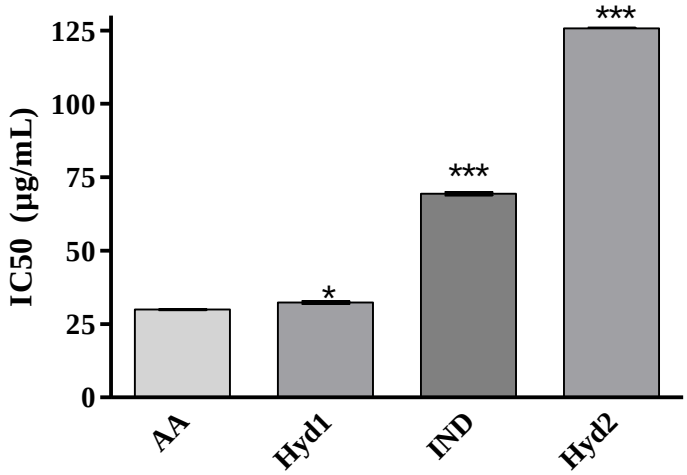

Figure 63. IC_{50}values of **Hyd1**, **Hyd2**, **IND**, and **AA**;
Values are expressed as mean ± SD, n= 3;*******: $p < 0.001$, *****: $p < 0.05$.

Remarkably, isoniazid **INH** did not exert any scavenging effect. Research findings indicate that **INH** was activated and stimulated by superoxides, causing oxidative reactions which can affect nucleic acid, macromolecules, and proteins [129]. Taken all together, the synthesis of **INH** analogs (**Hyd1** and **Hyd2**) improves **INH**-adverse effects from an oxidative activator to a potent antioxidant agent. This can be explained by quantum chemical parameters of both molecules. Antioxidant activity was enhanced by steric hindrance [130]; molecules with increased steric hindrance are supposed to exert stronger radical scavenging effect [131]. These results are in good agreement with previous data which confirm that hydrazones analog from **INH** possess a highest superoxide anion scavenging activity [132].

IV.2.2.3.2. Hydrogen peroxide scavenging effect

Hydrogen peroxide may be formed in tissues during oxidative stress and is not considered a reactive species. In animal cells, its reaction with iron ions contributes to generation of the hydroxyl radicals which are harmful species [133]. The scavenging capacity of the synthesized hydrazones and **IND** towards hydrogen peroxide is shown in **Figures 64** and **65**. Results reveal an excellent scavenging effect of **Hyd2** with inhibition percentage of 81.86% and IC_{50} of 4.46 ± 0.2 µg/mL when compared with **IND** which has similar effect with a percentage of 85.53% and IC_{50} of 4.60 ± 0.26 µg/mL. However, **Hyd1** exhibited lower effect than **Hyd2** with inhibition percentage of 45.30%,

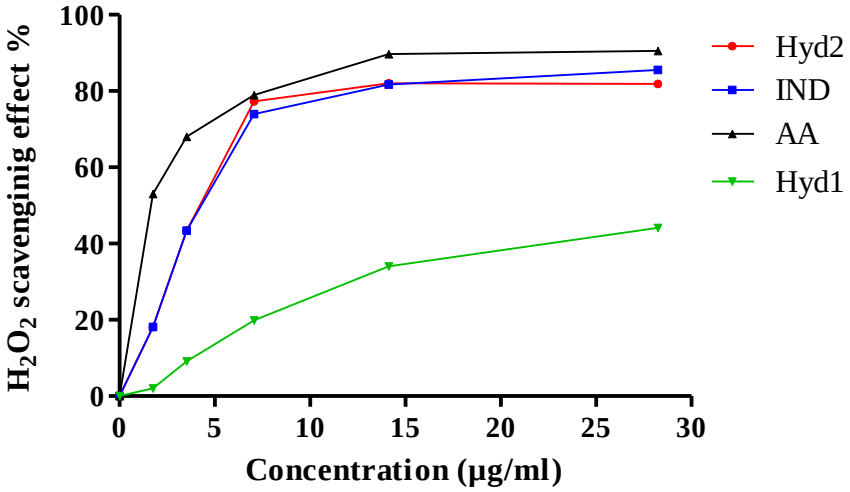

Figure 64. Hydrogen peroxide scavenging effect of **Hyd1**, **Hyd2**, **IND**, and **AA**.

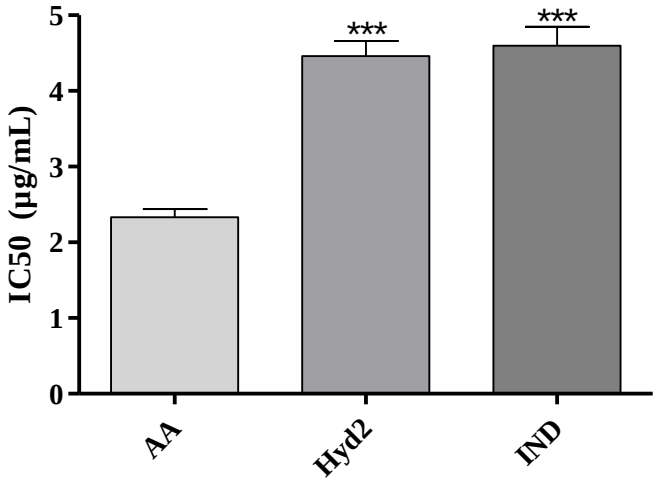

Figure 65. IC_{50} values of **Hyd2**, **IND**, and **AA**
Values expressed as mean ± SD, n= 3;*******: $p < 0.001$.

All of these results indicate the potent antioxidant effect of **Hyd2** which is an indole derivative. **IND** is one of this family which exhibited an excellent activity against different types of free radicals such as reactive oxygen species (ROS) and reactive nitrogen species (RNS) [134]. Structure-activity relationships study of **Hyd2** and **IND** displayed in **Figure 66**, show the presence of indole ring which is the main contributor in free radicals scavenging effect of the indole-derivatives that is an electron-rich ring with high resonance stability and lowest activation energy wall [135]. In addition, the presence of an amide group and a carbonyl functionality contributes to the antioxidant potential [136]. Furthermore, the presence of hydrogen atom in α-position is an essential site for free radical scavenging activity [137].

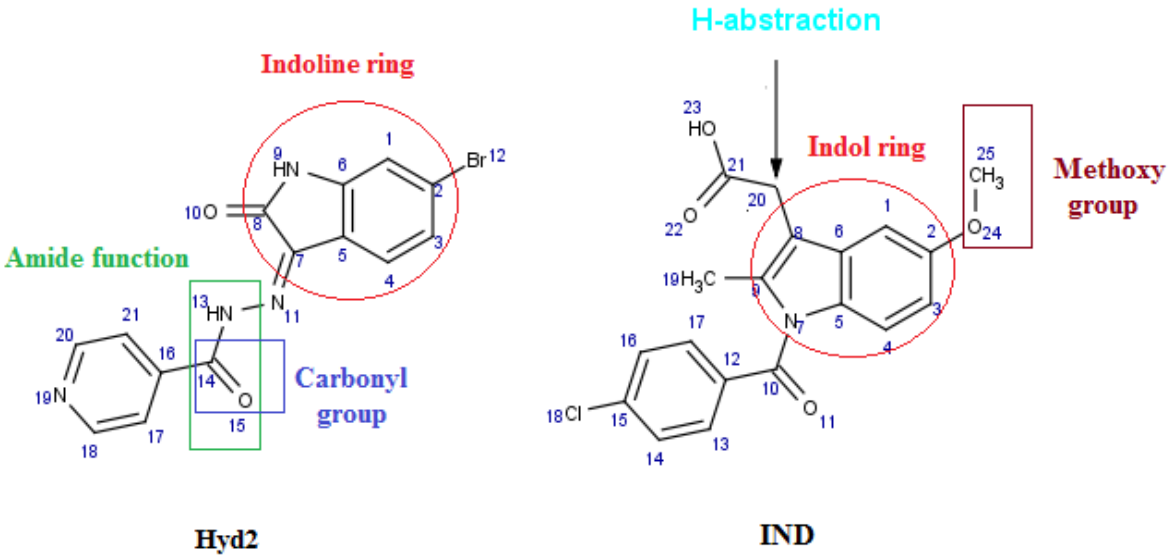

Figure 66. Structures of **Hyd2** and **IND**

IV.2.2.4. *In vivo* antioxidant activity evaluation

Due to the good predicted results and the high free radical-scavenging effect and to the similar structure to indole-derivatives, which are considered potential antioxidant agents [138], **Hyd2** was selected for *in vivo* investigation, against oxidative stress induced by the drug **INH**. Results of this study indicated that intraperitoneal injections of isoniazid at 151 mg/kg led to an increase in malondialdehyde (MDA) formation, decrease in the activities of enzymatic antioxidants such as CAT, and a decrease in non-enzymatic antioxidants such as GSH when compared with the control.

We found that oxidative stress induced by **INH** is associated with lipid peroxidation expressed by the increase in the level of MDA from 76.9 ± 1.74 to 79.61 ± 2.67 nmol/g tissue. This number was decreased to 68.02 ± 2.27 and 60.46 ± 4.63 nmol/g tissue, when animals

were treated with **Hyd2** at 15 and 30 mg/kg, respectively (**Table 23**). The reduced GSH is one of non-enzymatic antioxidant present in the liver which scavenges reactive toxic metabolites of anti-tubercular drugs; liver damage was observed when GSH stocks were significantly decreased [139]. The oxidative stress of **INH** is accompanied by a decrease in reduced GSH level (from 79.9 ± 12 µmol / mg to 68.48 ± 4.28 µmol / mg compared to of the control group).This reduction was attenuated by the administration of **Hyd2** at 15 and 30 mg/kg (71.93 ± 5.83 and 71.29 ± 10 µmol/mg protein respectively). Results of the enzymatic antioxidant, CAT activities of treated mice are presented in **Table 23**. After treatment with **INH** at 151 mg/kg, a decrease in CAT activities occurred compared to control (2.53 ± 0.39 U/mg Pr *vs* 5.07 ± 0.73 U/mg Pr). There were not significant differences between CAT activities of groups treated with **INH** at 151 mg/kg combined with oral administration of **Hyd2** at 30 mg/kg, and 15 mg/kg (3.83 and 3.19 U/mg protein, respectively). The decreased CAT activity could be due to the enhanced generation of ROS during isoniazid metabolism [140] that is deactivated by CAT as well as to the activation of the peroxide oxidation of lipids, proteins, nucleic acids, and other macromolecules. In the literature, the **INH**-hydrazone analog SH11 was reported to have a good effect against **INH**-induced oxidative hepatic damage [141]. Taken all together, we conclude that the potent antioxidant effect of **Hyd2** reduced the consumption of endogenous antioxidants which could be responsible for the reduction in oxidative stress during **INH** toxicity.

Table 23. Effect of **Hyd2** on oxidative stress parameters.

Groups	**CAT (U/mg protein)**	**MDA (nmol/g tissue)**	**GSH (µmol/mg protein)**
Control	5.07 ± 0.19	76.9 ± 1.74	79.90 ± 12
INH 151 (mg/kg)	2.53 ± 0.63***	79.61 ± 2.67**ns**	68.48 ± 4.28***
Hyd2 (15 mg/kg)	3.19 ± 1.09***	68.02 ± 2.27**	71.93 ± 5.83***
Hyd2 (30 mg/kg)	3.83 ± 0.84***	60.46 ± 4.63***	71.29 ± 10***

Values expressed as mean ± SEM, n= 5 animals /group;***: $p < 0.001$, **: $p < 0.01$,
ns: no significant differences.

IV.2.2.5. Hepatoprotective effect

Liver and biliary system injuries are the principle problems in the anti-tubercular treatment, were evaluated in patients received anti-tubercular drug, one of these drugs was **INH** [142]. The increased risk of hepatotoxicity with **INH** has been attributed to its metabolism, the plasma half-life of acetylisoniazid (**INH** metabolite) is rapidly converted to its active

metabolites; these are related to the higher incidence of liver necrosis caused by **INH** [143]. In this study, the hepatotoxic effect of **INH**, and the possibility of **Hyd2** to protect liver against **INH**-adverse effects was evaluated in mice.

IV.2.2.5.1. Body and organs weight estimation

During experiments, body weight of mice development was measured each day. Results in **Figure 67** indicate a decrease in the body weight of both treated groups; **INH**-treated group and **Hyd2**-treated group, whereas, stability in body weight from control group (NaCl) was observed. In addition, a decrease was observed in organ weight of treated animals (**Table 24**). These results demonstrate the weight loss of mice during this experiment.

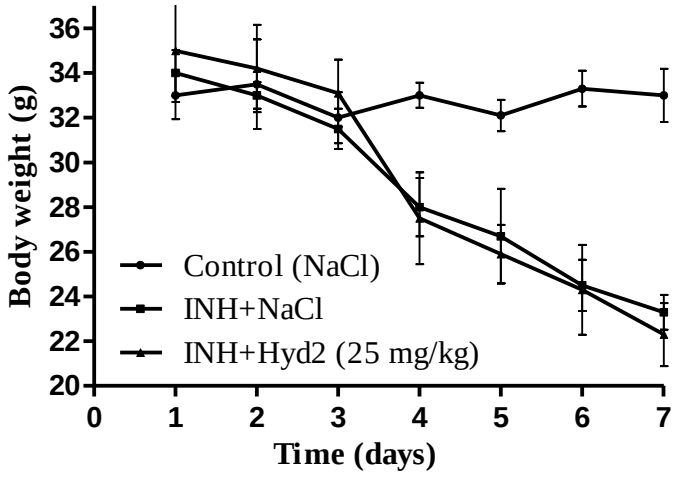

Figure 67. Body weight estimation during 7 days; Values expressed as mean ±SEM, n= 5 animals /group

Table 24. Organs weight estimation

Organs	Control	NaCl+INH (400 mg/kg)	INH+Hyd2 (25 mg/kg)
Liver	1.883 ± 0.98	1.6394 ± 0.13***	1.2823 ± 0.19***
Kidneys	0.329 ± 0.10	0.3859 ± 0.15**	0.3267 ± 0.01**ns**

Values expressed as mean ± SEM, n= 5 animals /group; ***: $p < 0.001$, **: $p < 0.01$, **ns**: no significant differences

IV.2.2.5.2. Biochemical parameters

Results of the protective effect of **Hyd2** against **INH** hepatotoxicity, are shown in **Table 25**. According to Roussel Uclaf Causality Assessment Method (RUCAM) [144], the drug **INH** has calculated R value of 5.51, which indicates the hepatocellular injury effect of this drug. In addition, ALT increased significantly by two fold, an indication to loss of hepatocellular

integrity and the hepatotoxic effect of **INH** [145]. For **Hyd2**, a decrease was observed in ALP (3.17 K A Units), and ALT (22.65 UI/L), low increase in AST (149.01 UI/L). These results indicate the hepatoprotective effect of **Hyd2**.

Table 25. Hepatoprotective effect of **Hyd2**

Parameters	**Control** (NaCl)	**NaCl+INH** (400mg/kg)	**INH+Hyd2** (25mg/kg)
ALP(K A Units)	5.46	6.27***	3.17***
AST (UI/L)	132.1	302.88***	149.01**
ALT (UI/L)	34.55	74.79***	22.65***
Urea (g/L)	0.69	0.16***	0.66**ns**
Creatinine (mg/L)	21.95	28.23***	26.34***

Values expressed as mean ± SEM, n= 5 animals /group; ***: $p < 0.001$, **: $p < 0.01$, **ns**: no significant differences.

IV.2.2.5.3. Histological analysis

Morphology of the mice liver samples representing the tested groups is shown in **Figure 68**. The control group animals (received NaCl) had normal liver histology. Steatosis and necrosis were detected in hepatotoxicity groups (received NaCl+ INH; 400 mg/kg), and the frequency of congestion was observed in **Hyd2**-treatment group (received **INH**; 400 mg/kg + **Hyd2**; 25 mg/kg). From these results, a significant protective effect of **Hyd2** was observed against **INH**-induced liver injury. These results complete the above effects of **INH** oxidative stress that **Hyd2** has a potent free radical scavenging capacity which contributed in the hepatoprotective effect.

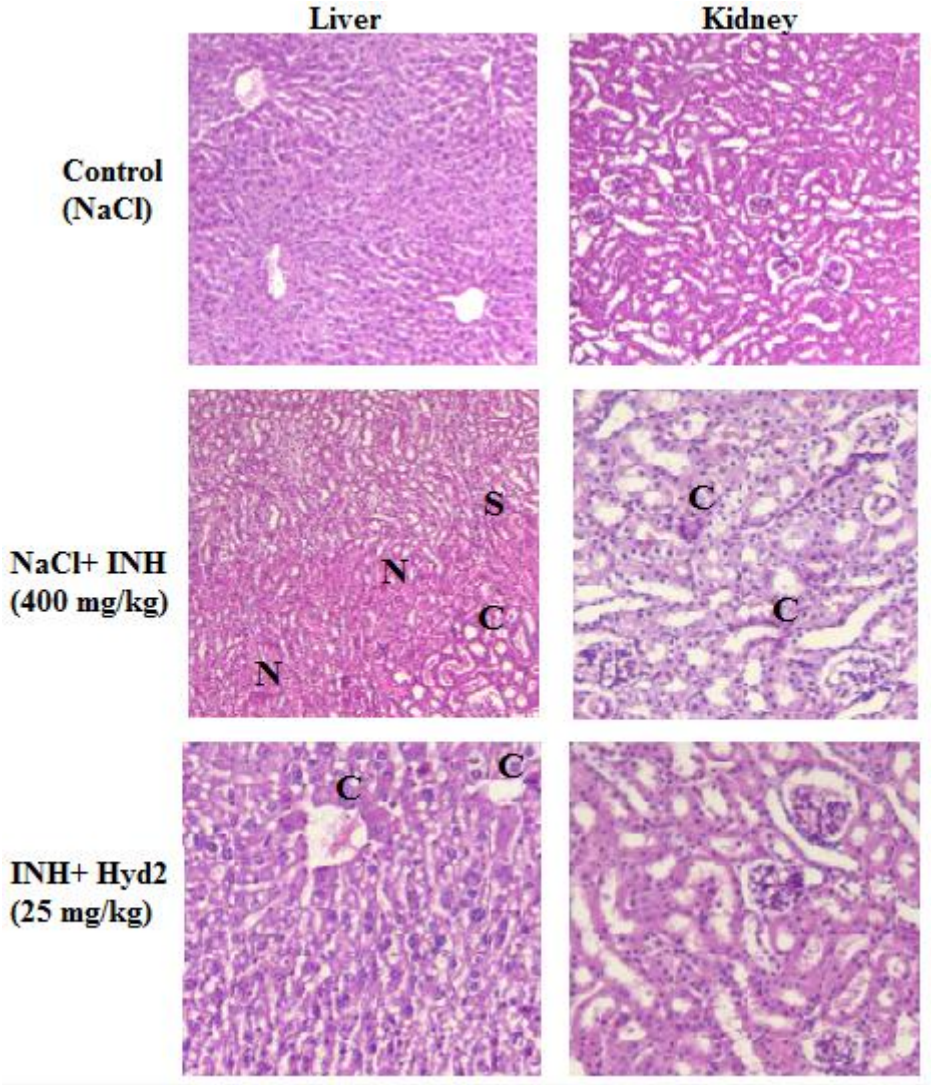

Figure 68. Histopathological analysis of mice females' liver and kidney treated with **Hyd2** in hepatotoxicity assay (x10 and x 40). **C**: congestion, **S**: steatosis, **N**: necrosis.

IV.2.2.6. *In vitro* biodegradability evaluation

Fungi micro-organisms play an important role in the degradation of chemicals [57]. In this context, *Aspergillus niger* is one of filamentous fungal strains which are capable of degrading phenols [146]. In this study, *in vitro* biodegradability evaluations of **Hyd1**, **Hyd2** and **INH** were carried out using the fungus *Aspergillus niger*, and were compared with nicotinamide (vitamin B3) **NA** [147]. Results revealed no-biodegradability of **Hyd2** and showed the fungi growth in mineral medium containing **INH**, **Hyd1** and **NA** as indicated by the increase in fungi growth diameter after 48, 72, 96, 120, and 144 h as depicted in **Figures 69** and **70**.

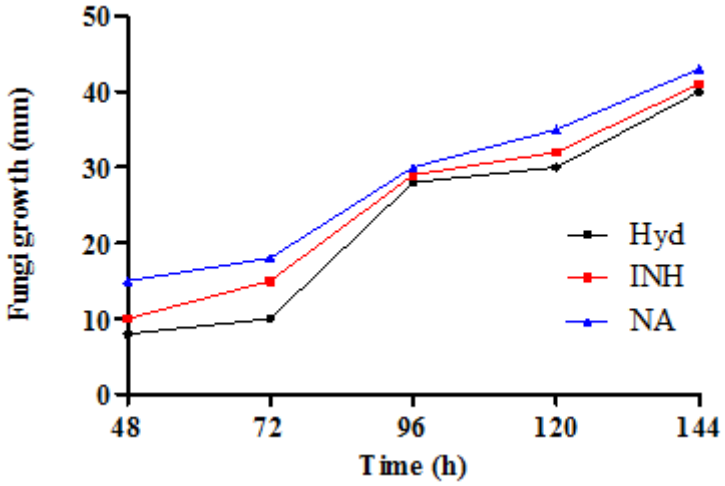

Figure 69. Biodegradation of **Hyd1**, **INH**, and, **NA** by *Aspargillus niger*

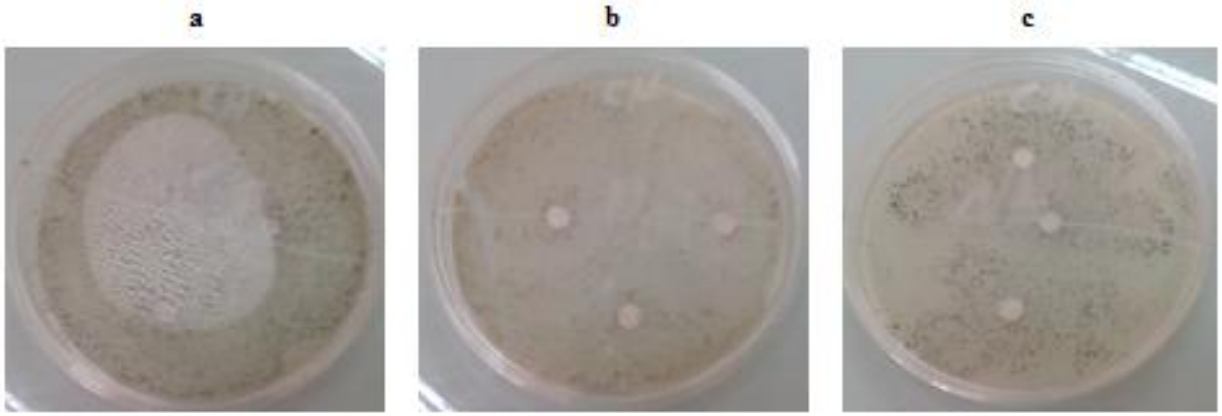

Figure 70. Diameter of *Aspargillus niger* growth after 7 days in mineral media containing; **a**) **NA**, **b**) **Hyd1**, and **c**) **INH**.

Conclusions

Conclusions

In this study, we synthesized new hydrazones; (N'-[(*E*)-(4-chloro-3-nitrophenyl) methylidene] pyridine-4-carbohydrazide (**Hyd1**), and N'-[(3*Z*)-6-bromo-2-oxo-2,3-dihydro-1*H*-indol-3-ylidene] pyridine-4-carbohydrazide (**Hyd2**), from the condensation reaction of anti-tubercular drug isoniazid (**INH**) and 4-chloro-3-nitrobenzaldehyde or 6-bromoindoline-2,3-dione, respectively, in absolute ethanol. The synthesized hydrazones were characterized by a panel of spectroscopic techniques such as UV, IR, NMR (^{1}H, ^{13}C), mass spectrometry, and by elemental analysis. Molecular structure properties of **INH, Hyd1,** and **Hyd2** were investigated using density functional theory (DFT) via B3LYP/6-31G (d,p) method in DMSO and gas state. Results demonstrated that **Hyd2** was more bioactive than **Hyd1** and **INH** with the lowest ΔE_{gap}= 0.1356 a.u. In addition, physicochemical proprieties such as lipophilicity, H-bond donor/acceptor, topological polar surface area, and number of rotatable bonds were calculated using the package Marvin; results showed that both hydrazones are in good agreement with the drug discovery rule of Lipinski, in which **Hyd2** has the excellent absorption percentage (80.20%).

On the other hand, *in silico* toxicological studies were undertaken using online software programs; from toxicophores, acute toxicity, carcinogenicity, hepatotoxicity, mutagenicity, immunotoxicity, cytotoxicity, and skin sensitization; these studies showed low toxic effect of **Hyd1** and **Hyd2**, with predicted LD_{50}values of 1816 and 984.60 mg/kg, respectively. Additionally, reduction in the hepatotoxic effect was observed with values of 42% for **Hyd1** and 32% for **Hyd2**. Adverse effects predicted of **Hyd1** are the mutagenicity and the immunotoxicity (71%, 80%). The anti-tubercular effect was predicted, results demonstrated the persistence of the effect in both compounds with predicted values of 84.6 and 83.9% from **Hyd1** and **Hyd2**, respectively. Results of *in vitro* toxicity evaluation using microorganism (bacteria and fungus) indicated no toxic effect of these compounds at the high dose of 2000 µg/mL. *In vivo* toxicological studies demonstrated no toxic effect against mice at a high dose of 1000 mg/kg. Antioxidant effect was evaluated by superoxide anion (by chemical and electrochemical methods) and hydrogen peroxide assays. Results revealed that **Hyd1** exhibits higher effect towards superoxide anion and lower effect towards hydrogen peroxide with 32.37± 0.45 µg/mL comparable with that of Ascorbic acid (**AA**), whereas, **Hyd2** exhibits higher effect towards hydrogen peroxide with an IC_{50} of 4.46 ± 0.2 µg/mL, comparable with that of indomethacine (**IND**). Due to the low toxicity and high antioxidant effect, **Hyd2** was selected for *in vivo* antioxidant and hepatoprotective effect against **INH**-induced oxidative stress and hepatotoxicity. Results confirm and demonstrate the antioxidant and the hepatoprotective effect of **Hyd2**. For

biodegradability, results of both *in silico* and *in vitro*, showed the biodegradability of the synthesized hydrazones by simple microorganisms.

In conclusion, from the anti-tubercular drug **INH**, which possesses a negative effect to human health by a catalytic role in oxidative reactions (hepatotoxicity), we synthesized new hydrazones with high predicted anti-tubercular effect and low toxicity and have higher antioxidant effects.

References

References

[1] D.K. Kölmel, E.T. Kool, Oximes and hydrazones in bioconjugation: mechanism and catalysis, *Chemical Reviews*. 117 (2017) 10358-10376.

[2] Ł. Popiołek, Hydrazide-hydrazones as potential antimicrobial agents: overview of the literature since 2010, *Medicinal Chemistry Research*. 26 (2017) 287–301.

[3] A.N. Unissa, L.E. Hanna, S. Swaminathan, A note on derivatives of isoniazid, Rifampicin, and pyrazinamide showing activity against resistant *Mycobacterium tuberculosis*, *Chemical Biology* & *Drug Design*. 87 (2016) 537–550.

[4] A. Kajal, S. Bala, N. Sharma, S. Kamboj, V. Saini, Therapeutic Potential of Hydrazones as Anti-Inflammatory Agents,*International journal of medicinal chemistry*. 2014 (2014) 1–11.

[5] A. Kivrak, C. Yilmaz, M. Konus, H. Koca, S. Aydemĭr, J. A. Oagaz, Synthesis and biological properties of novel 1-methyl-2-(2-(prop-2-yn-1-yloxy)benzylidene) hydrazine analogues, *Turkish journal of chemistry*. 42 (2018) 306–316.

[6] H.G. Bonacorso, G.R. Paim, L.M.F. Porte, E.P. Pittaluga, M. A.P. Martins, N. Zanatta. 6-Hydrazinonicotinic acid hydrazide: a useful precursor for chemo- and regioselective synthesis of new heteroaryl-linked pyridinohydrazones. *Arkivoc.* viii (2012) 214–225

[7] X. Su, I. Aprahamian, Hydrazone-based switches, metallo-assemblies and sensors, *Chemical Society Reviews*. 43 (2014) 1963–1981.

[8]J. Patocka1, R. Pita, K. Kuca, Gyromitrin, mushroom toxin of gyromitraspp,*Military Medical Science Letters*. 81 (2012) 61–67.

[9] M. S. Abdelfattah, K. Toume , M. A. Arai , H. Masu , M. Ishibashi, Katorazone, a new yellow pigment with a 2-azaquinone-phenylhydrazone structure produced by *Streptomyces sp*. IFM 11299, *Tetrahedron Letters* .53 (2012) 3346–3348.

[10] G. Le Goff, J. Ouazzani, Natural hydrazine-containing compounds: biosynthesis, isolation, biological activities and synthesis, *Bioorganic & medicinal chemistry***.** 22 (2014) 6529–6544.

[11] F. Li, Y. Miao, L. Zhang, S. A. Neuenswander, J. T. Douglas, X. MA, Metabolomic Analysis Reveals Novel Isoniazid Metabolites and Hydrazones in Human Urine, *Drug Metabolism and Pharmacokinetics*. 26 (2011) 569–576.

[12] R. Brehme, D. Enders, R. Fernandez, J. M. Lassaletta, Aldehyde N,N-Dialkylhydrazones as Neutral Acyl Anion Equivalents: Umpolung of the Imine Reactivity, *European Journal of Organic Chemistry*. 34 (2007) 5629–5660.

[13] N.P. Belskaya, W. Dehaen, V.A. Bakulev, Synthesis and properties of hydrazones bearing amide, thioamide and amidine functions, *Arkivoc* (2010) 275–332.

[14] S. Rollas, N. Gülerman, H. Erdeniz, Synthesis and antimicrobial activity of some new hydrazones of 4-fluorobenzoic acid hydrazide and 3-acetyl-2,5-disubstituted-1,3,4oxadiazolines, *Farmaco Edizione Scientifica*. 57 (2002) 171–174.

[15] A.B. Thomas, R. K. Nanda, L.P. Kothapalli, S.C. Hamane. Synthesis and biological evaluation of Schiff's bases and 2-azetidinones of isonocotinylhydrazone as potential antidepressant and nootropic agents, *Arabian Journal of Chemistry*. 9 (2016) 79–90.

[16] N.B. Patel, F.M. Shaikh, Synthesis of New Pyridine Based 4-Thiazolidinones Incorporated Benzothiazoles and Evaluation of Their Antimicrobial Activity, *Journal of Sciences, Islamic Republic of Iran.* 21 (2010) 121–129.

[17] N. Singh, R.Ranjana, M.Kumari, B.kumar, A Review on Biological Activities of Hydrazone Derivatives, *International Journal of Pharmaceutical* and *Clinical Research*. 8 (2016) 162–166.

[18] M.A. Elhakeem, A.T. Taher, S.M. Abuel-Maaty, Synthesis and anti-mycobacterial evaluation of some new isonicotinylhydrazide analogues, *Bulletin of Faculty of Pharmacy*, Cairo University. 53 (2015) 45–52.

[19] N. Nayak, J. Ramprasad, U. Dalimba. New INH–pyrazole analogs: Design, synthesis and evaluation of antitubercular and antibacterial activity, *Bioorganic* & *Medicinal Chemistry Letters***.** 25 (2015) 5540–5545.

[20] F.A.R. Rodrigues, A.C.A. Oliveira, B. C. Cavalcanti, C. Pessoa, A.C. Pinheiro, M, V. N. de Souza. Biological Evaluation of Isoniazid Derivatives as an Anticancer Class, *Scientia Pharmaceutica*. 82 (2014) 21–28.

[21] R.S. Amim, G.S.S. Firmino, A.C.P.D. Rego, A.L. Nery, S.A.G. Da-Silva, M.V.N. de Souza, C. Pessoa, J.A.L.C. Resende, J.D. Figueroa-Villarf, J.A. Lessa. Cytotoxicity and Leishmanicidal Activity of Isoniazid-Derived Hydrazones and 2-Pyrazineformamide Thiosemicarbazones. *Journal of the Brazilian Chemical Society*. 27 (2016) 769-777.

[22] M. Malhotra, S. Sharma, A. Deep, Synthesis, characterization and antimicrobial evaluation of novel derivatives of isoniazid, *Medicinal Chemistry Research*. 21 (2012) 1237–1244.

[23] R.A. Cordeiro, C.V.S. Melo, F.J.F. Marques, R. Serpa, A.J.J. Evangelista, E.P. Caetano, J. Mafezoli, M.C.F. Oliveira, M.R. Silva, T.J.P.G. Bandeira, J.L.B. Moreira , R.S.N. Brilhante, M.F.G. Rocha, J.J.C. Sidrim. Synthesis and in vitro antifungal activity of isoniazid-derived hydrazones against *Coccidioides posadasii*, *Microbial Pathogenesis*. 98 (2016) 1–5.

[24] A.H Adi, H.J Alturkmani, Physiologically lucky: the role of medical physiology in modern medical education: an interview, *Perspective Medical Education*. 2 (2013) 99–103.

[25] S. Howida, A. Seif, Physiological changes due to hepatotoxicity and the protective role of some medicinal plants, *Beni-Suef University Journal of Basic and Applied Sciences.* 5 (2016) 134–146.

[26] M. Blumenthal, G.K.L. Ferrier, C. Cavaliere, Total sales of herbal supplements in United States show steady growth. *Herbal Gram*. 71 (2006) 6–64.

[27] T. Lynch, A. Price, The effect of cytochrome P450 metabolism on drug response, interactions, and adverse effects, *American Family Physician* .76 (2007) 391–396.

[28] M. Sabate, L. Ibanez, E. Perez, X. Vidal, M. Buti, X. Xiol, A. Mas, C. Guarner, M. Forne, R. Sola, J. Castellote, J. Rigau, J.R. Laporte, Risk of acute liver injury associated with the use of drugs: a multicentre population survey, *Alimentary pharmacology & therapeutics*. 25 (2007) 1401–1409

[29] M. Porceddu, N. Buron, C. Roussel,, G. Labbe, B. Fromenty, A. Borgne- Sanchez. Prediction of liver injury induced by chemicals in human with a multiparametric assay on isolated mouse liver mitochondria. *Toxicological Sciences*.129 (2012) 332–345.

[30] E.S. Björnsson, O.M. Bergmann, H.K. Björnsson, R.B. Kvaran, S. Olafsson, Incidence,presentationand out comes in patients with drug- induced liver injury in the general population of Iceland. *Gastroenterology*.144 (2013) 1419.

[31] G. Danan, R. Teschke, RUCAM in drug and herb induced liver injury: The update, *International journal* of *molecular sciences*. 17 (2016) 1–33.

[32] S. Russmann, G. A. Kullak-Ublick, I. Grattagliano, Current Concepts of Mechanisms in Drug-Induced Hepatotoxicity, *Current medicinal chemistry.* 16 (2009) 3041–3053.

[33] D. Singh, W.C. Cho, Gh. Upadhyay. Drug-Induced Liver Toxicity and Prevention by Herbal Antioxidants: An Overview, *Frontiers in physiology*. 6 (2015)1–18.

[34] A. Koul, E. Arnoult, N. Lounis, J. Guillemont, K. Andries, The challenge of new drug discovery for tuberculosis.*Nature*. 469 (2011) 483–490.

[35] A.N. Unissa, S. Subbian, L. E. Hanna, N. Selvakumar, Overview on mechanisms of isoniazid action and resistance in Mycobacterium tuberculosis. *Infection genetics and evolution***.** 45 (2016) 474–492.

[36] P. Poprac,K. Jomova, M. Simunkova, V. Kollar, C.J. Rhodes, M. Valko, Targeting free radicals in oxidative stress-related human diseases. *Trends in pharmacological Sciences*. 38 (2017) 592–607.

[37] G.D. Deavall, E.A. Martin, J.M. Horner, R. Roberts. Drug-Induced Oxidative Stress and Toxicity, *Journal of toxicology*. 2012 (2012) 1–13.

[38] S. Tafazoli, M. Mashregi, P.J. O'Brien, Role of hydrazine in isoniazid-induced hepatotoxicity in a hepatocyte inflammation model, *Toxicology and applied pharmacology.* 229 (2008) 94–101.

[39] K.A. Rickman, K.L. Swancutt, S.P. Mezyk, J.J. Kiddle, Isoniazid: Radical-induced *oxidation* and reduction chemistry. *Bioorganic* & *medicinal chemistry letters***.**23 (2013) 3096–3100.

[40] G.S. Timmins, S. Master, F. Rusnak, V.Deretic, Nitric Oxide Generated from Isoniazid Activation by KatG: Source of Nitric Oxide and Activity against Mycobacterium tuberculosis. *Antimicrobial agents and chemotherapy*. 48 (2004) 3006–3009.

[41] P. Wang, K. Pradhan , X. Zhong , X. Ma. Isoniazid metabolism and hepatotoxicity. *Acta Pharmaceutica Sinica B.* 6 (2016)384–392.

[42] I.G. Metushi, T. Nakagawa, J. Uetrecht. Direct oxidation and covalent binding of isoniazid to rodent liver and human hepatic microsomes: humans are more like mice than rats. *Chemical research in toxicology*. 5 (2012) 2567–76.

[43] Y.M. Koen, N.A. Galeva, I.G. Metushi, J. Uetrecht, R.P. Hanzlik, Protein Targets of Isoniazid-Reactive Metabolites in Mouse Liver in Vivo, *Chemical research in toxicology*. 29 (2016) 1064–1072

[44] A.K. Verma, A. Yadav, S.V. Singh, P. Mishra, S.K. Rath, Isoniazid induces apoptosis: Role of oxidative stress and inhibition of nuclear translocation of nuclear factor (erythroid-derived 2)-like 2 (Nrf2), *Journal of life sciences*. 199 (2018) 23–33.

[45] A.D. Becke, Density-functional thermochemistry. III. The role of exact exchange, *The journal of chemical physics*. 98 (1993) 5648–5652.

[46] M.J. Frisch, G.W. Trucks, H.B. Schlegel, G.E. Scuseria, M.A. Robb, J.R. Cheeseman, et al., Gaussian 09, Revision A.02, Gaussian, Inc., Wallingford CT, 2009.

[47] J.B. Foresman, A. Frisch, Exploring Chemistry with Electronic Structure Methods, Gaussian, Pittsburg, Pa, USA, 1995.

[48] L. Pauling, The Nature of the Chemical Bond, Cornell University Press, Ithaca, NY, USA, 1960.

[49] P. Senet, Chemical hardnesses of atoms and molecules from frontier orbitals, *Chemical physics letters.* 275 (1997) 527–532.

[50] R.G. Parr, R.G. Pearson, Absolute hardness: companion parameter to absolute electronegativity, *Journal of the American chemical society*. 105 (1983) 7512–7516.

[51] Z. Bouanane, M. Bounekhel, M. Elkolli, F. Abrigach, M. Khoutoul, R. Bouyala, R. Touzani, A. Hellal, Synthesis, structural, catecholase, tyrosinase and DFT studies of pyrazoloquinoxaline derivatives, *Journal of molecular structure*. 1139 (2017) 238–246.

[52] G. Malloci, G. Serra, A. Bosin, A.V. Vargiu, Extracting conformational ensembles of small molecules from molecular dynamics simulations: ampicillin as a test case, *Computation*. 4 (2016) 1–16.

[53] Ch. Ji, F. Svensson, A. Zoufir, A. Bender, eMolTox: prediction of molecular toxicity with confidence, *Bioinformatics*. 34 (2018) 2508–2509.

[54] P. Banerjee, A. O. Eckert,A. K. Schrey, R.Preissner, ProTox-II: a web server for the prediction of toxicity of chemicals, *Nucleic acids research*. 46 (2018) 257–263.

[55] R.C. Braga, V.M. Alves, E.N. Muratov, J. Strickland, N. Kleinstreuer, A. Trospsha, C.H. Andrade. Pred-Skin: A Fast and Reliable Web Application to Assess Skin Sensitization Effect of Chemicals. *Journal of chemical information and modeling*. 57 (2017) 1013–1017.

[56] V.V. Poroikov, D.A. Filimonov, W-D. Ihlenfeldt, T.A. Gloriozova, A.A. Lagunin, Y.V. Borodina, A.V. Stepanchikova, M.C. Nicklaus, PASS Biological Activity Spectrum Predictions in the Enhanced Open NCI Database Browser. *Journal* of*chemical information* and *computer sciences*. 43 (2003) 228–236.

[57] L.B.M. Ellis, D. Roe, L.P. Wackett, The university of Minnesota biocatalysis/ biodegradation database: the first decade, *Nucleic Acids Res*. 34 (2006) 517–521.

[58] W.M. Eldehna, M. Fares, M.M. Abdel-Aziz, H.A. Abdel-Aziz, Design, Synthesis and Antitubercular Activity of Certain Nicotinic Acid Hydrazides, *Molecules*. 20 (2015) 8800–8815.

[59] R.K. Devappa, S.K. Rajesh, V. Kumar, H.P. Makkar, K. Becker, Activities of *Jatropha curcasphorbol* esters in various bioassays, *Ecotoxicology and environmental safety*.78 (2012) 57–62.

[60] S.M. Dhiyaaldeen, Z.A. Amin, P.H. Darvish, I. F Mustafa, M.M. Jamil, E. Rouhollahi, M.A. Abdulla, Protective effects of (1-(4-hydroxy-phenyl)-3-mtolyl-propenonechalcone in indomethacin-induced gastric erosive damage in rats, *BMC veterinary research.*10 (2014) 1–14.

[61] R. Gowri, V. Madhavan, Evaluation of antioxidant activity of ethanolic extract of *Sphaeranthusamaranthoides Burm.f, International Journal of Drug Development and Research*. 5 (2013) 320–329.

[62] C. Le Bourvellec, D. Hauchard, A. Darchen, J.L. Burgot, M.L. Abasq, Validation of a new method using the reactivity of electrogenerated superoxide radical in the antioxidant capacity determination of flavonoids, *Talanta*. 75 (2008) 1098–1103.

[63] D. Mukhopadhyay, P. Dasgupta, D. Sinha Roy, S. Palchoudhuri, I. Chatterjee, S. Ali, S. Dastidar, A sensitive In vitro spectrophotometric hydrogen peroxide scavenging assay using 1,10 phenanthroline, *Free Radicals and Antioxidants*. 6 (2016) 124–132.

[64] N. Georgieva, V. Gadjeva, D. Dimitrova, Study on the influence of isoniazid alone or combined with new synthetized isoniazid structural analogues upon catalase activity, *Bulgarian journal* of *veterinary medicine*. 7 (2004) 9–16.

[65] S. Aouachria, S. Boumerfeg, A. Benslama, F. Benbacha, T. Guemmez, S. Khennouf, L. Arrar, A. Baghiani. Acute, sub-acute toxicity and antioxidant activities (in vitro and in vivo) of *Reichardia picroide* crude extract. *Journal of Ethnopharmacology*. 208 (2017) 105–116

[66] L. Tebbouche, D. Hank, S. Zeboudj, A. Namane, A. Hellal, Evaluation of the phenol biodegradation by *Aspergillus niger*: application of full factorial design methodology, *Desalination* and *Water Treatment*. 57 (2015) 1–7.

[67] A. Bendjeddou, T. Abbaz, A.K. Gouasmia, D. Villemin, Molecular structure, HOMO-LUMO, MEP and Fukui function analysis of some ttf-donor substituted molecules using DFT (B3LYP) Calculations, *International research journal of pure and applied chemistry*. 12 (2016) 1–9.

[68]A. Hellal, S. Chafaa, N. Chafai, L. Touafri, Synthesis, antibacterial screening and DFT studies of series of a-aminophosphonates derivatives from aminophenols. *Journal of molecular structure*. 1134 (2017) 217–225.

[69] O. Toure, C.-G.Dussap, A. Lebert, Comparison of Predicted pKa Values for Some Amino-Acids, Dipeptides and Tripeptides, Using COSMO-RS, ChemAxon and ACD/Labs Methods,*Oil & Gas Science and Technology-Revue* d' *IFP Energies nouvelles*. 68 (2013)281–297.

[70] J.I. WELLS: Pharmaceutical Preformulation, 1st Ed. EillsHoowood Ltd., London, UK (1998):25

[71] M. Rupp, R. Körner, I.V. Tetko, Predicting the p*Ka* of small molecules. *Combinatorial chemistry & high throughput screening*. 14 (2011) 307–327.

[72] G. Vistoli, A. Pedretti, B. Testa. Assessing drug-likeness – what are we missing?, *Drug Discovery Today.* 13, (2008) 285–294.

[73] J.X. Mao, Charges in molecules: a classical concept in modern computational chemistry, *Journal of postdoctoral* research. 2 (2014) 15–18.

[74] I. Sidir, Y.G. Sidir, M. Kumalar, E. Tasal, Ab initio Hartree-Fock and density functional theory investigations on the conformational stability, molecular structure and vibrational spectra of 7-acetoxy-6-(2,3-dibromopropyl)-4,8- dimethylcoumarin molecule, *Journal of molecular structure*. 964 (2010) 134–151.

[75] M. Mehri, N. Chafai, L. Ouksel, K. Benbouguerra, A. Hellal, S. Chafaa, Synthesis, electrochemical and classical evaluation of the antioxidant activity of three aaminophosphonic acids: experimental and theoretical investigation, *Journal of molecular structure*. 1171 (2018) 179–189.

[76] R. Ruzziconi, S. Spizzichino, L. Lunazzi, A. Mazzanti, M. Schlosser, B values as a sensitive measure of steric effects, *Chemistry-* A *European Journal*. 15 (2009) 2645–2652.

[77] A.J. Arnott, R. Kumar, S, Lobo, Lipophilicity Indices for Drug Development, *Journal of pharmacokinetics and biopharmaceutic*s. 1 (2013) 31–36.

[78] J.M. Pallicer, J. Sales, M. Rosés, C. Ràfols, E. Bosch, Lipophilicity assessment of basic drugs (log Po/w determination) by a chromatographic method, *Journal of chromatography A*, 1218 (2011) 6356–6368.

[79] J. Kujawski, M. K. Bernard, A.Janusz, W.Kuzma, Prediction of logP: ALOGPS Application in Medicinal Chemistry Education, *Journal of Chemical Education*. 89 (2012) 64–67.

[80] C.A. Lipinski, F. Lombardo, B.W. Dominy, P.J. Feeney, Experimental and computational approaches to estimate solubility and permeability in drug discovery and development settings, *Advanced Drug Delivery Reviews.* 46 (2001) 3–26.

[81] G. Schaftenaar, J. de Vlieg, Quantum mechanical polar surface area, *Journal* of *computer-aided molecular design*. 26 (2012) 311–318.

[82] T. *Ö*sterberg, U. Norinder, Prediction of Polar Surface Area and Drug Transport Processes Using Simple Parameters and PLS Statistics, *Journal* of *computer-aided molecular* design. 40 (2000) 1408–1411.

[83] A. Husain, A. Ahmad, S.A. Khan, M. Asif, R.Bhutani, F.A. Al-Abbasi, Synthesis, molecular properties, toxicity and biological evaluation of some new substituted imidazolidine derivatives in search of potent anti-inflammatory agents, *Saudi pharmaceutical journal***.** 24 (2016) 104–114.

[84] A. Ibáñez-Escribano, J.J. Nogal-Ruiz, A. Gómez-Barrio, V.J. Arán, J.A. Escario, In vitro trichomonacidal activity and preliminary *in silico* chemometric studies of 5-nitroindazolin-3-one and 3-alkoxy-5-nitroindazole derivatives. *Parasitology*. 143 (2016) 34–40.

[85] B.R. Arwa, B.B. Vladimir, In silico toxicology: computational methods for the prediction of chemical toxicity, *WIREs Computational molecular science.* 6 (2016) 147–172.

[86] I. Rusyn, G.P. Daston, Computational Toxicology: Realizing the Promise of the Toxicity Testing in the 21st Century. *Environ Health Perspect* 118 (2010) 1047–1050.

[87] Z. Wang, N. R. Clark, A. Ma'ayan, Drug Induced Adverse Events Prediction with the LINCS L1000 Data, *Bioinformatics.* 32 (2016) 2338–2345.

[88] G.H. Hakimelahi, G.A. Khodarahmi. The Identification of Toxicophores for the Prediction of Mutagenicity, Hepatotoxicity and Cardiotoxicity, *Journal of the Iranian chemical society*. 2 (2005) 244–267.

[89] R. Benigni, Predicting the carcinogenicity of chemicals with alternative approaches: recent advances, *Expert opinion on drug metabolism & toxicology* 10 (2014) 1199–1208.

[90] M. Casalegno, G. Sello, Carcinogenicity prediction of noncongeneric chemicals by augmented top priority fragment classification, *Computational biology and chemistry*. 61 (2016) 145–154.

[91] C.Y. Liew, Y.C. Lim, C.W. Yap, Mixed learning algorithms and features ensemble in hepatotoxicity prediction, *Journal* of *computer-aided molecular* design .25 (2011) 855–871.

[92] B.K Gunawan, N. Kaplowitz. Mechanisms of Drug-Induced Liver Disease, *Clinics in liver disease*. 11 (2007) 459–475.

[93] A. Chowdhury, A. Santra, K. Bhattacharjee, S. Ghatak, D. R. Saha, G.K. Dhali, Mitochondrial oxidative stress and permeability transition in isoniazid and rifampicin induced liver injury in mice, *Journal of hepatology*. 45 (2006) 117–26.

[94] Z. Ji, N.S. Ball, M. J. LeBaron, Global Regulatory Requirements for Mutagenicity Assessment in the Registration of Industrial Chemicals, *Environmental and molecular mutagenesis***.** 58 (2017) 345–353.

[95] V. Leiro, A. Fernandez-Villar, D. Valverde, L. Constenla, R. Vazquez, L. Pineiro, A. Gonzalez-Quintela, Influence of glutathione S -transferaseM1and T1homozygous null mutations on the risk of antituberculosis drug-induced hepatotoxicity in a Caucasian population, *Liver International*. 28 (2008) 835–839.

[96] A.K. Schrey, J. Nickel-Seeber, M.N. Drwal, P. Zwicker, N. Schultze, B. Haertel, R. Preissner, Computational prediction of immune cell cytotoxicity. *Food and chemical toxicology*. 107 (2017) 150–166.

[97] Q. Li, M. Minami, T. Hanaoka, Y. Yamamura, Acute immunotoxicity of p-chloronitrobenzene in mice: II. Effect of *p*-chloronitrobenzene on the immunophenotype of murine splenocytes determined by flow cytometry, *Toxicology*. 137 (1999) 35–45.

[98] M. Zhang, D. Aguilera, C. Das, H. Vasquez, P. Zage, V. Gopalakrishnan, J. Wolff, Measuring Cytotoxicity: A New Perspective on LC50, *Anticancer research***.** 27(2007) 35–38.

[99] P. Bu, S. Narayanan, D. Dalrymple, X. Cheng, A.T.M. Serajuddin, Cytotoxicity assessment of lipid-based self-emulsifying drug delivery system with Caco-2 cell model: Cremophor EL as the surfactant, *European journal of pharmaceutical sciences***.** 91 (2016) 162–171.

[100] J. Liu, P.S. Kern, G.F. Gerberick, O.A. Santos-Filho, E.X. Esposito, A.J. Hopfinger, Y.J. Tseng, Categorical QSAR models for skin sensitization based on local lymph node assay measures and both ground and excited state 4D-fingerprint descriptors, *Journal* of *computer-aided molecular design*. 22 (2008) 345–366.

[101] J. Macan, D. Rimac, S. Kezic , V.M. Varnai, Occupational and non-occupational allergic contact dermatitis: a follow-up study, *Dermatology* 227 (2013) 321-329.

[102] H.A. Dabbagh, F. Azami, H. Farrokhpour, N. Chermahini, UV-Vis, NMR and FTIR spectra of tautomers of vitamin C. experimental and DFT calculations, *Journal of the Chilean chemical society*. 59 (2014) 2588–2594.

[103] A.O. Aptula, D.W. Roberts, Mechanistic applicability domains for non-animal based prediction of toxicological end points: general principles and application to reactive toxicity, *Chemical research in toxicology*. 19 (2006) 1097–1105.

[104] A. Nandy, S. Kar, K. Roy, Development and validation of regression-based QSAR models for quantification of contributions of molecular fragments to skin sensitization potency of diverse organic chemicals, *SAR and QSAR in environmental research*. 24 (2013) 1009–1023.

[105] C. Goebel, P. Aeby, N. Ade, N. Alepee, A. Aptula, Guiding principles for the implementation of non-animal safety assessment approaches for cosmetics: skin sensitization, *Regulatory toxicology and pharmacology*. 63 (2012) 40–52.

[106] World Health Organization. Global Tuberculosis Report; World Health Organization: Geneva, Switzerland, 2015.

[107] G.F.S. Fernandes, D.H. Jornada, P.C. Souza, C.M. Chin, F.R. Pavan, J.L. Santos, Current Advances in Antitubercular Drug Discovery: Potent Prototypes and New Targets, *Current medicinal chemistry*. 22 (2015) 3133–3161.

[108] R. Maccari, R. Ottanà, M.G. Vigorita, In vitro advanced antimycobacterial screening of isoniazid-related hydrazones, hydrazides and cyanoboranes: Part 14. *Bioorganic* & *medicinal chemistry letters.* 15 (2005) 2509–2513.

[109] S. Kauthale, S. Tekale, M. Damale, J. Sangshetti, R. Pawar, Synthesis, antioxidant, antifungal, molecular docking and ADMET studies of some thiazolylhydrazones. *Bioorganic* & *medicinal chemistry letters.* 27 (2017) 3891–3896.

[110] A. Chollet, L. Mourey, C. Lherbet, A. Delbot, S. Julien, M. Baltas, J. Bernadou, G. Pratviel, L. Maveyraud, V. Bernardes-Génisson, Crystal structure of the enoyl-ACP reductase of Mycobacterium tuberculosis (InhA) in the apo-form and in complex with the active metabolite of isoniazid pre-formed by a biomimetic approach ,*Journal of structural biology*. 190 (2015) 328–337.

[111] C. Pinedo-Rivilla, J. Aleu, I.G. Collado, Pollutants biodegradation by fungi, *Current organic chemistry*. 13 (2009) 1194–1214.

[112] S. Vorberg, I.V. Tetko, Modeling the biodegradability of chemical compounds using the online chemical modeling environment (OCHEM), *Molecular informatics*. 33 (2014) 73–85.

[113] D.L. Vladoiu, M.N. Filimon, V. Ostafe, A. Isvoran, Effects of herbicides and fungicides on the soil chitinolytic activity. A molecular docking approach, *Ecological* chemistry and engineering *s*-chemia. 22 (2015) 439–450.

[114] S.F. Nishino, J.C. Spain, Oxidative pathway for the biodegradation of nitrobenzene by *Comamonas sp*. strain JS765, *Applied and Environmental Microbiology*. 61 (1995) 2308-2313.

[115] R.M. Silverstein, F.X. Webster,D.J. Kiemle, "Ch. 2: Infrared spectrometry", In: "Spectrometric Identification of Organic Compounds", 7th edition, John Wiley & Sons, Inc., USA, 2005, 72–126.

[116] R.L. Shriner, C.K.F. Hermann, T.C. Morrill, D.Y. Curtin,R.C. Fuson,"Ch. 7: Infrared spectrometry", In: "The systemic identification of organic compounds", 8th edition, John Wiley & Sons, Inc., USA, 2004, p. 194–227.

[117] H.S.N. Kumar, T. Parumasivam, F. Jumaat, P. Ibrahim, M.Z.Asmawi, A. Sadikun, Synthesis and evaluation of isonicotinoylhydrazone derivatives as antimycobacterial and anticancer agents, *Medicinal chemistry research*. 23(2014) 1–11.

[118] P.F.M. Oliveira, B. Guidetti, A. Chamayou, C. André-Barrès, J. Madacki, J. Korduláková, G. Mori, B.S. Orena, L.R. Chiarelli, M.R. Pasca, C.L herbet, C. Carayon, S. Massou, M. Baron, M. Baltas, Mechanochemical Synthesis and Biological Evaluation of Novel Isoniazid Derivatives with Potent Antitubercular Activity,*Molecules.* 22 (2017) 1–27.

[119] C.H. Walker, Ecotoxicity testing of chemicals with particular reference to pesticides, *Pest Management Science*. 62 (2006) 571–583.

[120] Y. Wang, Z.H. Ning, H.W. Tai, S. Long, W.C. Qin, L.M. Su, Y.H. Zhao, Relationship between lethal toxicity in oral administration and injection to mice: Effect of exposure routes, *Regulatory toxicology and pharmacology***.** 71 (2015) 205–212.

[121] S. Parasuraman, Toxicological screening, *Journal Pharmacology Pharmacotherapeutics*. 2 (2011) 74–79.

[122] M.S. Baliga, G.C. Jagetia, J.N. Ulloor, M.P. Baliga, P. Venkatesh, R. Reddy, K.V.N. M. Rao, B.S. Baliga, S. Devi, S.K. Raju, V. Veeresh, T.K. Reddy, K.L. Bairy, The evaluation of the acute toxicity and long term safety of hydroalcoholic extract of *Sapthaparna (Alstoniascholaris)* in mice and rats. *Toxicology Letters*. 151 (2004) 317–326.

[123] E.G. Giannini, R. Testa, V. Savarino, Liver enzyme alteration: a guide for clinicians, *Canadian Medical Association journal*. 172(2005) 367–379.

[124] S. Rollas, Ş.G. Küçükgüzel, Biological Activities of Hydrazone Derivatives, *Molecules*. 12 (2007) 1910-1939.

[125] H. Khither, W. Sobhi, A. Khenchouche, A. Mosbah, M. Benboubetra. In-vitro Antioxidant Effect of Thymoquinone. *Annual Research & Review in Biology* 25 (2018) 1–9.

[126] D. Nikolic, R.B.V. Breemen, DNA Oxidation Induced by Cyclooxygenase-2,*Chemical research in toxicology*.14 (2001) 351–354.

[127] H. Tao, J. Zhou, T. Wu, Z. Cheng, High-throughput superoxide anion radical scavenging capacity assay, *Jourtnal agriculture food chemistry*. 62 (2014) 9266–9272.

[128] D.T. Sawyer, J.L. Roberts, Electrochemistry of oxygen and superoxide ion in dimethylsulfoxide at platinum, gold and mercury electrodes, *Journal of Electroanalytical Chemistry.* 12 (1966) 90–101.

[129] J.Y. Wang, R.M Burger, K. Drlica, Role of superoxide in catalase-peroxidase mediated isoniazid action against mycobacteria, *Antimicrobial agents and chemotherapy*. 42 (1998) 709-711.

[130] H. Gocer, I. Gulcin, Caffeic acid phenethyl ester (CAPE): correlation of structure and antioxidant properties, *International journal of food science and nutrition*. 62 (2011) 821–825.

[131] M.S. Salga, I. Sada, A. Mustapha, Influence of Steric hindrance on the antioxidant activity of some schiff base ligands and their copper (II) complexes, *Oriental journal* of *chemistry*. 30 (2014) 1529–1534.

[132] N. Georgieva, V. Gadjeva, Isonicotinoylhydrazone analogs of isoniazid: relationship between superoxide scavenging and tuberculostatic activities, *Biochemistry (Moscow)*. 67 (2002) 588–591.

[133] S. Sumathi, R. Anuradha. In vitro antioxidant activity of methanolic extract of flower of *Couroupitaguinensis* Aubl. *Journal of Chemical* and *Pharmaceutical Research*. 8 (2016) 618–623.

[134] M S. Estevão, L.C. Carvalho, D. Ribeiro, D. Couto, M. Freitas, A. Gomes, L.M. Ferreira, E.Fernandes, M.M.B. Marques, Antioxidant activity of unexplored indole derivatives: Synthesis and screening, *European journal of medicinal chemistry*. 45 (2010) 4869–4878.

[135] B. Poeggeler, R.J. Reiter, D-X.Tan, L-D. Chen, L.C. Manchester, Melatonin, hydroxyl radical-mediated oxidative damage, and aging: A hypothesis, *Journal of pineal research*. 14 (1993) 151–168.

[136] D-x Tan, R.J. Reiter, L.C. Manchester, M-t. Yan, M. El-Sawi, R.M. Sainz, J.C. Mayo, R. Kohen, M. Allegra, R.Hardeland, Chemical and Physical Properties and Potential Mechanisms: Melatonin as a Broad Spectrum Antioxidant and Free Radical Scavenger, *Current topical medicinal chemistry.* 2 (2002) 181–197.

[137] N. Belkheir, B. Bouguerne, F. Bedos-Belval, H. Duran, C. Bernis, R. Salvayre, A. Nègre-Salvayre, M. Baltas. Synthesis and antioxidant activity evaluation of a syringic hydrazones family, *European Journal of Medicinal Chemistry*. 45 (2010) 3019-3026

[138] S. Suzen, S.S. Cihaner, T. Coban, Synthesis and Comparison of Antioxidant Properties of Indole-Based Melatonin Analogue Indole Amino Acid Derivatives, *Chemical biology & drug design*. 79 (2012) 76–83.

[139] R. Suresh, N. Naik, S. Vandana, M. Panda. Hepatoprotective effect of Ginkgo select Phytosome in rifampicin induced liver injurym in rats: Evidence of antioxidant activity. *Fitoterapia*. 79 (2008) 439–445.

[140] J.M. Mates, C. Perez-Gomez, I. Nunenez de Castro, Antioxidants enzymes and human diseases, *Clinical Biochemistry*. 32 (1999) 595–603.

[141] N. Georgieva, Z. Yaneva, G. Nikolova, S. Simova, Schiff base SH11 with tuberculostatic and radical scavenging activities against INH-induced oxidative hepatic damage, *Advances in Biosciences and Biotechnological*. 3 (2012) 1068–1075.

[142] K. Gholami, E. Kamali, M. Hajiabdolbagh, G. Shalviri, Evaluation of anti-tuberculosis induced adverse reactions in hospitalized patients, *Pharmacy Practice*. 4 (2006) 134–138.

[143] Z. Hussain, P. Kar, S.A. Husain, Antituberculosis Induced Hepatitis: risk factors, prevention and management", *Indian journal of Experimental Biology*. 41 (2003) 1226–1232.

[144] J-H. Kim, W.S. Nam, S.J. Kim, O.K. Kwon, E.J. Seung, J.J. Jo, R. Shresha, T.H. Lee, T.W. Jeon, S.H. Ki, H.S. Lee, S. Lee, Mechanism Investigation of Rifampicin-Induced Liver Injury Using Comparative Toxicoproteomics in Mice. *International Journal Molecular Sciences*. 18 (2017) 1417.

[145] S. Eminzade, F. Uras, F.V Izzettin,Silymarin protects liver against toxic effects of anti-tuberculosis drugs in experimental animals, *Nutrition & metabolism*. 18 (2008)1–8.

[146] V. Santos, V.R. Linardi, Biodegradation of phenol by a filamentous fungi isolated from industrial effluents- identification and degradation potential. *Process biochemistry*. 39 (2004) 1001–1006.

[147] N.H Dang, H.L. Le, W. Chune Li, The culture conditions on the mycelium growth, antioxidant capacity of *cordycepsmilitaris* (strains AG-1 and PSJ-1). *Academia journal of biotechnology*. 4 (2016) 430–439.

Abstract

The new hydrazones; N'-[(*E*)-(4-chloro-3-nitrophenyl)methylidene]pyridine-4-carbohydrazide (**Hyd1**), N'-[(3*Z*)-6-bromo-2-oxo-2,3-dihydro-1*H*-indol-3-ylidene] pyridine-4-carbohydrazide (**Hyd2**) were synthesized *via* condensation of 4-chloro-3-nitro-benzaldehyde or 6-bromoindoline-2,3-dione and isoniazid (**INH**) in ethanol in the presence of a few drops of acetic acid. These synthesized compounds were characterized by a number of spectroscopic methods including UV, IR, NMR (1H, 13C), and mass spectrometry, and by elemental analysis. Molecular structure properties of **INH**, **Hyd1** and **Hyd2** were investigated using the package Marvin and density functional theory (DFT) via B3LYP/6-31G (d,p) methods, whereas the antioxidant effect was evaluated *in vitro* by superoxide anion (chemical and electrochemical methods) and hydrogen peroxide assays, and *in vivo* against oxidative stress and hepatotoxicity induced in mice by **INH**. Results obtained from this investigation indicate high effect of the **Hyd1** towards superoxide anion with an IC_{50} value of 32.37 ± 0.45 mg/mL, which is comparable with that of ascorbic acid (**AA**), and a high effect of **Hyd2** against hydrogen peroxide (IC_{50} = 4.46 ±0.2 µg/mL) which is comparable with that of Indomethacine (**IND**). In addition, **Hyd2** exhibited hepatoprotective effect against **INH**-oxidative stress and hepatotoxicity. Furthermore, toxicity of the synthesized compounds was evaluated by *in silico*, *in vitro*, and *in vivo* methods, using software programs, microorganisms, and animals. Results show low predicted toxicity of **Hyd2**, no toxic effect against bacteria and fungi at a high dose of 2000 mg/mL and no toxic effect against mice at a high dose of 1000 mg/kg of both hydrazones. Anti-tubercular effect prediction of both hydrazones, indicated an excellent effects with probabilities of 84.6 and 83.9% from **Hyd1** and **Hyd2**, respectively. Biodegradability predictions of the synthesized hydrazones were carried out using online computer software programs (UMBBD) and by *in vitro* assay using the degradation in mineral media. Results demonstrate that these hydrazones are biodegradable by simple microorganisms.

Keyword: Hydrazones, Synthesis, Antioxidant, Prediction, Toxicity, Biodegradation

Résumé

Les nouveaux hydrazones; N '- [(*E*) - (4-chloro-3-nitrophényl) méthylidène] pyridine-4-carbohydrazide (**Hyd1**), N' - [(3*Z*) -6-bromo-2-oxo-2,3-dihydro- Le 1*H*-indol-3-ylidène] pyridine-4-carbohydrazide (**Hyd2**) a été synthétisé par condensation du 4-chloro-3-nitro-benzaldéhyde ou de la 6-bromoindoline-2,3-dione et de l'isoniazide (INH) en éthanol en présence de quelques gouttes d'acide acétique. Ces composés synthétisés ont été caractérisés par de méthodes spectroscopiques, notamment UV, IR, RMN (1H, 13C) et spectrométrie de masse, ainsi que par analyse élémentaire. Les propriétés de structure moléculaire de INH, Hyd1 et Hyd2 ont été étudiées à l'aide du paquet Marvin et de la théorie de la densité fonctionnelle (DFT) via les méthodes B3LYP / 6-31G (d, p), alors que l'effet antioxydant a été évalué *in vitro* par des dosages d'anion superoxyde (methodes chimiques et electrochimiques) et de peroxyde d'hydrogène. et *in vivo* contre le stress oxydatif et l'hépatotoxicité induits chez la souris par l'INH. Les résultats obtenus au cours de cette étude indiquent un effet élevé de **Hyd1** sur l'anion superoxyde avec une IC50 de 32,37 ± 0,45 mg / mL, ce qui est comparable à celui de l'acide ascorbique (AA), ainsi que l'effet élevé de **Hyd2** contre le peroxyde d'hydrogène (IC50 = 4,46 ± 0,2 µg / mL), ce qui est comparable à celui de l'indométhacine (**IND**). En outre, **Hyd2** présente un effet hépatoprotecteur contre le stress oxydant et l'hépatotoxicité de l'INH. De plus, la toxicité des composés synthétisés a été évaluée par des méthodes *in silico*, *in vitro* et *in vivo*, à l'aide de logiciels, de micro-organismes et d'animaux. Les résultats montrent une faible toxicité prévue d'**Hyd2**, aucun effet toxique contre les bactéries et les champignons à une dose élevée de 2 000 mg / mL et aucun effet toxique contre les souris à une dose élevée de 1 000 mg / kg des deux hydrazones. La prédiction de l'effet antituberculeux des deux hydrazones indique des excellents effets avec des probabilités de 84,6 et 83,9% pour **Hyd1** et **Hyd2**. Les prédictions de biodégradabilité des hydrazones synthétisées ont été réalisées à l'aide de logiciels informatiques en ligne (UMBBD) et d'un test *in vitro* utilisant la dégradation en milieu minéral. Les résultats démontrent la biodégradabilité de ces hydrazones par de simples microorganismes.

Mots clés: Hydrazones, Synthèse, Antioxydante, Prédiction, Toxicité, Biodégradation

ملخص

تم تحضير الهيدرازونات الجديدة 4-(كلورو-3-نيتروفنيل) مثيلدين بيردين -4-كربوهايدرازيد **(هايد1)** و 3-(6-بروموـ-2-اوكسو.3.2-دايهايدرو -1-اندول-3-يلدين)بيردين-4-كاربوهايدرازيد **(هايد2)** عن طريق تفاعل التكثيف للايزونيازيد مع 4-كلورو-3-نايتر-بنزالدهايد **او** 6-بروموانـدولين-ديون- في الايثـانول مع قطرات من حمض الاستيك على التوالي. تم تحليل المركبات بعدد من الطرق الطيفية بما في ذلك الأشعة فوق البنفسجية ، الأشعة تحت الحمراء-الرنين المغناطيسي النووي- الطيف الكتلي والتحليل العنصري، ثم درست خصائص التركيب الجزيئي للهايدرزونات باستخدام حزمة مارفاين والنظرية الوظيفية للكثافة. في حين تم تقييم التأثير المضاد للأكسدة بواسطة أنيون سيباراكسايد (باستعمال الطريقة الكيميائية والكهروكيميائية) و هيدروجين بيروكسيد و ضد الإجهاد التأكسدي والتسمم الكبدي للفئران الناجم عن الايزونيازيد. تشير النتائج التي تم الحصول عليها من هذا الفحص إلى تأثير عال لـ**(هايد1)** تجاه أنيون سيباراكسايد32.37 ميكروغرام/مل والتي يمكن مقارنتها مع حمض الأسكوربيك. فيما بينت النتائج التاثير العالي ل**(هايد2)** تجاه هيدروجين بيروكسيد 4.46 ميكروغرام/مل والتي يمكن مقارنتها مع الاندومتاسين. كما بينت النتائج تاثير **(هايد2)** المضاد للإجهاد التاكسدي والواقي من التسمم الكبدي عند الفئران. إلى ذلك ، تم تقييم سمية المركبات ، باستخدام برامج الحاسوب ، الكائنات الدقيقة والحيوانات. تظهر النتائج سمية منخفضة متوقعة لـ**(هايد2).** لا تأثير سام ضد البكتيريا والفطريات بجرعة عالية من 2000 ميكروغرام / مل ولا تأثير سام ضد الفئران بجرعة عالية من 1000 ملغم / كغ من كلا الهيدرازونات.كمايشير تنبؤ التأثيرات المضادة للسل ان لكل من الهيدرازونات تأثيرات ممتازة مع احتمال 84.6 و 83.9٪. كما نفذت تنبؤات التحلل الحيوي للهيدرازونات باستخدام برامج حاسوبية على الإنترنت وتم تنفيذها في المختبر باستعمال الوسط المعدني. واظهرت إمكانية التحلل البيولوجي لهذه الهيدرزونات بواسطة كائنات دقيقة بسيطة.

الكلمات المفتاحية هايدرزون. تركيب .مضاد للتأكسد. تنبؤ. السمية. التحلل البيولوجي